2023-01-18

Influence of Polymer Structure, Cation Type, and Substrate on Ionomer Thin Film Hydration Properties

Eskandari, Hamideh

UNIVERSITY OF CALGARY

Influence of Polymer Structure, Cation Type, and Substrate on Ionomer Thin Film Hydration Properties

by

Hamideh Eskandari

A THESIS

SUBMITTED TO THE FACULTY OF GRADUATE STUDIES

IN PARTIAL FULFILMENT OF THE REQUIREMENTS FOR THE

DEGREE OF DOCTOR OF PHILOSOPHY

GRADUATE PROGRAM IN CHEMICAL AND PETROLEUM ENGINEERING

CALGARY, ALBERTA

JANUARY, 2023

Abstract

Low carbon energy systems are undeniable solutions for addressing environmental and climate change issues facing the world. Hydrogen-fueled polymer electrolyte fuel cell (PEFC) are at the forefront of clean energy technology solutions since they are producing no particulate emissions and only water as a by-product at the point source (cars) and can improve air quality. Critical to their widespread adoption is the need for a reduction in the PEFC stack cost which is mainly attributed to the expensive Platinum (Pt) catalyst and development of new materials in catalyst layer. This work aims at investigating the effect of material (such as ionic polymer or ionomer type, substrate and contamination) and operational conditions (such as temperature and relative humidity, RH) on hydration behavior (water uptake and proton conduction) of ionomer thin film in catalyst layer, and then developing a correlation describing how those parameters effect hydration properties (water uptake and proton conductivity) of the ionomer thin film. The results of this study will enable the engineers to better optimize the performance of their produced PEFCs.

In this work, we reported the water content and proton conductivity properties of thin-film ionomers (30 nm) at 80 °C over a wide range of relative humidity (0−90%) for seven different ionomers differing in the side-chain structure, including the number of protogenic groups, with the equivalent weight ranging from 620 to 1100 g/mol of sulfonic acid.

The results show that the acid content or equivalent weight of the ionomer is the strongest determinant of both the swelling and the proton conductivity of ionomer films at a given relative humidity. The proton conductivity of low-equivalent-weight ionomers was higher than that of higher-equivalent-weight ionomers. Significantly higher values of both water content and proton conductivity are observed at 80 °C compared to those at 30 °C, implying that room temperature data are not reliable for estimating ionomer properties in the fuel cell catalyst layer.

We also studied the impact of exchange of protons with cobalt ions on the humidity dependent (0−90% RH) hydration and conductivity of ~30 nm thin ionomer films at a fuel cell-relevant temperature (80 °C). A significant suppression (up to 2 orders of magnitude at low RH) in ionic conductivity was observed for all ionomers upon exchange of protons with cobalt ions, evidently because the water content of the ionomer films decreases upon Co^{2+} exchange. The most interesting finding of the study is that a large variation in conductivity between the H^+ form and Co^{2+} form of ionomer films at a given RH is significantly minimized when conductivity is correlated with the water content.

Then we focused on how carbon and Pt substrate impact the 10 nm ionomer swelling rate under different RHs. It was found that films on Pt substrate, have higher swelling rate than those on carbon and SiO_2 substrates. These results prove the evidence of better water network and higher proton conductivity in ionomers on Pt substrate, indicating that the interactions between ionomers and substrate affects internal structure of ionomers as well as the film surface especially in ultra thin films (< 10 nm). Moreover, water sorption studies on ionomer thin films shows that water absorption is slower than water desorption. It could indicate that the rate of water absorption controlled by the rate of interfacial transport and swelling while the desorption rate mainly controls by interfacial mass transport.

Acknowledgements

I would like to express my sincere gratitude to my supervisor, Prof. Kunal Karan, for the guidance, encouragement, and support he provided during my time as his PhD student at the University of Calgary. This work would not have been possible without the mentorship and guidance of Dr. Karan. I am grateful to the members of my thesis committee, Dr. Anne Maria Benneker, Dr. Sathish Ponnurangam, Dr. Edward (Ted) PL Roberts, Dr Venkataraman Thangadurai and Dr. Shudipto Konika Dishari for the time they put in reading my thesis and for their valuable comments. I would like to thank Dr. Devproshad Paul and Alan Young from Ballard Power Systems Co. for providing valuable suggestions, ideas, and feedback while conducting my research. I thank all the past and present students and researchers of Karan Research Group.

I would like to acknowledge the Natural Sciences and Engineering Research Council of Canada (NSERC) program, Ballard Power Systems and UCalgary scholarships for the financial support to undertake this research. I would like to thank all of the faculty and staff in the Chemical and Petroleum Engineering Department for their help and support throughout my study at University of Calgary.

Finally, I am grateful beyond words to my dearest family, my parents and specially my husband, Mohammad. I would especially express my sincere gratitude to Mohammad, for his continued support, and numerous sacrifices he has made to help me reach this point. I express my heartfelt thanks to my parents for their encouragement and blessings and also for keeping faith on me, not just along this PhD journey but always.

Dedication

To my dear husband,

Mohammad

To my lovely son,

Adrian

Table of Contents

List of Figures

List of Tables

List Acronyms

A

C

E

G

H

I

L

M

N

O

P

Q

R

S

V

Chapter One: General Introduction

1.1.Project background

Nearly 80% of greenhouse gas emissions are attributed to fossil fuel usage and the production of carbon dioxide (CO_2) is considered to be the central reason for global climate change. Besides, fossil fuels are responsible for local air pollution and human health problem due to emission of particulate matter during combustion [1].

Around 24% of energy related global greenhouse gas emissions in the world comes from transportation vehicles running on fossil fuels [2]. The number of car passengers worldwide is anticipated to increase to 2.5 billion by 2050 (Figure 1.1b) [3]. Long-term exposure to air pollution contributed to the deaths of 6.1 million people in 2016 with strokes, heart attacks, lung disease and lung cancer causing many of them [4]. This means an increased level of pollution and healthcare problems associated rise in direct and indirect costs [5]–[7]. Moreover, this contributes to global warming which in turn causes climate change. The effects of climate change are a threat to human existence and must be enthusiastically and adequately put under check. This will keep the global temperature rise to below 2 °C as suggested by the Paris Agreement [8], [9].

Using hydrogen chain (electrolyzer, hydrogen storage, and fuel cells) as energy storage and conversion technologies has attracted significant attention as a solution for the technological gap toward a net-zero CO_2 emission society [13].

An alternative to fossil fuels utilizing combustion system is electrochemical energy conversion devices. Batteries, fuel cells, and electrochemical capacitors (ECs) are the most well known systems for electrochemical energy storage and conversion [14]. Hydrogen-fueled polymer

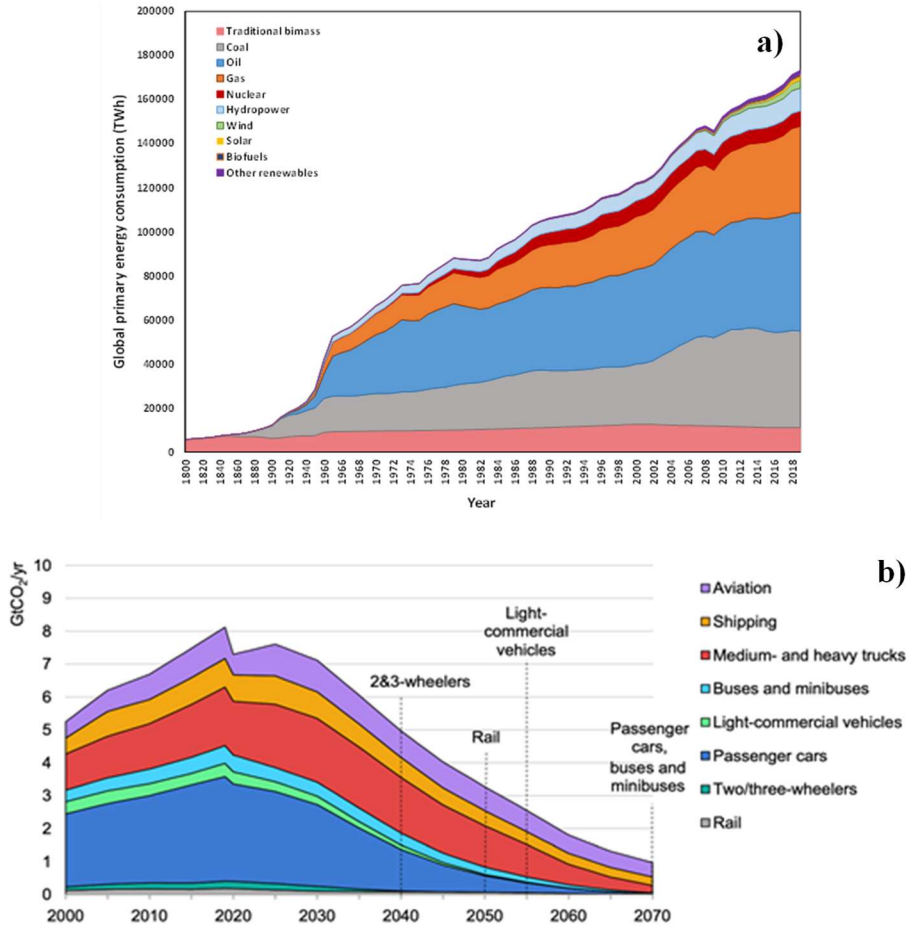

Figure 1.1. a) Global primary energy consumption per annum, reproduced with the permission from Ref [1]. b) Global CO2 emissions in transport by mode in the sustainable development. The dotted line indicates the year which various transport stopped consuming fossil fuels. Reprinted with the permission from Ref [1], [10]

electrolyte fuel cell (PEFC) are at the forefront of clean energy technology solutions since they are producing no particulate emissions and only water as a by-product at the point source (cars) and can improve air quality [7]. It is anticipated by the International Renewable Energy Agency (2020) that the hydrogen energy cost will become competitive with conventional energy sources by 2030. So, several countries have planned to have hydrogen energy industries and infrastructure ready or the arrival of full commercialized hydrogen application [15]–[18]. The costs of hydrogen related

technology are decreasing continuously due to the progress in technology and supply chain. This would be great step in commercialization of this technology [18]. In fact, some companies already have commercialized their fuel cell vehicles like Toyota (Mirai) [19], Honda (Clarity) [20] and Hyundai (Tucson) [21].

Critical to further widespread adoption of PEFCs is the need for a reduction in the PEFC stack cost without comprising the performance. Both cost and performance are primarily attributed to the PEFC catalyst layer. It has been estimated that the expensive Platinum (Pt) catalyst contributes to 40% of the fuel cell system cost [22]. A significant factor affecting the performance are the intrinsic activity of the catalyst and the transport characteristics of the cathode catalyst layer. The catalyst layer (CL) consists of Pt/C aggregates which are covered by ionomer thin film. Electrons and protons conduct via carbon and ionomer respectively (Figure 1.2). Oxygen diffuses through ionomer film to get to the active layer of Pt/ ionomer interface. Hence, oxygen diffusivity and proton transport are impacted by ionomer density and ionic domain of ionomer. For maximum utilization of these catalysts and high in operando electrochemical performance, facile transport of the reactant of the electrochemical reactions, i.e., electrons, protons and gases (e.g., hydrogen and oxygen) must be ensured. That helps to boost the performance of the fuel cell system which will conduct to a reduction in catalyst layer cost significantly. Thus, understanding the properties of ionomer thin films in catalyst layer is considered to be one of the important problems for the PEFC research and development [22], [23].

As elaborated in the next chapter, there is a need to investigate and quantify the effect of material (such as ionic polymer or ionomer type, substrate, and contamination), operational conditions (such as temperature and relative humidity) and preparation process (e.g., annealing temperature) on the hydration-controlled properties, i.e., water uptake and proton conduction, of

ionomer thin films. Such data will help to correlate aforementioned fuel cell operating parameters and their hydration properties (water uptake and proton conductivity). The results of this study will help the technology developers to make data-driven informed choice regarding material selection and operational parameters (such as temperature and relative humidity (RH)) of PEFCs and also provide guidance on electrode processing conditions. The data will also serve as input for computational models of catalyst layer, which can be applied to optimize the performance of PEFCs.

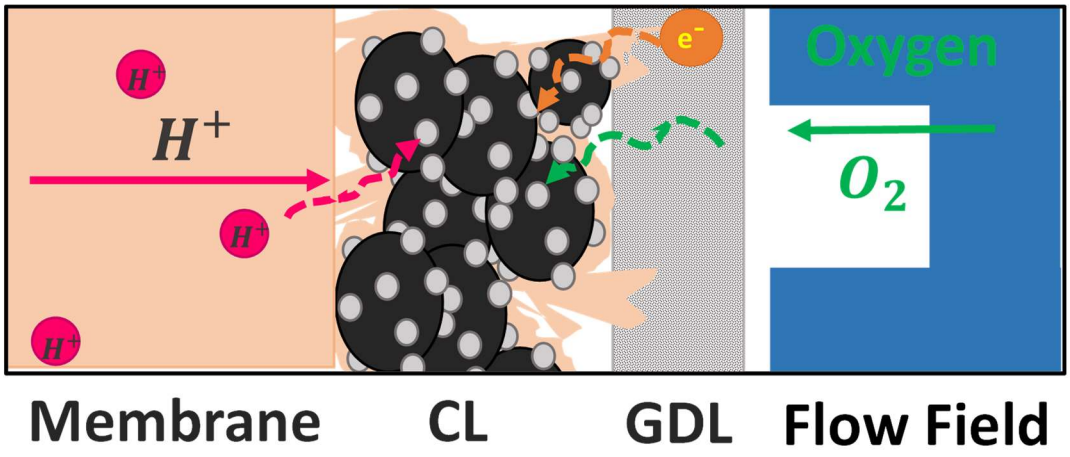

Figure 1.2. Schematic of polymer electrolyte membrane (PEM) fuel cell catalyst layer.

1.2.Research objective

The primary goal of my research is to investigate and quantify the impact of ionomer composition (side-chain length and equivalent weight (EW)) on the properties of ionomer thin films. Another key goal of my research is to examine the impact of cation contamination, arising from leaching of cobalt (Co) from alloy catalysts, on ionomer thin film properties. In addition, the research is aimed at understanding whether and how the hydration properties (water content and proton conduction) of the films are dependent on physical characteristics such as film thickness,

fabrication variables such as substrate type, and local environmental variables such as relative humidity, and temperature. To attain the broader research goal, four sub-tasks discussed below were be undertaken

i) The effects of equivalent weight (EW) and side-chain characteristics of ionomer on hydration properties of the ionomer. The overall objective was to quantify the role of ionomer structure (EW and side chain length and structure) on water uptake and proton conduction of thin film. A number of sub-objectives were planned including: a) investigating the effect of temperature on the ionomer thin film hydration properties. b) investigating the effect of thickness on ionomer thin film properties. in this part tried to achieve the 10 nm thickness (relevant to PEFC CLs, i.e., 4-10 nm) for ionomers. c) achieve a universal correlation between proton conductivity and water content.

ii) The effects of cation-exchange on the water uptake and proton conductivity of ionomer thin film (as a function of RH) of thin films of ionomers differing in molecular structure or EW.

The key objective was to investigate the impact of cobalt ions on water uptake and proton conductivity of ionomer thin films. A number of sub-objectives were planned including a) development of a method for preparing cobalt exchanged ionomer thin films and measuring the hydration properties of the ion exchanged ionomers. b) investigation of the role of ionomer structure (EW and side chain length) on the impact of cobalt exchange on ionomer thin films hydration properties. c) determine the existence of a universal correlation between proton conductivity and water content for cobalt exchanged ionomers.

iii) The effects of different substrates and humidity cycling on the water uptake and kinetics of water uptake in ionomer thin films. The key objective was to investigate the role of

wettability of substrate and ionomer hydration hysteresis on ionomer thin film swelling via measuring the thickness changes at different RH.

1.3.Thesis Structure

The thesis comprises 7 chapters and the main contributions related to the three specific objectives stated above are presented in Chapters 4, 5 and 6. The following is a brief description of the content of each chapter.

Chapter 1. General Introduction: This chapter contains an overview of research topic and motivation behind this research work. This chapter also contains a guideline on the overall thesis goals.

Chapter 2. Literature review and Relevant Background: This chapter contains the background knowledge on the fundamental of PEFC, CL and ionomer thin films. A review of existing literature as it relates to the ionomer cation contamination, ionomer/substrate interaction and ionomer EW and side chain structure has also presented . Finally, research gap and challenges as it existed at the time of conception of the thesis has been identified through extensive literature review related to this research topic.

Chapter 3. Experimental Techniques: In this chapter, the experimental techniques adopted in this study have been described.

Chapter 4. Humidity-dependent hydration and proton conductivity of the perfluorosulfonic-acid (PFSA) ionomer thin films at fuel cell relevant temperature: Effect of ionomer equivalent weight and side-chain characteristics. In this chapter, the water uptake, and

the proton transport properties of ~30 nm ionomer thin films are investigated as a function of ionomer EW and ionomer sidechain structure and length. This chapter also discuss the effect of thickness on ionomer thin film properties. Ellipsometry and Electrochemical impedance spectroscopy (EIS) were employed to determine the water uptake and protonic conductivity of the thin films respectively. A detailed protocol, experimental methodology, data collection and data interpretation are described.

Chapter 5. Conductivity and hygroscopic expansion of ionomer thin films: Effect of cobalt exchange and thermal/aqueous treatment. This chapter highlights the effects of cation (cobalt ion) contamination on ionomer thin films. In this work water uptake and proton conduction of ionomer thin films of thickness ~ 30 nm are investigated as a function of RH at two different doping level (fully exchanged and non- exchanged). In addition, the chapter elucidates the role of ionomer side chain and EW on the impact of cobalt contamination on ionomer thin film properties.

Chapter 6. Water sorption in ionomer thin films: Investigation of substrate and hysteresis effects. This chapter highlights the effects of substrate wettability on ionomer thin film (10 nm) swelling (water uptake). Moreover, this chapter investigate the hysteresis effect on ionomer water uptake in thin films and the kinetics of water uptake. The diffusion coefficient of water absorption and desorption were studied through hydration cycling for 10 nm ionomer thin films. Quartz Crystal Microbalance (QCM) was used for kinetic studies in this chapter.

Chapter 7. Conclusions and Recommendations for Future Work: This chapter provides a summary of key findings and future directions relevant to the development and optimization of materials for PEFC CL.

Chapter Two: Literature Review and Relevant Background

This chapter provides a general background of polymer electrolyte fuel cell (PEFC) technology including an introduction to the key components of PEFC and their function. The intent is to present the existing research gaps and challenges via a concise literature review on the key papers on the specific topic and in the field.

2.1. Polymer Electrolyte Fuel Cell (PEFC)

A fuel cell is an electrochemical device that converts chemical energy directly into electricity. Its origin can be traced to the early 1840s [24]. Fuel cells are often classified based on the type of membrane used. One type of fuel cell, known as the polymer-electrolyte fuel cell (PEFC) –made of proton-conducting polymer electrolyte membrane (PEM, mainly Nafion) and Platinum (Pt)-based materials as catalyst – has received remarkable attention in the past decades due to their performance (fuel-to-electricity conversion efficiency of 60%) [25]. The promise of high efficiency, zero point-source CO2 and particulate matter emissions, and the potential for independence from traditional energy sources make PEFCs highly desirable energy conversion device. Tremendous progress has been made in the PEFC technology over the past decade, but some challenges remain unaddressed [22], [26].

In the following section, first, the key components of PEFC are discussed, and then selected R&D works pertinent to the thesis topic are summarized.

2.1.1. Key components of PEFC

Polymer electrolyte membrane fuel cell is composed of several components including polymer electrolyte membrane (PEM), catalyst layers (CLs), and gas diffusion layers (GDLs), shown in Figures 2.1. Akin to a battery, a PEFC has an anode and a cathode that are separated by an electrolytic medium that allows only ions to conduct but not electrons. Humidified hydrogen gas is fed to the anode side and humidified oxygen is fed to the cathode side. Humidification is necessary to ensure proton conduction in the PEM and the ionic polymer in the CLs, as elucidated later. Hydrogen (H_2) diffuses through the anode-side GDL to arrive at the anode CL where hydrogen oxidation reaction (HOR) takes place (Eq. 1) and hydrogen molecules are split into protons and electrons at the platinum/ionomer interface. The released protons are transported through the PEM towards the cathode; this drives the electrons off the anode through an external circuit to the cathode. At the cathode CL, the protons released at anode, oxygen (O_2) gas diffused through cathode-side GDL, and electrons travelled across external circuit will undergo a chemical reaction called oxygen reduction reaction (ORR) (Eq.2) through which water and heat are produced [27], [28]. The produced water is partially utilized for humidification purposes of the membrane because the membrane's performance (i.e., proton conductivity) is highly dependent on its water content.

$$\text{HOR: } H_2(g) \rightarrow 2H^+ + 2e^- \tag{2.1}$$

$$\text{ORR: } 4H^+ + 4e^- + O_2(g) \rightarrow 2H_2O(l) \tag{2.2}$$

The overall reaction can be described as follows (Eq. 3):

$$2H_2 + O_2 \rightarrow 2H_2O \tag{2.3}$$

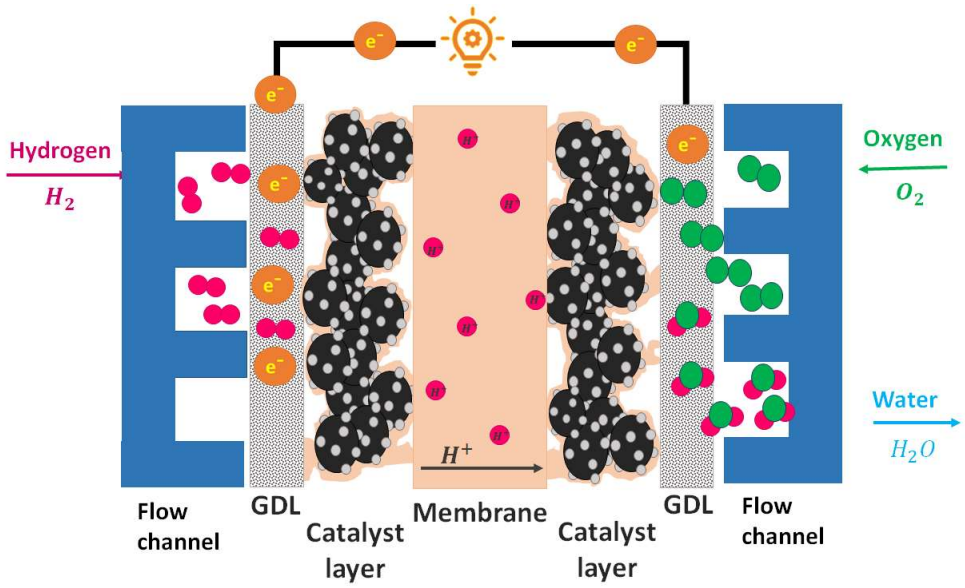

Figure 2.1. Schematic representation of a PEM fuel cell.

The main role of PEM is that it only allows positively charged ions (H^+) to pass through. GDL is responsible for facilitating diffusion of reactants (i.e., O_2, and H_2) across the catalyst layer, and controlling the humidity in catalyst layer and membrane through supplying humid gases, removing produced water off the catalyst layer, and conducting electrons from the flow-channels to the CLs. Sufficient hydration of ionomer in the catalyst layer and membrane is needed to ensure high proton conductivity, since proton conduction is highly mediated by water. The electrochemical reactions and transport of all key species occur in the CL. Thus, the CL can be said to be the heart of a fuel cell. The CL is discussed in the following section, since this thesis is concerned with one of the key material components of CL.

2.1.2 Catalyst layer (CL)

PEFC CL is typically a 5-10 μm thick, porous nanocomposite of Pt/C catalyst (Pt supported on carbon nanoparticles) and an ionic polymer or ionomer. The platinum nanoparticles are 2-5 nm and are supported on ~ 30 nm carbon black particles. The ion-conducting polymer film coating these Pt/C particles are only a few nanometers (4-10 nm) in thickness (Figure 2.2) [22], [29]–[32]. The ionomer thin film facilitates the transport of protons to catalyst particles (e.g., Pt) where electrochemical reactions occur. Also, it helps in removing the produced water out of CL. To state simply, electrons conduct through the carbon to reach the external circuit, and oxygen and protons through the ionomer to access the surface of catalyst nanoparticles [31].

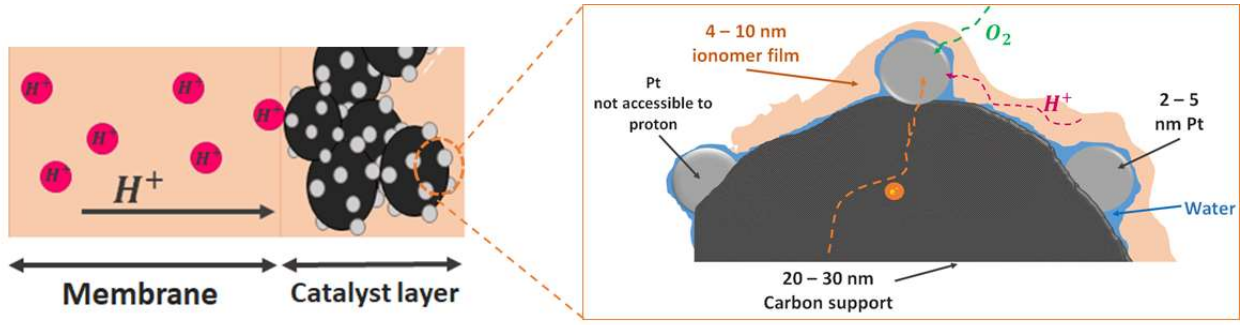

Figure 2.2. Schematic of fuel cell catalyst layer.

As mentioned earlier, the transport of protons, oxygen gas, and water take place in the ionomer thin film of cathode CL. The proton conduction through the ionomer film is highly dependent on water content of the ionomer. Any introduction of non-proton cation into the ionomer thin film during preparation or operations stages could also significantly affect the ion conduction through the ionomer. As a result of poor proton conductivity of the cation-contaminated ionomer, the performance of fuel cell can be adversely impacted due to poor access of catalyst sites by the

protons. A dense ionomer thin film would notably impact the local oxygen transport, because the oxygen diffusion through ionomer will be drastically constrained. Confinement and interfacial interactions are known to influence polymer thin film characteristics. There is now evidence that they also affect ionomer thin film properties (discussed later in section 2-3-1). All these facts evidently demonstrate the crucial role of the ionomer thin film in a CL. Driven by the need to - reduce cost, enhance performance, and increase durability, there is a considerable focus on the development of new materials as well as operations at elevated temperatures. However, integration of a new catalyst and catalyst support material or changes in operating conditions would require considerations of how the ionomer interactions with the new materials and operating conditions impacts its key functional property (proton conductivity). Availability of new ionomer materials has expanded the portfolio of ionomers permitting the selection of a suitable ionomer for new catalyst/catalyst support material or new operating conditions. Some of the key research developments and their impact on ionomer are summarized below.

2.1.2.1. Decreasing the Pt content in CL, for instance, using Pt – alloys catalyst

Significant efforts have been made to reduce the amount of the expensive Pt metal in CL by introducing Pt-alloys and core–shell type nanostructure catalysts (e.g., a cobalt core with a Pt shell) [33], [34]. However, it has been reported that the alloying metals such as Co and Ni leach out of the catalyst and migrate from the ionomer/catalyst interface to the CL ionomer and into the membrane [35]–[38]. These ions can exchange with protons in the ionomer and potentially impact the ionomer properties such as proton conductivity and water uptake [36], [37], [39], [40]. The extent to which these properties are affected by and how different the ionomers respond to metal leach-out are still unknown and not quantified.

2.1.2.2. Increasing the operating temperature of fuel cell up to 110 ˚C

High operational temperature (between 100 and 200 °C) would have several advantages over the low temperature condition (60 to 80 °C), as it helps in promoting the cathode kinetics, and improving heat management in the fuel cell. High temperature operation demands designing new ionomers with high conduction under low RH. Several new ionomers that are variations of fluorocarbon ionomer and, also, new hydrocarbon ionomers have become available in last five years. However, the RH dependent proton conductivity –which is correlated to fuel cell operating conditions– of these ionomers is not available, particularly for thin films of less than 50 nm. This makes data-driven ionomer material choice difficult [41].

2.1.2.3. Interaction of ionomers with supporting substrates

Carbon materials such as graphene or carbon nanotubes, which are carbon corrosion resistant are being considered as catalyst supports. Recently, Orfanidi et al have claimed that nitrogen-group functionalization of commonly used carbon black support, i.e. Vulcan Carbon, improves ionomer coverage of Pt/C and also induces changes in internal structure of ionomers [42], [43]. The interaction of ionomers with supporting substrates, which could contain different type of carbon, may affect ionomer properties (such as, proton transport and water content) but have not been studied [42], [44]

Clearly, understanding the behavior of the ionomer thin films – particularly, the impact of ion contamination arising from leaching of alloy metals of Pt alloy catalysts, humidity, and substrate on ionomer properties (such as proton conduction and water content) – is crucial for robust design and guidance of material selection for PEFCs. Next, the ionomer material commonly used in PEFCs is introduced.

2.1.3. Ion-containing polymer (Ionomer)

Ionomers belong to the class of ionic polymers. Ionomers were defined in 1970s by Eisenberg as polymers containing 10-15 mol% ionic groups are known as an ionomer [30], [45]. Generally, when we refer to the term "ionomer", we are concerned with the properties of the ionic polymer in solid state. The perfluorosulfonic-acid ionomers (PFSA) are the most widely employed ionomers for PEFC applications. PFSA ionomers are made of fluorocarbon chains tethered upon copolymer of poly(tetrafluoroethylene) (PTFE) with side chains ending with polar sulfonic acid ionic group, SO3H [30] (Figure 2.3). High thermal and chemical stability of their fluorinated backbone and the chemical nature of their side chains, i.e., the sulfonic group [46], made them a promising candidate for PEFC applications. Equivalent weight (EW) is commonly used to represent the degree of sulfonation in PFSA ionomers that is negatively correlated to the ion exchange capacity (IEC). In other words, EW decreases when IEC increases [31]. Nafion, 3M, and Aquivion are among the most common PFSA ionomers used in the industry. The differences in the structure of these ionomers are shown in Figure 2.3. The commonalities amongst these ionomers are Teflon backbone and sulfonic acid end group. On the other hand, the differences are in the side chain length and the composition of the side chain. Nafion was designed and developed by DuPont in the 1960s. Since then, it has been widely employed as a benchmark PEM in fuel cells.

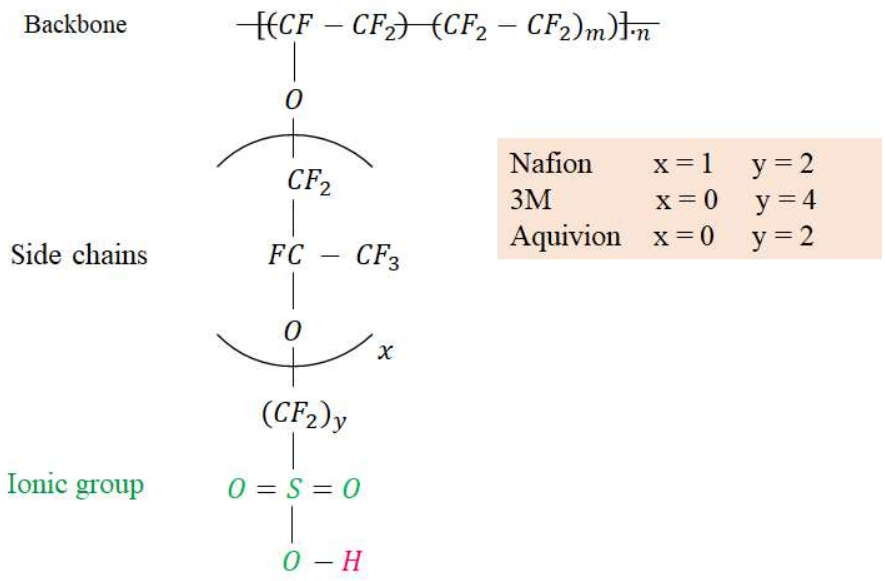

Figure 2.3. Chemical structure of PFSA ionomers.

2.1.3.1. Phase segregated morphology and hydration related properties of PFSA ionomers

Properties, structure, and functionality of ionomers are primarily dictated by their hydration-dependent nanostructure that can be categorized into hydrophilic transport pathways and hydrophobic polymer matrix [30], [31]. Electrostatic forces drive the aggregation of ion-pairs ($SO3^{-}$/H3O+) in dry conditions forming ionic clusters. These strong electrostatic forces also serve to cross-link the low-energy fluorocarbon backbones. When exposed to humid environment, the affinity of sulfonic acid for water results in hydration of the ionomer. The fluorocarbon backbones are hydrophobic and want to minimize their interaction with water. The extent of water sorption by ionomer at a given relative humidity is a result of the net chemical/mechanical force balance. The chemical forces are associated with the hydration of ions while mechanical force is imposed by the rigid backbone. The hydrated PFSA ionomer is known to have a well-defined phase-segregated structure comprised of water-filled ionic channels/clusters and water-free matrix. The

morphology of this phase segregation gives PFSAs their unique ion transportation characteristic [31].

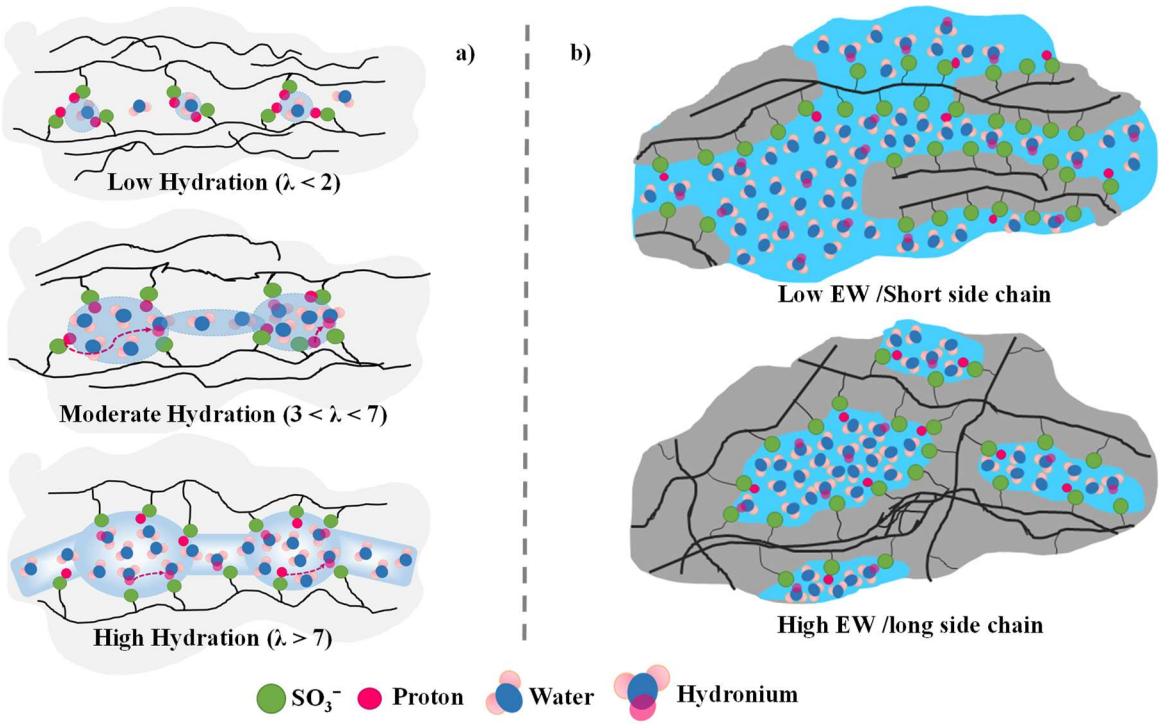

Figure 2.4. Schematic representation of cluster-network at a) different hydration level [47], [48], and b) different EW and side chain length [31].

Under dry conditions, where the water content λ (number of water molecules per sulfonic group) is less than 2.0, the sulfonic acid is not dissociated. Neither the protons nor the sulfonic group is fully hydrated. Fully hydrated proton (first shell) has 4 water molecules. The ionic clusters are also poorly connected. Both factors result in poor conduction at low water content (Figure 2.4a).

When the water content of ionomer increases ($3 < \lambda < 7$) due to exposure to humid environment, the small isolated ionic clusters start to grow in size. This results in the formation of

a percolating interconnected network of ionic clusters (Figure 2.4a). The hydration of the protons also leads to separation from the counter-ion and improved mobility of the protons. Thus, both enhanced mobility of protons (local effect) and better ionic domain connectivity dramatically increases the conductivity.

Further increase in water content ($\lambda > 7$) of ionomer through increasing RH, provides the hydrophilic domain with more water molecules enabling them to grow improving their connectivity. The protons and sulfonic groups are fully hydrated and separated from each other; i.e., sulfonic acid is largely dissociated resulting in a further improvement in the mobility. This enables the ions/protons to travel easier across the ionomer mainly because of the presence of free water molecules [30], [31] (Figure 2.4a).

The EW of ionomer and the length of its sidechains also impact its transport properties. Low EW ionomer simply implies that there is more acidic material within the fluorocarbon matrix. The length of the sidechain can be thought to affect the size of ionomer cluster. The ion-pair in ionomers with large side-chains, even if they are spaced apart, would be able to reach out to the ion-pair of another side-chain and cluster. Short-side chains will have steric inhibition in reaching out too far. Thus, the length of side chains and spacing between then would be expected to impact the size of cluster and thereby the distribution and connectivity of the ionic cluster. For these reasons, shorter sidechains and smaller EWs (i.e., shorter backbones) result in better connectivity, since water forms better dispersed domains. This leads to the formation of less tortuous transport pathways. However, in ionomers with longer sidechains and higher EWs (i.e., longer backbones) it can be hypothesized that the water forms larger but disconnected domains. This would result in

the formation of more tortuous transport pathways and correspondingly to inferior connectivity especially at low water content [49]–[51] (Figure 2.4b).

When the thickness of ionomer decreases, especially to the length scale of less than 50 nanometers, the confinement effect (discussed in more detail later in this section) could significantly impact the ionomer response (more specifically, the phase segregation) to changes in RH, EW, and sidechain lengths.

Water content (λ): This parameter defined as the number of water molecules per sulfonic acid group quantifies the local water accessible by the acid group sites. It increases monotonically with the humidity of the environment, i.e., RH (Figure 2.5).

As discussed above, water content affects the effective concentration of mobile protons and their mobilities through controlling the extent of sulfonic acid dissociation and the dilution of protons. The connectivity and tortuosity of the water corridors in the hydrophilic domains of ionomer, indeed, affect the long-range proton transport. Therefore, quantifying the water content of ionomer would significantly help us in understanding how proton conduction is correlated with ionomer structure (Figure 2.5) [30].

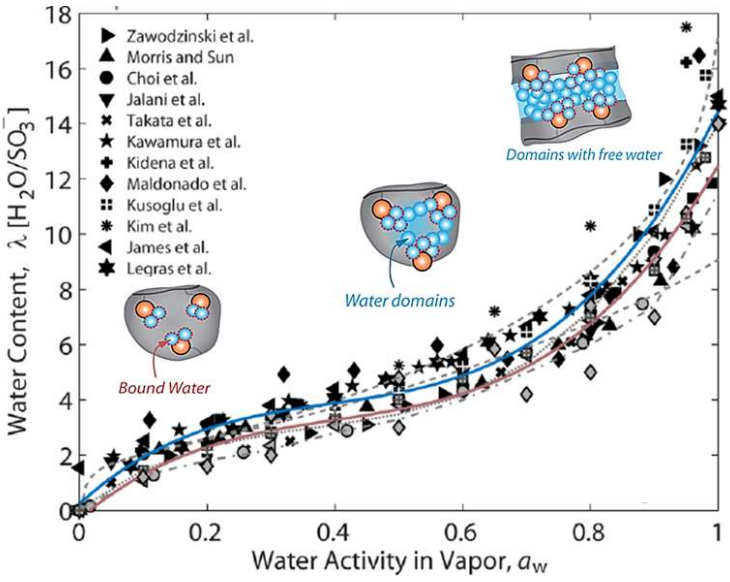

Figure 2.5. Nafion membrane water content as a function of water activity reported by different groups with schematic representation of different states of water. Reprinted from [31] with permission.

Proton conductivity is the most important functional property of ionomers for use in polymer-electrolyte- based electrochemical devices. It is primarily controlled by water content, which in turn is affected by the environmental relative humidity. Strong affinity of sulfonic acids for water is the driving force for initial sorption of water to dry ionomers [30], [52].

Ionomer proton conductivity (σ) is a function of various parameters: proton mobility (μ_{H^+}), concentration of charge carrier (C_{H^+}), and structure of the ionomer thin film – defined as an unknown function of porosity (φ_w) and tortuosity (τ_w) – . It is represented by the following equation:

$$\sigma = (\mu_{H^+})(C_{H^+})f(\varphi_w, \tau_w) \tag{2.4}$$

Any change in these factors may result in an increase/decrease in proton conduction of ionomer. The proton mobility depends on water environment, while the concentration of charge carrier is fixed for a given ionomer, as it depends on the number of counterions (SO_3^- groups) on the ionomer backbone. The lower the equivalent weight of ionomer, the higher number of sulfonic groups for given mass of ionomer it has. This corresponds to having more protons [53]–[56].

When the water content is low ($\lambda < 2$), the sulfonic acid groups do not dissociate. Thus, the hydronium ions stay bound exhibiting significantly low mobility and conduction occurs primarily by vehicular mechanism. By increasing the water content to intermediate levels (λ = 2-8), the sulfonic groups dissociate but the protons stay close to the sulfonic groups. Within an ionic cluster, there may be sufficient water to form a connected network of water. If the clusters are also connected, then proton conduction both within a cluster and between the cluster could occur by Grotthus hopping, wherein protons transit via hydrogen bonding in the surrounding water molecules. At high water content of λ>8, complete dissociation of sulfonic groups occurs, and the produced hydronium ions get distant from the sulfonic groups. The protons are highly mobile and there is connected network of water molecules. This ensures proton conduction to occur via Grotthus hopping mechanism [57]–[59].

2.1.3.2. Influence of confinement and contamination on hydration related properties of PFSA ionomers

Thickness effect. Thickness of ionomer films could significantly alter the properties of ionomers. For studies of non-ionic polymers, we know that when the thickness of polymer film tends to the characteristic length of its polymer-chain, its structure and properties can begin to deviate strongly from that of the bulk material. This thickness dependency of polymer thin film

properties is generally described as confinement effects [60]. These effects in thin film ionomers could originate from either the interactions between polymer and substrate [61] or the preferential orientation of the polymers on the substrate. Similar behavior can be expected for ionomers. Thus, although the PFSA ionomer, or more precisely Nafion ionomer, has been extensively studies in its bulk form, its structure and properties, especially those relevant to fuel cells cannot to be extrapolated to thin film form [62].

Very little was known about PFSA ionomer thin film properties a decade ago. In fact, there was little discussion or questions raise about whether ionomer thin films would exhibit significantly different characteristics than its bulk form. The intense research over the past 7-8 years, including those by Karan group has now conclusively established that the ionomer thin films have significantly different properties than their bulk counterpart [30], [31]. It is now known that once the film thickness reaches below 100 nm, a strong interplay between the confinement and substrate interactions controls the ionomer's nanostructure (such as ionic domain size, and backbone and side chain orientation) and properties (such as water uptake and proton conduction). As the film thickness approaches 10s of nanometers, i.e., comparable to CL ionomers, the impact of substrate interactions becomes even more dominant. Thus, in the thin-film regime, ionomer properties significantly deviate from those of the bulk form (i.e., PEM), and the magnitude of these deviations depends on the substrate and the operating conditions (e.g., RH and temperature). It is reported that the ion conductivity of thin-film ionomer could drop by $1/7^{th}$ compared to the bulk ionomer for planar electrodes [63]. Similar behavior is also observed for water uptake, swelling dimension, and transport properties of thin-film ionomer [54]. These changes in properties of thin-film ionomer are mainly attributed to thickness, polymer-substrate interactions, and structural changes [63]. Lower proton conduction than the bulk films primarily due to confinement effects

has been observed for Nafion thin films [27], [54], [64]. Nafion thin films (less than ~100 nm) showed lower swelling [65], [66], water uptake amounts (Figure 2.6b) and rates[65], [67]–[69], ionic conductivity (Figure 2.6a), water diffusion [53], [70], and contact angles [53], [70]. Further, different groups have reported different properties. While Karan group had reported RH-dependent proton conductivity, they did not report water content. Other groups reported water content but did not study the proton conduction characteristics. Furthermore, the effect of materials parameters such as ionomer type and substrate have not been systematically studied, making it difficult to develop a generalized understanding of how these parameters affect hydration properties.

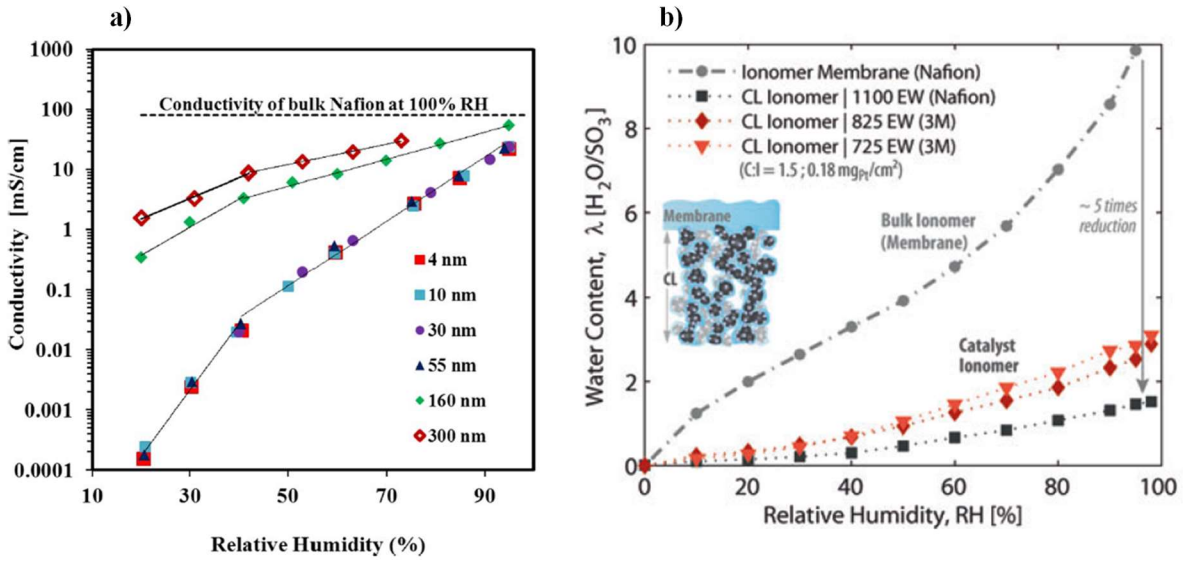

Figure 2.6. (a)Proton conductivity of the Nafion nano thin films, of various thickness ranging 4 nm to 300 nm, at 25 ◦ C as a function of RH, reprinted from [65] with permission,(b) comparison of water uptake behavior of catalyst layer (CL) ionomers (measured without the membrane). Reprinted from [31] with permission.

Cation contamination. As discussed earlier, significant effort has been directed towards the reduction of the cost of PEFCs through decreasing the amount of expensive Pt in the metal-based catalyst. To this end, both non-Pt group metal and low-Pt content alloy catalysts have been explored [29], [71]. Innovative approaches in alloying Pt with transition metals (such as Co, and Ni) resulted in designing new electrocatalysts with activities close to those of pure Pt catalyst [71]–[73]. The world's first serially produced commercial fuel cell vehicle, Toyota Mirai utilizes Pt-Co catalyst [19], [22], [35]. Although significant cost reductions have been achieved using Pt-Co/Ni as a catalyst, but the performance losses became more pronounced because of Co/Ni loss and migration to membrane. As a consequence of Pt-Co/Ni degradation [35]–[37], [74], the metal cations (Mn+) migrate from catalyst to thin film ionomer and ionomer membrane primarily because they have higher affinity towards sulfonate ($SO3^-$) end groups than H+, as depicted in Figure 2.7. For this reason, the effect of cation contamination/exchange on the properties of membrane has been received significant attention from industry researchers over the past decade.

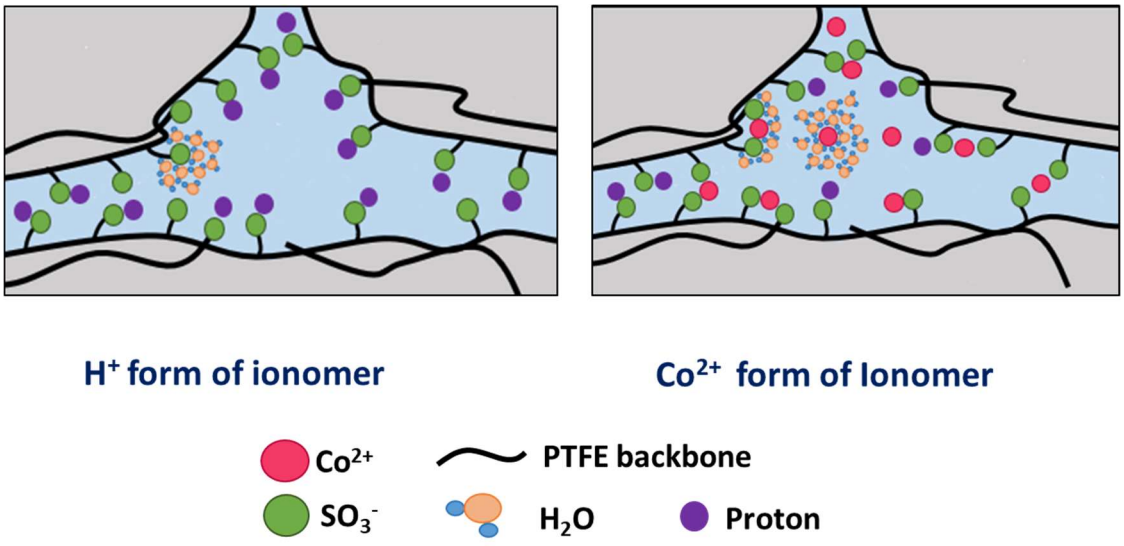

Figure 2.7. Schematic of hydrated ionomer morphology in H^+ and Co^{2+} forms.

It is evident that exchange of cations (such as, $Co^{2+,}$ Na^{+}, Li^{+}, K^{+}, Cs^{+}, Ca^{2+}, Ni^{2+}, Fe^{3+}, Al^{3+}, etc.) had a severe effect on the performance and durability of the PEFC due to significant decrease in conductivity of the membranes [75]–[80]. Metal cation contaminants have shown to replace protonic sites, reduce transference number of conductive species, lower ionomer/membrane conductivity [79]–[81], and hinder oxygen-reduction reaction [39], [76], [82], [83]. Mitigating these negative impacts is of critical importance to meeting durability and lifetime requirements of PEFCs for market purposes [84]. In bulk PFSA ionomers, metal cations impact water sorption, conductivity, gas-transport coefficients, density, mechanical properties, and morphological structure [81], [85]–[88] Therefore, it is expected that metal cations impact the properties of ionomer thin films.

Although, there is a tremendous amount of literature on the effect of cation-exchange on the membrane properties (such as water uptake and ion conductivity), there are only limited exploration of the effect in nano-thin film ionomers. Hence, this work first aims at quantifying the impact of cation contamination (specifically Cobalt) on the hydration properties of nano-thin film ionomers.

2.2. Research gaps, goals, and approach

Considering the combination of material (EW, substrate type, cation contaminant), processing (annealing) and operational parameters (temperature, humidity), it is evident that there is a gap in quantitative data on how relevant hydration properties – water content and proton conduction are affected by these parameters. Arising from the lack of these data is the limitation of providing any CL material selection and processing guidance or understanding the impact of operational parameters on hydration properties. The lack of correlative data set, e.g., water content

as a function of RH and conductivity as a function of RH, on similarly prepared ionomer films prevents to support or deny any hypothesis on why ionomers of different thicknesses or material type exhibit different proton conductivity at a given operating conditions (temperature and RH). If an ionomer exhibiting low conductivity is also found to have lower water content, we can explain that the conductivity suppression is due to water content. The lack of correlative data set also precludes developing and testing hypothesis on the underlying reasons for any observed differences in proton conductivity – e.g., whether the mobility or the structural parameters (see equation 4) play any roles or not.

Research goals. The overall goal of the proposed research is to develop an improved understanding (through quantitative data acquisition) of the impact of selected material and processing parameters on the hydration properties – water content and proton conduction - of ionomer thin films. Since, the parameter space is large, films of only 2-3 film thickness and data at temperatures relevant to fuel cell operations will be studied. To attain the broader research goal, four sub-tasks discussed below will be undertaken:

i) Quantifying the effects of equivalent weight (EW) and side-chain characteristics of ionomer on the water uptake and proton conductivity (as a function of RH).

ii) Quantifying the effects of cation-exchange on the water uptake and proton conductivity (as a function of RH) of thin films of ionomers differing in molecular structure or EW.

iii) Quantifying the effects of different substrates on the water uptake (as a function of RH).

iv) Quantifying the effects of humidity cycling on the water uptake and it's kinetic in ionomer thin films (as a function of RH) .

Chapter Three: Experimental Techniques

This chapter presents the basic principle underlying each of the experimental techniques common to data collection in Chapters 4, 5 and 6. Specific information for experimental details for a particular chapter are provided in each chapter as needed.

3.1. Characterization techniques

3.1.1. Electrochemical Impedance Spectroscopy (EIS)

Electrochemical Impedance Spectroscopy (EIS) is a powerful technique that has been known to the electrochemistry community for more than a century. Electrochemical impedance spectroscopy (EIS) was carried out with a potentiostat. A small magnitude 10-100 mV sinusoidal voltage signal is applied to probe the impedance characteristics of a cell. Conductivity measurements were carried out on ionomer films coated on interdigitated array (IDA) of gold electrodes by following the approach described in earlier papers of our group [53], [56], [68], [89]. Briefly, impedance is measured on the ionomer films on IDA (Au electrode on SiO_2 substrate consists of 110 teeth with 100 μm gap between each teeth, shown in Figure 3.1, using two – microprobe applying AC voltage to the interface to measure the response, i.e., the impedance of the system.

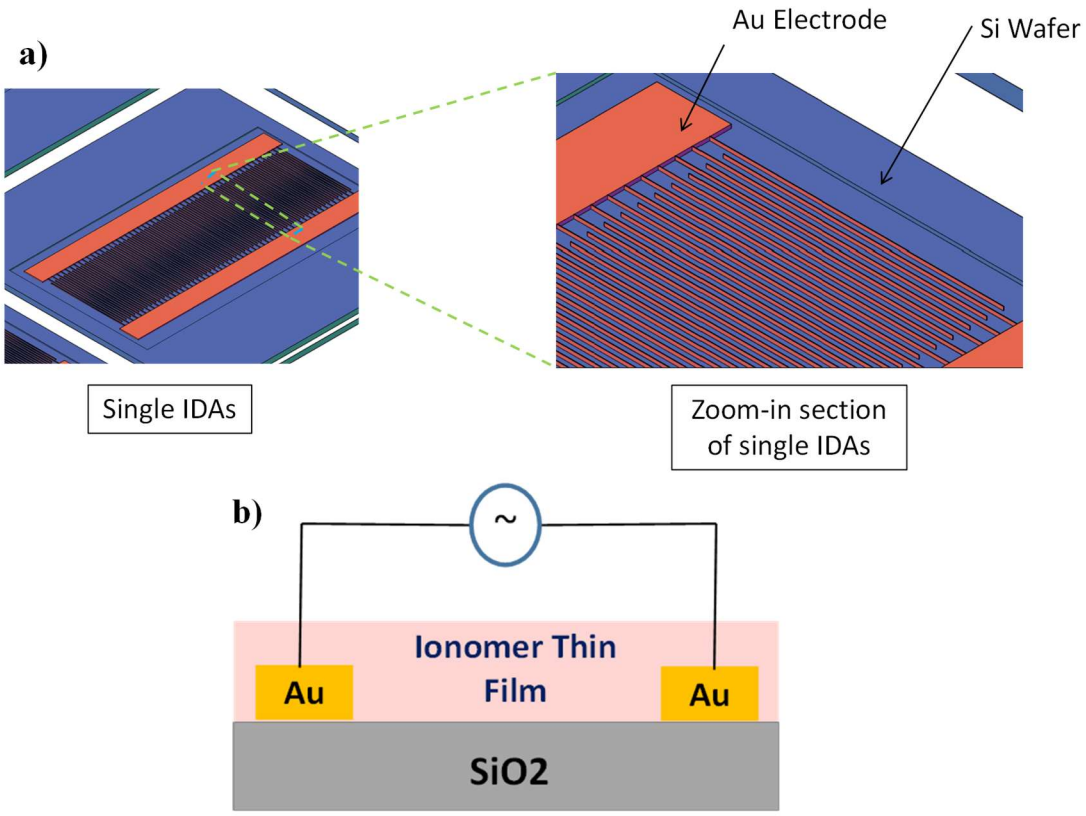

Figure 3.1. a) IDA of Au electrode supported by SiO2 terminated wafer. b) schematic representation of Nafion nanofilm on SiO2 supported IDA gold electrode. Gray/dark blue color represents SiO2, golden color represents Au electrode and light pink represents Nafion thin film.

In this work, the AC signal (100 mV) is applied over a wide range of frequencies (10 MHz to 0.01 Hz) to generate an impedance spectrum for the electrochemical cell under test. Z-view impedance software (Version 3.0a, Scribner Associates Inc.) was used to fit and analyse the equivalent circuit model to data.

The typical impedance response of ionomer thin films consists of a semicircle (at high frequency) and a vertical like line (at low frequency) (Figure 3.2 a) [65]. The impedance response of 10 nm Nafion film at different RH measured at 60 C have been presented in Figure 3.2 b [65]. The main goal of impedance measurement is to find the proton transport resistance in ionomer thin

films. Hence, an equivalent circuit model is fitted to the impedance response to extract the proton transport resistance of thin films. Figure 3.2 shows the equivalent circuit model that we used in this work.

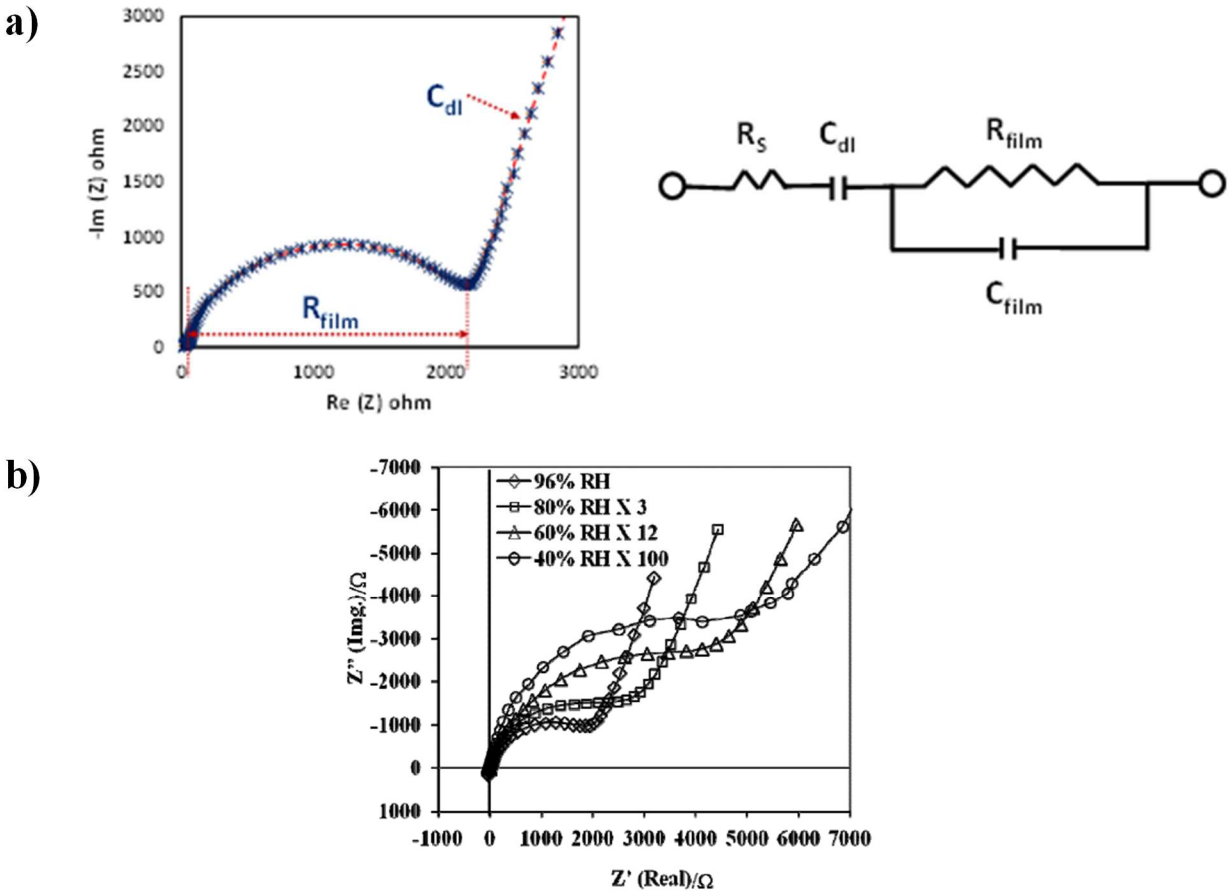

Figure 3.2. a)Typical impedance plot of Nafion thin film and the fitting with equivalent circuits. R_{film}, C_{film}, C_{dl}, and RS represent thin film resistance, thin film capacitance, double layer capacitance and serial resistance respectively. b) Nyquist impedance plots for 10 nm Nafion® film at 60 °C and different RH, reprinted from [65] with permission.

Nyquist plot is used to visualize the Impedance data. In this plot, the y-axis shows the imaginary part, and the x-axis is the real part. Starting from the origin of the plot, where the frequency is high, the frequency decreases as we move away from it. The observed semi-circle can be simply

modelled through defining an equivalent circuit of two parallel capacitor and resistor (Figure 3.2). This will enable us to find the absorbed film resistance R_{film}, as R_{film} is simply the diameter of the observed semi-circle. Using the measured Rf, then, one can calculate the film conductivity as follows [31]:

$$Conductivity\ \sigma_{film} = \frac{1}{R_{film}} \frac{d}{l\ (N-1)t} \tag{3.1}$$

where L, d, and N are the length, spacing, and number of teethes on the IDA, and t is the film thickness. More information could be find in Karan group papers [65].

Impedance measurement for this thesis: In this thesis, EIS was employed for film proton conductivity measurement. A two micro-probe setup connected with Biologic SP-200 potentiostat has been used for impedance measurement. Z view software has been used for data interpretation and model fitting.

3.1.2. Variable Angle Spectroscopy Ellipsometry (VASE)

Ellipsometry is one of the most widely used tools for measuring the optical properties, thicknesses of thin films with thicknesses ranging from a few nanometers to micrometers and roughness of the films. To simply describe the main principal underlying this technique, Ellipsometer composed of a light source which sends elliptically polarized light to the object under study. As these polarized light travels through the object, it can be reflected, diffused, transmitted, and scattered (Figure 3.3). The reflected and transmitted light from the object will then pass through a rotating polarization state analyzer. The light that is already elliptically polarized in analyzer will reach the detector. The detector converts those light into electronic signals and stores them as a function of the rotation angle (α). By comparing the output polarization from detector

with the original one from the light source, one can measure the changes in polarization, and extract the parameters.

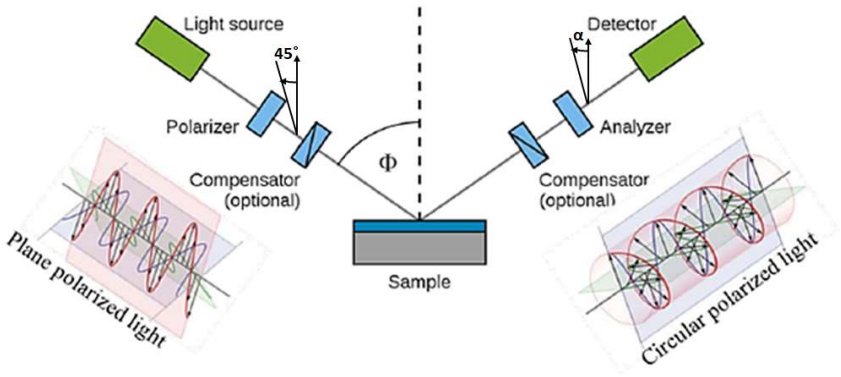

Figure 3.3. Typical Ellipsometry configuration [90].

Ellipsometry measurements were carried out using a VASE Ellipsometer (J. A. Woollam Co., Inc., USA). All the parameters like thickness, refractive index of the ionomer and other physical parameters can be acquired by fitting phase shift (difference) (Δ) and amplitude ratio upon reflection (tan (Ψ)) with different physical model using the WVASE32 software. The model used Frensel's equations to calculate a prediction of response (Equation 3.2). The calculated parameters are compared with the experimental results and the best fit is chosen based on an estimator like Mean Squared Error (MSE) (Figure 3.4). Using the true model would give us the best values for parameters like film thickness, roughness and optical parameters (i.e., refractive index).

$$\frac{r_p}{r_s} = \tan\Psi \; e^{-i\Delta} \tag{3.2}$$

Where r_p and r_s are intensities of the reflected light that are polarized in the plane and polarized perpendicular to the plane, respectively.

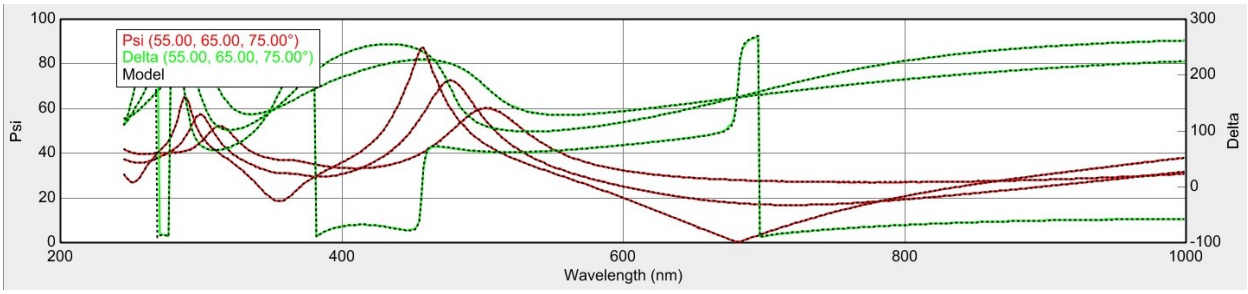

Figure 3.4. A sample of Variable Angle Spectroscopic Ellipsometric (VASE) data and a fitting model for a ~12 nm Nafion film on SiO_2 substrate.

Figure 3.5 shows the process of data analysis in Ellipsometry.

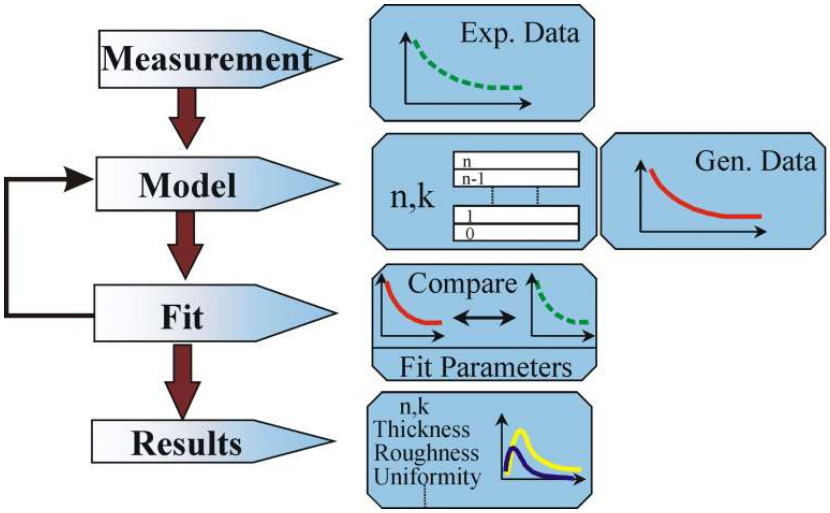

Figure 3.5: Flowchart of Ellipsometry data analysis [89].

Ellipsometry measurement conduced in this thesis: Ellipsometry has been used to investigate the thickness, the optical parameters, homogeneity and roughness of the films. All the experiments carried out in a controlled temperature and relative humidity using a built-in chamber in Ellipsometry. Ellipsometry measurements were carried out using aVASE Ellipsometer (J. A. Woollam Co., Inc., USA). The resulting Ψ and Δ spectrum was fitted with different physical model using the WVASE32 software setting a number of fitting parameters including thickness, surface roughness and optical constant. The difference in the thickness of the ionomer at a specific temperature and relative humidity and the thickness at same temperature but 0% RH yields the

swelling. The swelling data was converted to water content, λ, i.e., the number of the water molecules per acid groups of the ionomer is calculated [69], [81] according to the following equation:

$$\lambda = \frac{mol\ (H_2O)}{mol\ (SO_3)} = \left(\frac{m_{RH} - m_0}{m_0}\right)\left(\frac{EW}{M_{H_2O}}\right) = \frac{(h_{RH} - h_0)}{h_0}\left(\frac{EW}{M_{H_2O}}\right)\left(\frac{\rho_{H_2O}}{\rho_{ionomer}}\right) \quad (3.3)$$

where, EW is the equivalent weight of the ionomers in g/mol, M_{H2O} is the molecular weight of water which is 18.01 g/mol, ρ_{H2O} is the density of water (g/cm^3), $\rho_{ionomer}$ is the density of ionomer (g/cm^3), h_0 is the thickness of the ionomer thin film at dry condition and h_{RH} is the thickness of film equilibrated at a specific RH.

3.1.3. Quartz Crystal Microbalance (QCM)

Quartz Crystal Microbalance (QCM) has been used to investigate the water uptake in ionomer thin films. QCM is a kind of crystal oscillators that used to detect properties change (Mass changes) of films applied to the quartz sensor surface. The QCM device detect changes using frequency change of quartz crystal as a result od applied electrical potential.

The mass change detected on the surface of the crystal is calculated using the change in frequency (Δf) . QCM can measure mass changes between ng/cm^2 to 100 μg/cm^2. Mass detected can be given by the saurberry equation (Equation 3.4) which assumes that any additional film deposited on the crystal has same acousto-elastic properties as the quartz. This assumption has been shown to be sufficient for uniform, rigid, thin film deposits.

$$\Delta m = -\frac{\Delta f}{C_f} \quad (3.4)$$

where, C_f is a constant that depends on the property of the crystal used. For example, for a 5 MHz AT-cut quartz crystal at room temperature, C is approximately equal to 17.7 ng/(cm$_2$·Hz). This

means that the addition of 17.7 ng/cm^2 of mass on a 5 MHz quartz crystal causes a frequency change of 1 Hz.

In this work, Au coated QCM have been used and the thin film was coated uniformly using spin coater. The schematic of frequency changes in QCM is shown in Figure 3.6. To measure the mass associated with water taken up by ionomer, damped resonant frequency associated with ionomer coating has to be separated from depression in frequency associated with water uptake. As a result, mass of water absorbed has is referenced from both unloaded bare crystal frequency as well as dry ionomer coated frequency. Amount of water taken up by ionomer can be calculated via:

$$Mass\ uptake = \frac{m_{RH} - m_{dry}}{m_{dry}} = \frac{\Delta f_{RH} - \Delta f_{dry}}{\Delta f_{dry}} \tag{3.5}$$

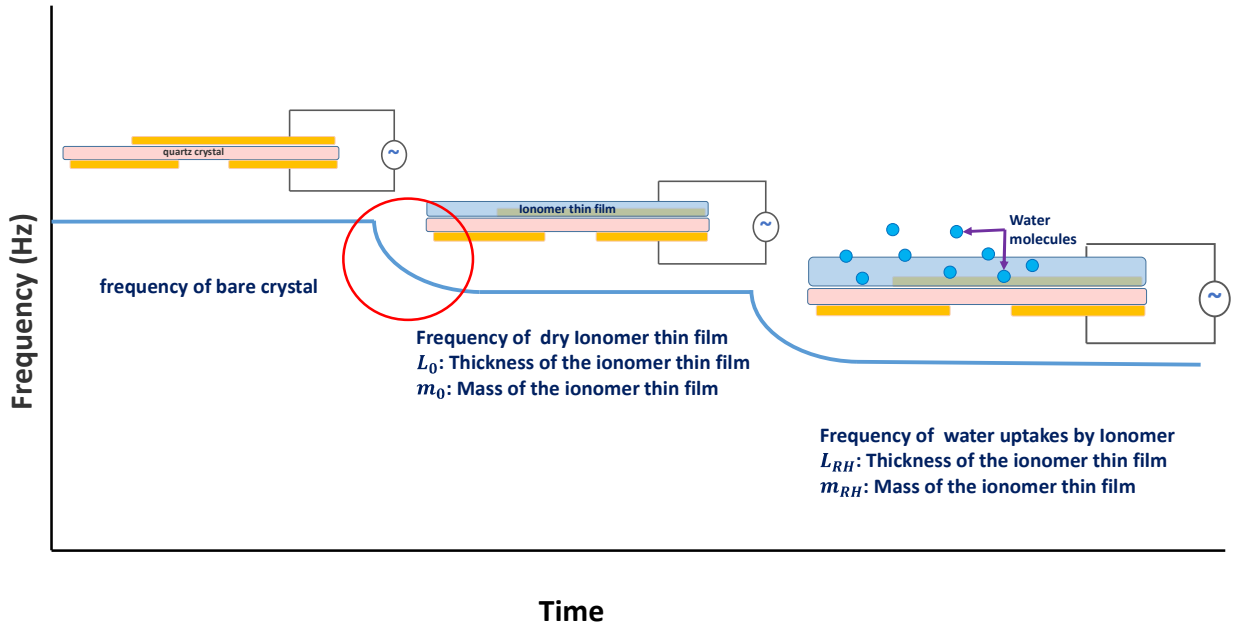

Figure 3.6:Schematic representation of frequency change for quartz crystal in different states – uncoated crystal to coated crystal followed by slow decrease during water sorption.

QCM measurement for this thesis: QCM measurements technique has been used for water uptake measurements via mass change and investigating the kinetics of water sorption in ionomer thin films. The QCM200 — 5 MHz QCM (SRS Stanford research system, USA) equipped with its Data Acquisition Software has been used for all the experiments.

Chapter Four: Humidity-Dependent Hydration and Proton Conductivity of PFSA Ionomer Thin Films at Fuel-Cell-Relevant Temperatures: Effect of Ionomer Equivalent Weight and Side Chain Characteristics

This chapter has been reproduced from "Humidity-Dependent Hydration and Proton Conductivity of PFSA Ionomer Thin Films at Fuel-Cell-Relevant Temperatures: Effect of Ionomer Equivalent Weight and Side-Chain Characteristics", ACS Appl. Mater. Interfaces 2022, 14, 45, 50762–50772, doi:10.1021/acsami.2c12667, with the permission from ACS (American Chemical Society). Dr. Devproshad K. Paul (Ballard Power Systems Inc) and Dr. Alan P. Young (Ballard Power Systems Inc) are the co-authors in the manuscript.

4.1. Introduction

Polymer electrolyte fuel cells (PEFCs) have gained significant interest in the recent years for transportation, materials handling, and stationary applications [94]. There is a continued demand for a further improvement in their performance and a reduction in their cost. Both of these technological goals for PEFCs are linked to the catalyst layers [95]. For cost reduction, high activity catalyst that are also durable are being explored [96], [97]. For performance enhancement, in addition to the efficient electrochemical kinetics of the oxygen reduction reaction, facile transport of species in the catalyst layer (CL) must be considered. This is because the technological goal for performance is to achieve higher current density at higher cell potential [98]. Higher current density implies high flux of all the reactants to and the products from the catalyst sites. For

PEFC cathode catalyst layer (CCL), this translates into the transport of oxygen, protons, and electrons to the catalytic site and of produced water away from the site. The material properties (e.g. conductivity) and catalyst microstructure (e.g. porosity, tortuosity) must be chosen and/or designed to minimize the higher gradients in the pertinent potential associated with quantity being transported, e.g. concentration of oxygen, and ionic potential of proton conducting phase, to minimize transport losses.

The conventional PEFC CL is a 5-10 μm thick nanoporous, nanocomposite comprising supported platinium or platinum-alloy catalyst and ionomer [29]. The Pt or Pt-alloy nanoparticles are 2-5 nm in diameter and are supported on a larger carbon black particles (~ 30 nm diameter). The ionomer forms an ultrathin coating (7-15 nm) on the aggregates of Pt/C particles and is often considered as a binder (Figure 4.1) [22], [29]–[32]. However, in addition to binding the Pt/C powder the ionomer serves many critical functionalities that impacts the performance of a CL. The most important role of the ionomer thin film is to facilitate the transport of protons to catalyst particles (e.g., Pt) where electrochemical reactions occur. It also ends up as a medium through which the gaseous oxygen reactant in the cathode catalyst layer must be transported from the pore to the reaction site, i.e. the Pt catalyst/ionomer interface. For high current density operations, facile transport of all these species must be ensured in the catalyst layer. New ionomer materials increase our access to a wide range of ionomers for designing catalyst layers made with new catalyst/catalyst support material and specific operating conditions such as low relative humidity operations.

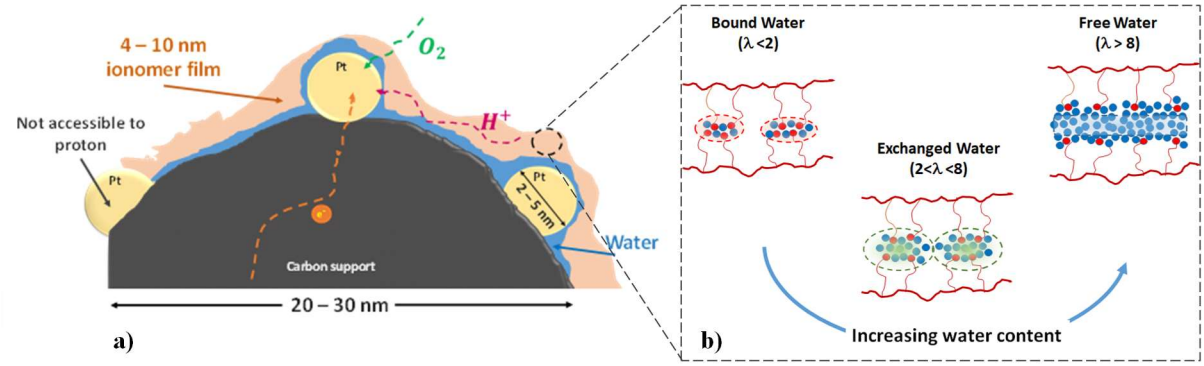

Figure 4.1. Schematic representation of (a) highly localized structure of the PEFC catalyst layer, (b) different states of water in ionomer thin film, reprinted with permission from [30]. Copyright 2019 American Chemical Society.

Perfluorinated ionomers, Nafion, 3M, and Aquivion, are commercially available and have been employed for catalyst ink formulation used for catalyst layer fabrication. The commonalities in these ionomers are the fluorocarbon, the Telfon-like backbone, and the sulfonic acid end group of the side chain. On the other hand, the differences between these ionomers arise from the differences in the length, composition, and average inter-side-chain distance of the side chains. Perfluoro imide acid (PFIA) is a new ionomer with a side-chain structure different from the classical perfluorinated sulfonic acid (PFSA) in that there are two protogenic groups in the side chain: the terminal sulfonic acid and the imide group in the middle of the side chain [99]. The aggregated effect of these differences may appear in the ionomer equivalent weight (EW), defined as grams of polymer per mole of the acid group. Whereas EW offers a quick measure of the acid content of the ionomer (low EW has high acid content and vice-versa), the structural differences induced by the differences in the side-chain characteristics is not captured by a single parameter. Whether such structural differences significantly impact the key functional property of the ionomer - its proton conductivity - remains unquantified for these material in thin film form.

Two ionomers may have the same EW but may vary in side-chain length or in side-chain interspacing. However, these differences may have different impact on the ionic cluster size and the mechanical strength of the hydrophobic matrix. These two properties have been identified as key factors influencing the water uptake in ionomers. Since, the hydration level of ionomer impacts several transport properties, it is important to study the influence of ionomer structure on its hydration behavior and its proton conductivity.

Only a few studies have investigated the effect of ionomer EW and sidechain structure on the cathode catalyst layer (CCL) and membrane properties [100]–[104] . In an early study, Buchi et. al reported O2 permeation in ionomer membranes of different EW ranging 1200 to 880 [105]. Recent studies have revealed a better picture of the effect of using low EW and short side-chain (SSC) ionomers on performance of the fuel cell. It has been shown that using SSC ionomer even when using lower amount of ionomer in CL (e.g. from 30% of Nafion to 20% of SSC ionomer) [106], [107] the performance of the fuel cell improved at operating condition of high temperature (>95 oC)and low relative humidity (< 50 %RH) [102], [106]–[110]. Several studies have investigated the impact and benefits (higher water uptake, proton conductivity and fuel cell performance improvement) of using low EW and SSC ionomers in CL and membrane for operations at high temperature (>95 oC) and dry condition (< 70 %RH) [50], [102], [104], [106]–[111]. Only a few works have studied the effect of EW and side chain structure (Nafion®, 3M PFSA and DOW ionomer) on morphology, water uptake, conductivity and other transport properties in the membrane [50], [51], [67], [110], [112]–[116] and thin film form [67], [112]. However, most of these studies have reported data at low temperatures, typically room temperature.

In summary, the properties of low-EW and SSC ionomers in the thin-film form pertinent to CL of ionomers and at fuel cell operating conditions (80 °C and a wide range of RH values) covering a wide range of ionomers with different side-chain structures and different EWs are not available. Specifically, the water content and proton conductivity data at fuel-cell-relevant temperatures are scarce. Also, the correlation between water content and proton conductivity is missing under fuel-cell relevant conditions and at any temperature. Hence, this study fills these gaps via reporting the hydration and proton conduction properties at 80 °C over a wide range of RH values (0−90%) to assess how strongly EW impacts these properties and whether a universal correlation between water content and proton conduction exists. A majority of experiments were carried out for ionomer films of a nominal thickness of 30 nm. This thickness is higher than the 7−15 nm thickness observed in catalyst layers but is amenable for fabricating films reproducibly for both water uptake and conductivity measurements. Selected experiments with thinner (10 nm) and thicker (80 nm) films were also carried out.

4.2. Experimental

4.2.1.Materials

Ionomers with different equivalent weight (EW) and side chain structure, depicted in Figure 4.2, were used: Nafion EW1100 (long side chain (LSC) PFSA); 3M PFSA EW1000, EW825, EW725 (medium side chain (MSC) PFSA); 3M PFIA EW620; Aquivion PFSA EW980 and EW830 (short side chain (SSC) PFSA). Nafion dispersion (EW1100) was obtained from Ion Power Inc. (USA) whereas the other 3M PFSA (EWs of 1000, 825, and 725) and PFIA (EW of 620) ionomers were provided by 3M Fuel cells Component Group, MN, USA and Aquivion ionomers (EWs of 980 and 830) were provided by Solvay.

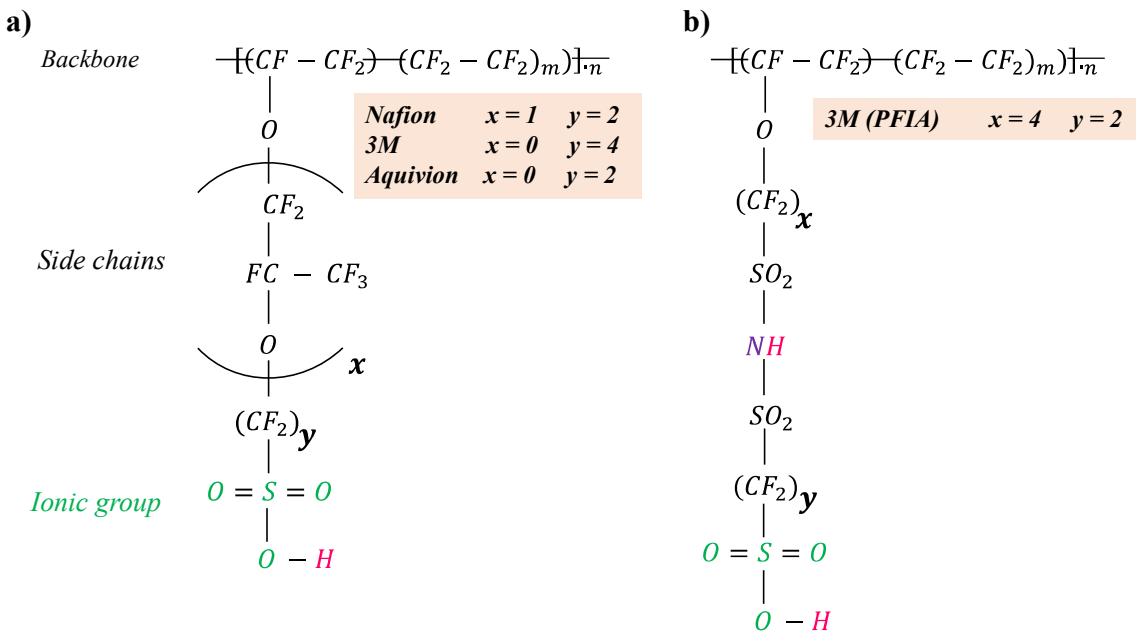

Figure 4.2. Chemical structures of (a) PFSA and (b) PFIA ionomer. The differences in the molecular structures of Nafion, 3M and Aquivion ionomers is denoted with specified values of x and y.

4.2.2. Thin film preparation and characterization

Thin films of 30 nm nominal thickness were prepared using spin coating. For preparation of ionomer thin film, the desired ionomer dispersion (1 wt%) were made by adding isopropyl alcohol to the stock ionomer dispersion. The diluted dispersion was ultrasonicated for 15 min and then placed at room temperature for 24 hours for equilibrating under ambient condition. Before spin coating, the dispersion was ultrasonicated for 10-15 min to make sure that the dispersion is homogenous and ready to use. The prepared dispersion was used to spin coat (at 5000 rpm and for 30 sec.) on the substrate.

For swelling experiments, films were coated on SiO_2/Si wafer whereas for conductivity measurements films were also coated on SiO_2 wafer but with interdigitated array (IDA) of gold

electrodes. The procedure to fabricate IDA electrodes can be found somewhere else [53], [56], [68], [69]. The spin-coated samples were kept in vacuum oven (22 mm of Hg or 2.93kPa) at 40℃ for 24 hours to dry out and make them ready for next steps. The film thickness was measured using M 2000 Ellipsometer (J. A. Woollam Co., USA) at different spot on the surface of the sample and they were around 30 ± 2 nm.

4.2.3. Conductivity measurement

Conductivity measurements were carried out on ionomer films on IDA electrodes by following the approach described in earlier papers from our group [53], [56], [68]. Briefly, impedance spectroscopy measurements on the films coated on IDA were performed using two microprobes connected to a SP - 200 potentiostat (Bio - Logic Science Instrument, USA). Electrochemical impedance spectroscopy (EIS) data modeling was perfomed using the analysis tool, Z Fit, in the EC-Lab Software. An environmental chamber (Model: MCB-1.2, CSZ products LLC., USA) was used to control relative humidity (RH) and temperature. A combined humidity and temperature sensor (EK-H4 Model, CMOSENS Tec., Switzerland) was utilized to monitor the local temperature and RH by placing the sensor near the sample.

4.2.4. Swelling measurement

The swelling of thin films at each humidity was determined by measuring the change in the film thickness at given RH compared to its thickness at zero humidity (i.e., dry film). A custom-built environmental chamber, capable of controlling temperature and humidity combined with M 2000 Ellipsometer (J. A. Woollam Co., USA) were employed to measure the thickness of thin film at various RHs. The details of the setup are provided elsewhere [69], [117].

For swelling calculation, a sample was first kept at dry conditions (i.e., RH of 0% in the environmental chamber) for more than 2 hours and the dry thickness (h_0) of the ionomer thin film was determined. Next, the RH of the system was increased in the increments of 20 up to 80% and finally to 90% RH. The sample was maintained at each RH for approximately half an hour to make sure that the system is equilibrated completely ($\Delta h / h_0 < 0.05\%$ per min). At the end, RH of the system was set to the 0% RH to let the film go back to dry state again.

The swelling data was converted to water content, λ, i.e., the number of the water molecules per acid groups of the ionomer is calculated [69], [81] according to the following equation:

$$\lambda = \frac{mol\ (H_2O)}{mol\ (SO_3)} = \left(\frac{m_{RH} - m_0}{m_0}\right)\left(\frac{EW}{M_{H_2O}}\right) = \frac{(h_{RH} - h_0)}{h_0}\left(\frac{EW}{M_{H_2O}}\right)\left(\frac{\rho_{H_2O}}{\rho_{ionomer}}\right) \quad (4.1)$$

where, EW is the equivalent weight of the ionomers in g/mol, M_{H2O} is the molecular weight of water which is 18.01 g/mol, ρ_{H2O} is the density of water (g/cm^3), $\rho_{ionomer}$ is the density of ionomer (g/cm^3), h_0 is the thickness of the ionomer thin film at dry condition and h_{RH} is the thickness of film equilibrated at a specific RH. In all calculations, it is assumed that the density and thickness of thin film are uniform all over the sample surface and that the film expands only in the direction perpendicular to the plane of the film. There is a likelihood of in-plane expansion of the films as noted in a recent paper [118] from our group but it is ignored in the present work. It must be noted that λ is set to be 0 for dry films, as assumed by many groups, although it has also been argued that even in dry state one hydronium ion may be associated with a sulfonic group. Each sample was first placed in the environmental chamber at 0% RH for two hours. The measured thickness h_0 at dry condition (RH of 0%) was used as the baseline. Then, the RH of the system was increased incrementally in 5 steps to reach a maximum RH of 90%. To ensure that the system is fully equilibrated at each RH, the sample was held at the specified RH for half an hour while the response was monitored.

4.3.Results and Discussion

4.3.1. Effect of temperature on proton conductivity and water uptake

Commercial polymer electrolyte fuel cells for transportation applications are designed for operations at temperatures significantly higher than room temperature. The US DOE performance targets for polymer electrolyte fuel cells are based on 80℃ operations[119]. Thus, the pertinent temperature for measurement of proton conduction and water uptake would be 80℃. However, many of the ionomer thin film properties including proton conductivity, swelling and water uptake have been measured ex-situ at room temperature, likely due to the lack of temperature control in the environmental chamber used for these measurements. From membrane studies [50], [51] and some of our own prior studies [56], [117], [120] on ionomer thin films, it is known that measurement temperature can influence ionomer properties. To investigate the extent of changes in proton conduction and swelling behavior of ionomer thin films with temperature, these properties for Nafion (EW1100) thin film was measured at two different temperatures of 30 and 80℃. These results are shown in Figure 4.3a and 3b, respectively. As can be noted from Figure 4.3a, the proton conductivity of the Nafion thin film is significantly higher at 80℃ compared to that at 30℃ especially at low RH. However, this difference decreases at higher RH. At 20% RH, the conductivity of the Nafion thin film at 80℃ is nearly two orders of magnitude higher than that at 30℃. At 90% RH, the conductivity difference decreases yet the conductivity at 80℃ is almost three times higher than that at 30℃. The conductivity values from the present study are in a good agreement with the Paul et al.[65] and shim et al.[121] results. For example, a conductivity of 3.2 mS/cm at 30 °C and 80% RH for the spin-coated Nafion film in the present study is comparable to the data reported by Shim et al [121] (2.8 mS/cm) for spin-coated Nafion films at 75% RH and

30 °C, which is lower than the values reported by Paul et al [65] (4.4 mS/cm) for self-assembled Nafion films. No data at 80 °C are available for comparison.

It is known that proton conductivity of the ionomers is highly dependent on its water content (λ) [30], [122]. The water content expressed as λ (representing the number of moles of water per sulphonic acid group) estimated from swelling data, according to equation (1), is reported in Figure 4.3b. Significant differences in the water content of the ionomer film at 30℃ and 80℃ are observed. The effect of temperature on the conductivity, surface wettability and ion mobility of Nafion thin films was also summarized in a recent article [30]. The difference in lambda value of ≈1 is observed at any given RH for 80℃ and 30℃. In the pioneering work on Nafion membrane conductivity, Zawodzinski et al. had correlated proton conduction as function of lambda and found an exponential dependency [115], [123]. Thus, a difference of 1 for lambda can result in a large difference in protonic conductivity. Upon plotting the conductivity of the Nafion thin film as a function of λ (Figure 4.3c), the differences in conductivity at 30 and 80 °C become much smaller, confirming that the proton conductivity of ionomer films is a strong function of water content. Small differences between the two datasets (30 and 80 °C) could be attributed to the differences in thermally activated properties such as proton mobility or diffusivity.

From a practical application point of view, the results in Figure 4.3a highlight the need to determine the ionomer thin film properties at fuel-cell-relevant temperatures. All subsequent results reported in this paper are those obtained from measurements at 80 °C.

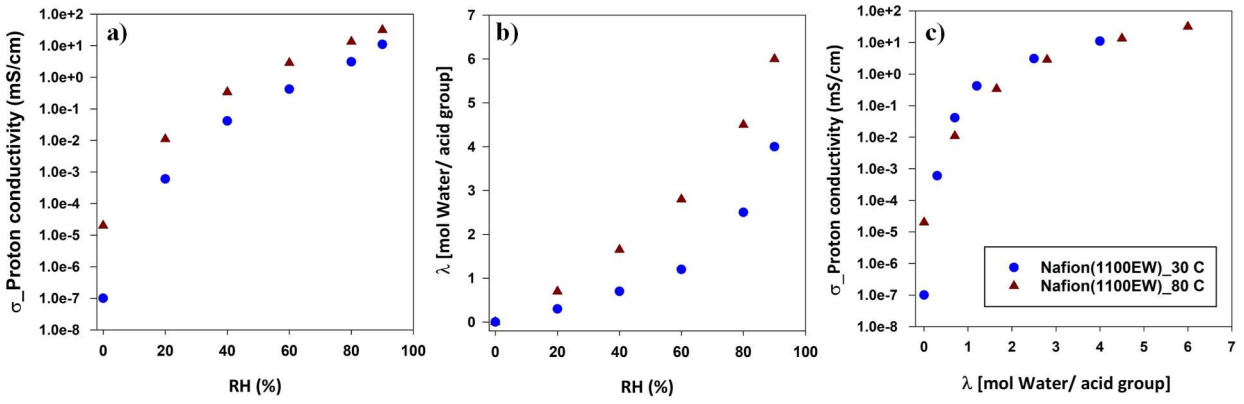

Figure 4.3. (a) Proton conductivity and (b) water content of Nafion thin film at 30˚C and 80˚C as a function of RH. (c) Proton conductivity of Nafion thin film at as a function of water content.

4.3.2. Effect of equivalent weight and sidechain on proton conductivity and water uptake

Figures 4.4a and 4b show the proton conductivity and water content, respectively, of different ionomers at 80℃ and different RH as a function of equivalent weight (EW). Higher EW ionomers have less acidic group than lower EW ionomers for a given mass of ionomer. If the density of the different EW ionomers is considered to be similar, then for ionomer films with comparable thickness, low EW ionomer films would have larger amount of acidic group than high EW ionomer films. Expectedly, the proton conductivity of ionomer thin films decreased with increasing EW (Figure 4.4a). On a semi-log plot, the σ exhibits a nearly linear dependency on EW at a given RH. Similar trend has been observed by Yandrasits [110] in saturated membrane (e.g., PFSA membranes equilibrated with liquid water). As it is shown in Figure 4.4d, ionomer thin films and membrane water content both have similar behavior towards the EW change; in both cases, the water content increased by decreasing EW.

The proton conductivity dependency on EW at a given RH is described by the following expression:

$$\sigma = a \exp\ (b \cdot EW) \qquad \Rightarrow \qquad \log\ (\sigma) = \log\ (a) + b \cdot EW \tag{2}$$

For example, at 90% RH the proton conduction dependency on EW is b=0.00285 mS/cm-EW; for 80% and 60% RH, b = 0.00373 and 0.00438 mS/cm-EW, respectively, while at 40% RH b = 0.0073 mS/cm-EW. The reason for examining the conductivity dependency on EW at a given RH is that relative humidity is an externally controllable parameter as opposed to water content of the ionomers.

The swelling rate of ionomer thin films also exhibits a similar dependency on EW (Figure 4.4c). It would be expected that upon normalizing the amount of water to the number of protogenic groups, i.e., the water content (λ), the differences would become small. Surprisingly, a linearly decreasing trend for water content as a function of EW was observed. PFIA (620 EW) has the highest water content (≈9 at 90% RH), followed by 3M (725 EW), and the lowest water content was observed for Nafion 1100 EW (≈6 at 90% RH). In a free acid, the water content would not be expected to differ depending on the amount of acid in equilibrium with water vapor at the same chemical potential (or RH). However, the normalized water content for ionomers, including in the thin-film form, does appear to vary with acid content. This interesting behavior of water uptake of ionomers has been a subject of discussion and debate for several years now, and many different models have been proposed [50], [67], [124], [125]. One of the earliest models to consider water uptake as a balance between chemical and mechanical forces was proposed by Eisenberg in 1970 [126]. More recent extension and application of this idea include works by Choi et al. [127], [128] and Kusoglu et al. [129]–[131]. It has been considered that rigidity of hydrophobic matrix puts mechanical constraints on the water uptake capacity of the hydrophilic ionic cluster. In fact, amongst the only known data for RH-dependent mechanical property of ionomer thin films, Page et al. [132]–[134] from NIST group had reported how thickness-dependent mechanical property

of thin films are correlated with water uptake. Thinner films had larger mechanical stress and correspondingly lower water uptake. Extension of this idea to our data would indicate that the rigidity of the backbone increases with increasing EW, which would then constraint the water uptake. Another factor is the ionic cluster size dependency of hydration energy [135]. It was observed that larger cluster size has lower hydration energy. Thus, in the limits of free floating sulphonic acids , it would be expected that such configuration would sorb most water and a single isolated sulphonic acid would have the least affinity of water. We would need both mechanical properties and cluster size data to ascertain how the side chain parameters – length and interspacing between side-chains – affect the two parameters. Measurement of mechanical properties of supported ionomer films requires specialized experiments [132]. The ionic cluster size can be determined from grazing-incidence small angle x-ray scattering (GISAXS) but require beamline access. For now, the experimental data provide a simple guidance that the acid content (i.e., EW) has the strongest influence on water content whereas the side-chain parameters have smaller influence.

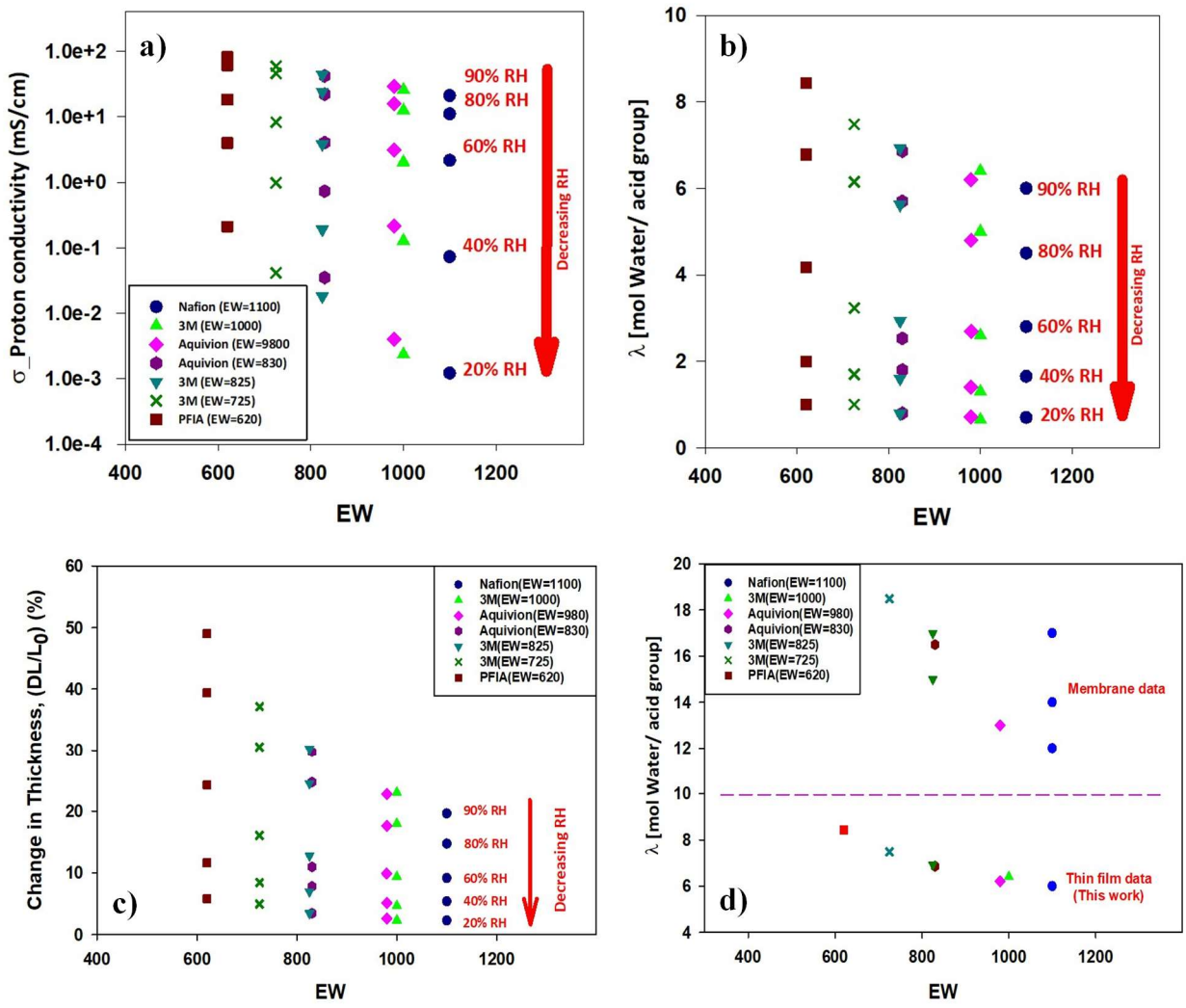

Figure 4.4. a) Proton conductivity, b) water content of ionomers at different RH and c) swelling rate of 30 nm ionomers as a function of EW measured at 80 ℃ while RH decreases; d) water content of different 30 nm ionomer thin films (at 90% RH and 80°C) and membrane at saturation as a function of EW [31], [67] .

4.3.3.Proton conductivity – water content (σ- λ) correlation

Conductivity of a charged species in a medium is classically described by the product of charge-carrier mobility and charge-carrier concentration. For ionomers, water content impacts both of these properties. Although the number of charge-carriers (protons) per mass of ionomer

can be computed from its EW, not all the charge-carriers are necessarily in a mobile state because the protons may be tightly bound to the counter ion (SO_3^-) at low water content. Indeed, at higher water content the sulphonic acid may fully dissociate when the protons and SO_3^- are fully hydrated. Protons need 4 water molecules to form their first hydration shell and SO_3^- is thought to need 2-3 water molecules to form its hydration shell [136]–[138]. Briefly, the ion-pair states in salt solution [139], [140] described as: (i) at low λ of up to 4, contact ion-pair (SO3-/H+) can be expected, (ii) at a λ of 6 to 7, the ion-pairs share the hydration water, and (iii) at greater than λ=7, protons can be considered to be dissociated from the sulphonic group. There is only one study where the state of water in the thin film form of Nafion was investigated [141]. In the study, the water content in Nafion films were considered to be anonymously high and as much as 15. The origin of the anomaly was later resolved [121] yielding a more reasonable values consistent with other studies including the present work. At low λ, nuclear magnetic resonance (NMR) revealed the water to be bound and only above λ of 6-7, free water was observed. These considerations were taken into account in the model developed for proton conduction in Nafion membrane in a much earlier work by Jalani and Dutta [127] and have also been discussed in works done by Kusoglu et al. [31] and Shrivastava et al [140]. It can be argued that for similar water content (λ), the mobility and the effective mobile concentration of protons would be similar for all ionomers. Now, PFSA ionomers are also known for their phase-segregated morphology comprising water-free hydrophobic matrix and hydrophilic domains containing clusters of ion-pairs when in dry state. Upon hydration, the shape and connectivity of the hydrophilic domains change, which then impact the effective transport of protons over a longer distance. Essentially, PFSA ionomers can be considered to be a composite of non-ionic matrix filled with pockets of acids connected irregularly via some tortuous

path. Accordingly, the proton conductivity of PFSA ionomers can be described to follow the following proportionality:

$$\sigma_{H^+} \propto [\mu_{H^+}][C_{H^+}][\frac{\varphi_W}{\tau}] \quad (3)$$

where, σ is proton conductivity which is a function of various parameters: proton mobility (μ_{H^+}) representing the concentration of "mobile" charge carrier (C_{H^+}), porosity (φ_W) , and tortuosity (τ_W).

Since water content impacts all three terms on the right side of the proportionality expression, the simplest approach to correlating proton conductivity of ionomers to its physical property is via its acid-group normalized water content (λ). Figure 4.5a shows the conductivity-water content (σ-λ) data for all ionomers. All ionomer films demonstrate similar dependency of conductivity on water content, i.e., very sharp rise in conductivity with small change in water content over the value of 0-4 and a slower increase in conductivity with water content at higher water content. It must be noted that the conductivity is plotted on a logarithmic axis.

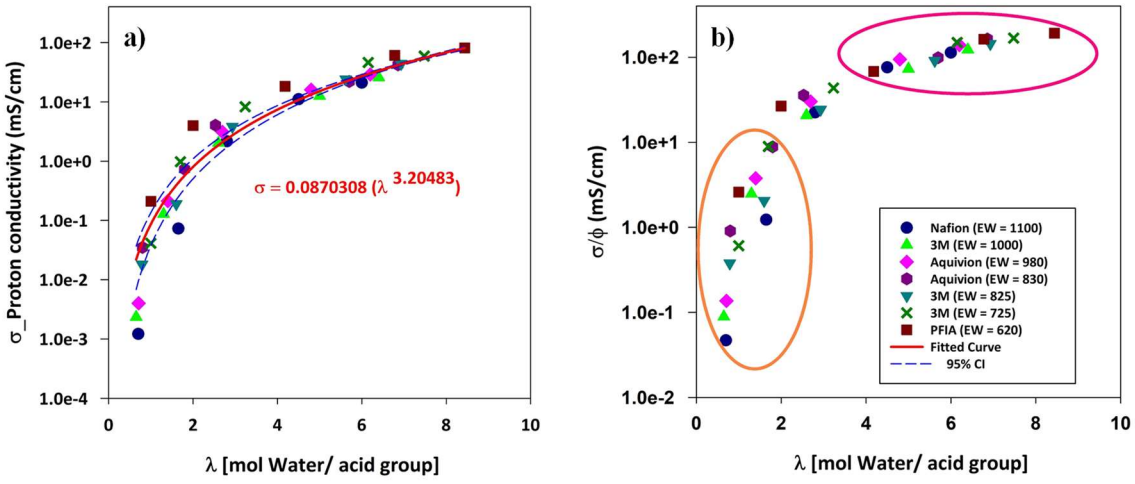

Figure 4.5. a) Proton conductivity, and b) water-volume fraction normalized proton conductivity of the ionomers as a function of water content (λ) at 80 °C.

First observation to be made is that the conductivity appears to be converging to a value of 100 mS/cm as water content tends to 9. Significant differences in the conductivity of ionomers can be noticed at low water content with highest value for PFIA 620EW ionomer and the lowest for highest EW ionomer, Nafion 1100. These differences could arise from the differences in their microscopic structure of the proton conducting phase (φ_W,τ) and intrinsic properties (C_{H^+}, μ_{H^+}). PFIA exhibits higher conductivity than PFSA ionomers at any given water content (λ). Upon normalizing the conductivity with water volume fraction, i.e., rearranging expression (3) as $(^{\sigma_{H^+}}/_{\varphi_W}) \propto [\mu_{H^+}][C_{H^+}][\frac{1}{\tau}]$, the PFIA data fall closer to the rest of the data. The higher water content and higher conductivity of PFIA in the membrane form were reported by Su et al.[142].They suggested that the enhanced conductivity is not only due to higher water uptake but also a combined impact of chemical interactions governing proton dissociation with water and more efficient proton transport [142].

The Mobility of protons in ionomers has been determined from pulse gradient NMR, which we do not have access to. As discussed earlier, solid state NMR of ionomers in thin film form is difficult to measure and only one such study exists [141]. Similarly, a direct measurement of tortuosity in any composite material is non-trivial and especially difficult to ascertain for the hydrophilic domain in the ionomer thin films. This leaves us with phase volume fraction as the only readily estimable quantity. A plot of σ/φ_W as a function of water content is reported in Figure 4.5b. The data in this figure reveal two regions – one above λ of 4 and one over λ ranging from 0 to 2. At λ>4, the (σ/φ_W) values for different ionomers seems to collapse to a single correlation line and depend only on the water content (λ). Since proton mobility is weakly dependent on the domain size [143], it may be inferred, as per proportionality of equation 3, that tortuosity would

be the only influencing factor responsible for the differences in conductivity at lower lambda. In the low λ range, the proton conductivity at any lambda varies by an order of magnitude.

4.3.4.Effect of film thickness

Polymer thin films including ionomer thin films are known to exhibit thickness-dependent properties [30]. In our earlier work on self-assembled Nafion (EW1100) films, a strong dependency of conductivity on the thickness for films below 50 nm was observed [65]. In the present study, all films were prepared by spin-coating. Differences in the internal structure of the studied ionomer films prepared by self-assembly and spin-coating can be found somewhere else [68]. Here, we have examined the thickness-dependency of proton conductivity and water content of films of three different nominal thicknesses (10, 30, and 80 nm) for three different ionomers. It must be noted that thickness-dependent properties of ionomer thin films have been discussed and summarized in recent articles [30], [31]. Effect of thickness on proton conduction was reported by Siroma et al. [66]; then Karan group [53], [69]; and more recently by Zhang, Kongkanand and Nagao group [63], [70], [144]. However, such data at fuel cell operating conditions of 80ºC is lacking. Here, we report proton conductivity and water content of PFSA ionomers for three different film thicknesses – 10 nm, 30 nm, and 80 nm - in Figure 4.6. As can be seen, proton conductivity and water content of the PFSA ionomers decreases by reducing the thickness of the film and it has good agreement with result of Nagao [70] and Karan [69] group work. At 40% RH, the water content increased one unit (λ=1) when film thickness increased from 10 to 80 nm, while the differences became four units (λ=4) at 90% RH. However, the conductivity changes show an opposite trend in that the differences in conductivity is larger at low RH (40%) despite small difference in water content upon film thickness increase from 10 to 80 nm and is smaller at high

RH (90%). At 40% RH, the conductivity increased two orders of magnitude by increasing the thickness while at 90% RH, the conductivity increased one order of magnitude.

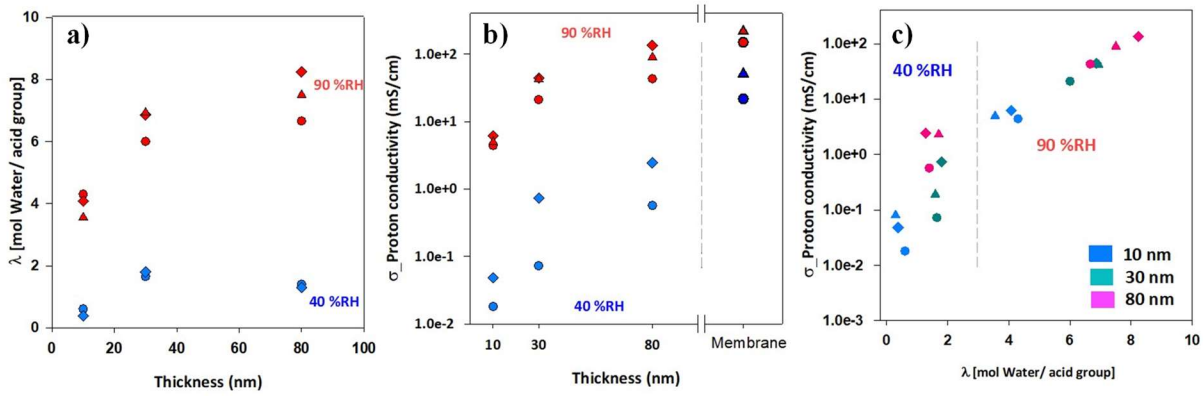

Figure 4.6. Thickness dependence of a) water content, b) proton conductivity, and c) proton conductivity as a function of water content at 80 oC and moderate (40%) and high (90%) relative humidities. ●: Nafion, ▲: 3M and ♦: Aquivion.

4.3.5. Discussion on correlating ionomer thin film data with CL ionomer properties

One of the motivations for the present study was to generate comprehensive data on ionomer thin films at fuel cell operations relevant temperature (80°C rather than the prevalent room temperature data) for several prominent ionomer varying over a wide range of equivalent weight. Ultimately, the idea is to use the thin film hydration and conductivity data as a guide for ionomer material selection for catalyst layer fabrication. To this end, it is useful to correlate thin film data and CL ionomer properties data. Two key ionomer properties that can affect the fuel cell performance are protonic conductivity and oxygen diffusivity of cathode CL ionomer.

Determination of CL ionomer conductivity is not straight-forward due to the heterogeneity of ionomer distribution and non-uniformity of ionomer film thickness. However, the total ionic resistance of the CL can be determined from impedance spectroscopy of a fuel cell operated in a N_2/H_2 configuration [145]. Similarly, oxygen transport resistance can be extracted from limiting

current density measurements but translating that value into Intrinsic diffusivity of oxygen is complicated because of variability of oxygen path length, i.e., variation in ionomer thickness (Figure 4.1) within the CL. On the other hand, model systems such as uniform ionomer film of well-defined thickness on planar system permit the determination of proton conductivity and film thickness-dependent water uptake. Thus, one to one comparison of the protonic conductivity of our thin films cannot be done with CL ionomer conductivity. As alluded to earlier, most of the prior data on conductivity and water content for ionomer thin films in the literature has not been reported at fuel cell operating temperatures (80ºC), which adds another caveat when comparing in-situ (fuel cell) CL ionomer properties with thin film data. Recently, the effect of ionomer EW on the CL ionomer properties, i.e., ionic resistance and oxygen transport resistance using in situ fuel cell electrochemical diagnostic measurements, at fuel cell operating conditions (80C) for eight PFSA ionomers with EW varying from 720 to 1100 gr/mol and having long, medium and short side chain (Nafion, 3M and Aquivion respectively) was reported by Ramaswamy et al. [112]. Thus, we can remove one of the confounding factors, i.e. the influence of temperature from the correlation.

Our ionic conductivity results imply that equivalent weight (or acid content) of the ionomer has the strongest impact on conductivity of the ionomer thin films. For membranes, Yandrasits [110] had also shown a strong correlation of conductivity with EW. Considering the thickness-dependent conductivity of ionomer thin films, there is always a question of whether the trends observed (e.g. EW dependency on conductivity) for membrane form would still hold for CL ionomer. Accordingly, we have compared the H+ conductance of cathode CL ionomer (Nafion®: LSC, 3M PFSA: MSC, Aquivion®: SSC with EW varying from 720 to 1100 gr/mol), calculated as inverse of H^+ transport resistance, reported by Ramaswamy [112] with the conductivity of

ionomer thin films (this work) both at 80°C. Both dataset, depicted in Figure 4.7a, show similar dependency on EW. It is worth noting that proton conduction in CL occurs through the thickness of catalyst layer but in-plane with respect to the ionomer film, and not through plane as sometimes incorrectly mentioned. While clear differences between the medium side chain ionomer and short-side as well as long-side chain ionomers were observed for CL protonic conductance, no such clear distinction was observed for the uniform thickness thin film protonic conductivity.

Oxygen permeability in Nafion membrane has been found to increase with relative humidity and explained in terms of increase in water content of the membrane, which provides a more facile pathway for oxygen diffusion at high water content than the diffusion through hydrophobic matrix. Similar analogy could be extended to oxygen diffusion through thin films of ionomer covering the Pt catalyst in the CL. However, some distinct differences may exist. The path length for transport of oxygen in membrane and CL ionomer differ significantly. The longer pathway (through tens of microns thickness) in membrane would imply that geometric effect such as tortuosity and inter-domain distances would be important. In the CL, the oxygen transport through the ionomer may not be subjected to long tortuous path and likely traverse only 1 or 2 interdomain distance in the through plane distance before it arrives at the catalyst site (Figure 4.1). If so, the oxygen transport resistance in ionomer thin films may be dependent on the "state" of the water – bound, exchanged or free – as shown in Figure 4.7b [30]. A restrictive transport would be expected under conditions of bound water ($\lambda<2$), and become more facile as λ increases to 6-8 when hydration shell is completed for both protons and sulphonic groups. The local oxygen transport resistance in CL is thought to be due primarily to the oxygen transport through the ionomer film [23]. Interfacial resistance at Pt/ionomer interface, rather than bulk diffusion through the film, is considered to be dominant resistance for the observed local transport resistance.

Nonetheless, water content of the ionomer film both at the interface and in the bulk may be important parameter controlling the oxygen transport resistance. It is pertinent to note that in a recent work from our group, the interfacial water determined from neutron reflectometry study was found to be ionomer side chain length dependent [209].

To correlate CL local oxygen transport resistance (R_{O2}) at 80^{o}C and 70%RH reported by Ramaswamy et al. with water content of ionomer phase, we used the water content of ionomer thin films at 80% RH from our study as a surrogate for the CL ionomer water content. It is our view that under conditions of transport resistance measurement, water would be produced locally at Pt/ionomer interface, thereby resulting in CL ionomer hydration levels slightly higher than ionomer film equilibrated at 70%RH. Also, it is recognized that the water content of CL ionomer may be different than water content for uniform ionomer thin films of the present study due to many reasons including film thickness and substrate (carbon versus SiO_2). For high EW ionomers, the lambda is low and correspondingly the R_{O2} is higher. At lower lambda (≈5), it appears that medium side chain (MSC) length ionomer has higher R_{O2} than shorter side chain (SSC) length ionomer. Although the data is limited, considering the MSC ionomers, a near leveling off of R_{O2} is observed as lambda approaches a value of 6-8. If this is correlated with the state of water, it can be speculated that under these conditions, the water in ionomer is in free state and more mobile. This free water may then improve the mobility of the oxygen as well. This idea of correlating oxygen transport resistance for different ionomers would require careful study of CL water content determination and determination of oxygen transport resistance. For now, the water content for ionomer thin films may be considered as the best approximation.

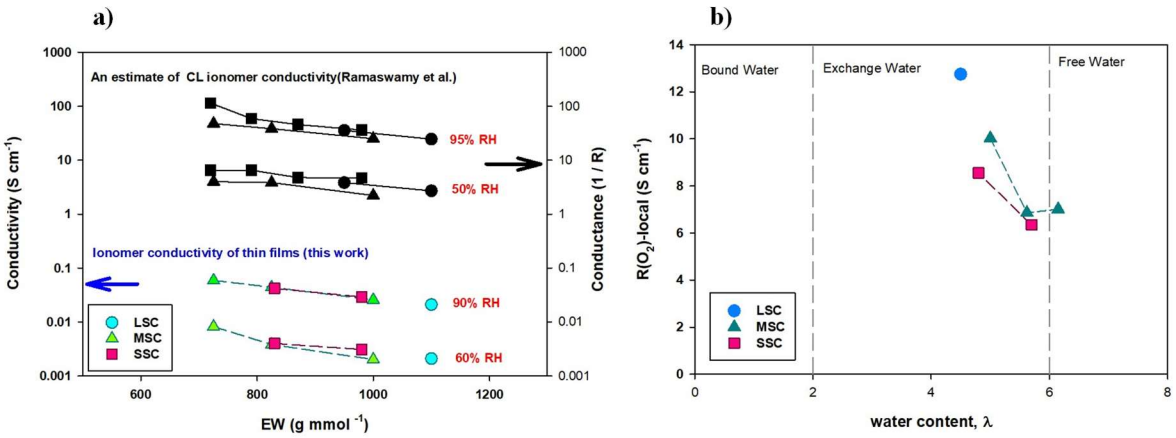

Figure 4.7. (a) ionomer conductivity of thin films (this work) at 60% and 90% RH and the CL ionomer conductivity at 50%RH and 95% RH (Ramaswamy et al., [112]) as a function of EW at 80°C, and (b) correlation of local O2 transport resistance reported by Rangaswamy with water content data for ionomer thin films.(Nafion: LSC, 3M PFSA: MSC, Aquivion: SSC and PFIA).

4.4.Conclusions

This study provides interesting insights into the hydration dependent properties, viz., water content and proton conductivity, of thin films (30 nm) for PFSA and PFIA ionomers at 80 °C with different equivalent weights (from 620 to 1100 g/mol of sulfonic acid) and varying side-chain lengths. The primary focus of our study, measurements of both water content and proton conductivity at 80 °C, which is a typical fuel cell operating temperature, revealed that the value of these properties was significantly higher than that at 30 °C. Since most of the studies in the literature have reported ionomer thin-film properties at room temperature, these results offer a cautionary note in so far as applying the results at 30 °C to fuel cell operating conditions. The acid content of the ionomer, i.e., the inverse of EW, was the strongest determinant of the water content and proton conductivity at any given relative humidity. Thus, water content and proton conductivity were found to decrease monotonically with increasing EW. A key contribution of the

present study is the examination of the correlation between water content and proton conductivity for seven ionomers. All ionomers exhibited an exponential type dependency of proton conductivity on water content. A single universal correlation for all ionomers could describe the trend, but the influence of side-chain characteristics, i.e., length and interspacing, was significant at low water content ($\lambda < 4$). The trends at higher water content appeared to exhibit proton conductivity, tending to reach an asymptotic value of ≈0.1 S/ cm.

Chapter Five: Conductivity and Hygroscopic Expansion of Ionomer Thin films: Effect of Cobalt Exchange and Thermal/Aqueous Treatment

This chapter has been reproduced from "Conductivity and Hygroscopic Expansion of Ionomer Thin Films: Effect of Cobalt Exchange and Thermal/Aqueous Treatment", J. Phys. Chem. C 2022, 126, 42, 17862–17874, doi: 10.1021/acs.jpcc.2c05629, with the permission from ACS (American Chemical Society). Copyright (2022) American Chemical Society. Dr. Vinayaraj Ozhukil Kollath (former postdoctoral fellow) is the co-author in the manuscript.

5.1. Introduction

Polymer electrolyte fuel cell (PEFC) powered vehicles offer the advantage of longer driving range and quick refueling while maintaining many of the advantages of battery powered electric vehicles. Tremendous progress has been made in the PEFC technology over the past decade but further reduction in cost, enhancement in durability, and improvement in performance is still needed [22], [26], [146], [147]. A key research focus has been to reduce the PEFC cost, which is attributed to the expensive Platinum (Pt) catalyst. Both non-Pt group metal and low-Pt content alloy catalysts are being explored in order to reduce the catalyst cost [29], [71]. Alloyed catalysts such as Pt_3Co and Pt_3Ni have low Pt content but demonstrate oxygen reduction reaction activity comparable to that of pure Pt nanoparticle catalyst [71], [148]–[150]. In fact, world's first serially produced commercial fuel cell vehicle, Toyota Mirai utilizes Pt-Co catalyst [19]. However,

it is now known that cobalt (Co) can leach out from the alloy catalyst during fuel cell operation and cause performance degradation under long-term operation [35], [151]. After long-term operation of Pt-Co based electrodes, cobalt has been found in the membrane as well as in the catalyst layers of PEFCs [35], [74], [152]–[154]. Upon Pt-Co/Ni catalyst degradation [27], [29], [30], [155], the generated metal cations (M^{n+}) migrate from the catalyst surface into the thin film of ionomer coating it and then into the polymer electrolyte membrane primarily because they have higher affinity towards sulfonate (SO_3^-) end groups of the ionomer/electrolyte compared to that between sulfonate ion and H^+ [58], [81] For this reason, the effect of cation contamination/exchange on the properties of membrane has been received significant attention over the past decade. The effect of cation contamination or cation exchange, in general [46], [88], [153], [156], [157], and that of cobalt cation, specifically on the membrane properties have been reported. [37], [39], [152].

From published work, it is evident that exchange of cations (such as, Co^{2+}, Na^+, Li^+, K^+, Cs^+, Ca^{2+}, Ni^{2+}, Fe^{3+}, Al^{3+}) has a severe effect on the performance and durability of PEFCs due to a significant decrease in the ionic conductivity of the membranes [33]–[38]. Metal cation contaminants exchange with protons, reduce the transference number of conductive species, lower the ionomer/membrane conductivity [31], [42], [43], and hinder the oxygen-reduction reaction [43]–[46]. Mitigating these negative impacts is of critical importance for meeting the durability and lifetime requirements of PEFCs that are increasingly using Pt-Co alloy catalysts in commercial stacks [84].

It is interesting to note that the presence of Co^{2+} even in a liquid electrolyte (H_2SO_4) results in a decrease in O_2 diffusivity, O_2 solubility, and the kinematic viscosity of the electrolyte [158]. In a recent study, the contamination effect of Co^{2+} in fuel cell operating condition was investigated

by injecting Co^{2+} ion solution through inlet air stream, and it was found that fuel cell voltage dropped significantly. The Co^{2+} effect was severe with decreasing temperature which led to a larger reduction in the ORR rate. Litster and co-workers[39], [159] have also investigated the oxygen transport properties of membrane of H^+ and Co^{2+} forms of Nafion ionomer. They employed Nafion 117 membranes with different levels of Co-exchange (un-exchanged, partially- exchanged and fully-exchanged). The oxygen permeability through the membranes were reported in its inverse form as oxygen transport resistance (R_{O2}), which was found to increase with an increasing level of Co exchange. It was pointed out that Co^{2+} migration and accumulation in the cathode mainly cause the maximum R_{O2}. The oxygen transport resistance increased by 100% at low water activity and less than 50 % at high water activity (saturated water activity) upon cobalt ion exchange of H+ form of Nafion membrane.

Migration of Co^{2+} cation was evaluated in the membrane electrode assembly (MEA) of an operating PEMFC using Synchrotron micro-X-ray fluorescence (μ-XRF). It showed that the Co^{2+} distributions was not simply in through-plane direction and a semi-quantitative two-dimensional (electrochemical and transport coupled) model is needed to describe the potential gradient at the MEA edge [35] . In another study, the effect of Co contamination on fuel cell performance was studied under different oxygen concentrations, using impedance spectroscopy for measuring membrane and electrode proton transport resistance. It was found that the Co contamination increased the membrane proton transport resistance by an order of magnitude and CCL resistance follows similar trend with Co contamination. [152].

These studies have established that the presence of Co^{2+} ions in cathode catalyst layer can adversely affect fuel cell performance. Thus, it would be expected that the leaching of Co from Pt-Co alloys catalysts would impact the ionomer properties in the catalyst layer first and subsequently

the membrane conductance. The ionomer in the catalyst layers (CL) of PEFCs exist as few nanometers thin ionomer films coating Pt or Pt-Co catalyst supported on carbon (Figure 5.1) [29], [30], [160]. The ionomer serves as a medium for long-range ion/proton transport and the hydrophilic ionic domains also provide a dominant pathway for oxygen transport to the catalyst surface. Thus, Co^{2+} exchanged ionomer can affect both ion conduction and oxygen transport in the PEFC catalyst layers wherein Pt-Co catalysts are employed.

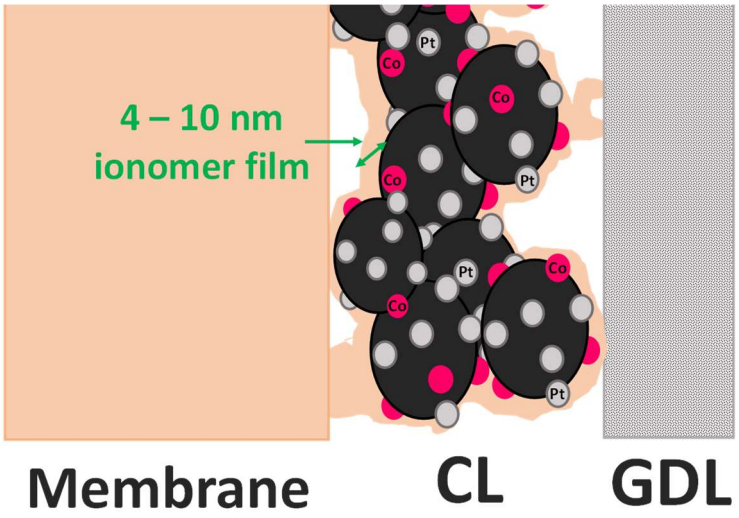

Figure 5.1. Schematic of ionomer catalyst layer in PEFC system

Whereas the impact of cations (compared to H^+) on the conductivity of membrane form of Nafion is known [36], [37], [69], [79]–[81], [161], the extent of such effects for Nafion and other ionomer thin films has not been well studied. It is known that the properties such as the ionic conductivity, water uptake, and swelling of the nanothin ionomer films are significantly different than those of the bulk material [66], [162]. For example, at a given RH, Nafion thin films exhibit lower conductivity compared to the bulk/membrane form and, also, a correspondingly lower water uptake, usually described in terms of the parameter λ, which is number of water molecules per sulfonic groups. However, even at comparable λ, the thin films show suppressed conductivity than

its membrane form [54], [66], [162]–[164]. In a recent study, Han et al [165] reported the ionic conductivity of H^+ form and Co^{2+} exchanged ionomer films of 40 nm and 120 nm thickness at a 98% RH (in the temperature range between 20 and 50 ºC). The found that the ionic conductivity of Co^{2+} exchanged films were suppressed compared to H^+ form of the thin ionomer film. This trends qualitatively follows the trend expected from membrane data. However, without the accompanying water uptake data, no insights can be drawn on how the Co exchange impacts the hydration level. The water content of ionomer impacts many aspects of the ionic conduction including the ion-pair dissociation, (which impacts the local mobility of ions) and the connectivity of the ionic channels (which impacts the longer-range transport of ions) [165]. Han et al also observed monotonically decreasing conductivity with increasing Co^{2+} content but only a slight increase in conductivity with temperature increase from 298K to 323K was observed. The effect of RH was not reported in their work. Cai et al reported membrane and CCL proton resistance from MEAs with different Co doping level as a function of relative humidity. They found that under dry conditions (~ 35% RH), Co contamination has greater impact on proton resistance increase. Moreover, it is observed that membrane and CCL resistance follow the same trend upon the increase in Co contamination [152].

In summary, to the best of our knowledge, there are two studies that report on the influence of Co^{2+} exchange on the conduction of ionomer thin films. One study reported ion conductivity of Nafion 1100 thin films of well-defined thickness (40 and 120 nm) [165] upon Co^{2+} exchange. Another study reported changes in CL ionomer (Nafion 1100) conductance for two different extents of Co^{2+} exchange [152]. Neither of these studies reported the water uptake of the ionomers and correlate the conductance to water content. Also, both studies have been limited to one type of ionomer – Nafion 1100. Recently, a number of commercial perflurosulphonic acid ionomers

have become available commercially, e.g. shorter side chain Perfluorosulfonic Acid (PFSA) ionomers (3M, Solvay) and 3M's Perfluoroimide Acid (PFIA) ionomer. However, no study has reported the impact of Co-exchange on water uptake and conductivity of nanometers thin films of ionomers with differences in equivalent weight (acid content) and the underlying compositional variation introduced by altering the side-chain length or side-chain inter-spacing.

In this work, we determine the hydration level and conductivity of 30 nm ionomer thin films over a range of humidity (0-90%) at 80℃. Seven different ionomers – Nafion EW 1100, 3M PFSA EW 1000, 825 and 725, Aquivion EW 980 and 830 and 3M PFIA EW 620 – were investigated. We also report the effect of thermal annealing and water exposure on water uptake and conductivity. The investigation of thermal annealing effect was not originally planned but became essential for comparing the hydration and ionic conductivity properties of H^+ and Co^{2+} forms of the ionomer films as explained in results and discussion section.

5.2. Experimental

5.2.1. Materials

Seven different ionomers varying in equivalent weight (EW) were investigated in this work (Figure 5.2). Nafion dispersion (EW1100) was obtained from Ion Power Inc. (USA) whereas the 3M PFSA and PFIA ionomers were provided by 3M Fuel cells Component Group, MN, USA and Aquivion ionomers were provided by Solvay Company (Italy). Commercially available 5 wt. % Nafion solution (in 25/75 water to alcohol mixture), EW 1100 g.mol $^{-1}$, from Ion Power was used to make diluted (1 wt. %) Nafion solution using isopropyl alcohol (IPA) (Sigma Aldrich) to have desired ionomer thin film thickness with spin coating method. Similar procedure is employed to prepare 3M PFSA and PFIA (Provided by 3M Fuel cells Component Group) and Aquivion

(Provided by Solvay) thin films. The diluted dispersion was placed at room temperature for 24 hours for equilibrating and sonicated again after equilibration to ensure that the dispersion is homogenous and ready to use. Ionomer thin films were Co^{2+} exchanged by soaking in 0.1 M aqueous cobalt sulfate solution (Alfa Aesar, Canada) for 48 h.

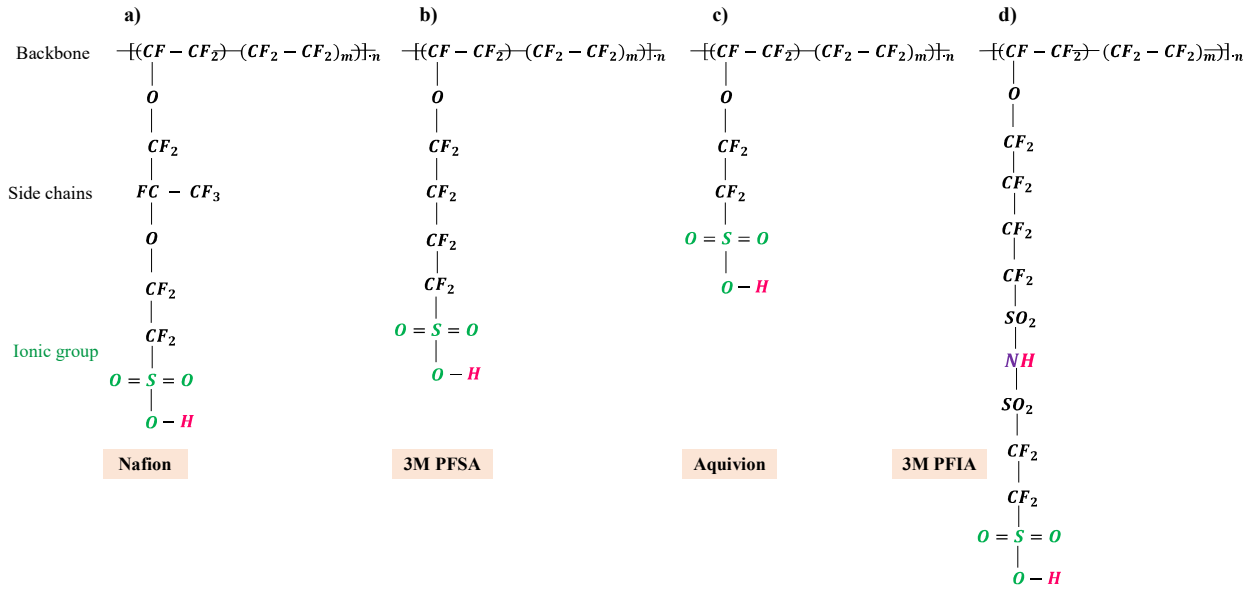

Figure 5.2. Chemical structures of ionomers which are used for investigation of Co exchanged thin films: (a) Nafion by Ion Power Inc Co., (b) PFSA by 3M Co, (c). Aquivion by Solvay Co. and (d) PFIA by 3M Co.

5.2.2. Thin film preparation and basic characterization

Thin films of nominal thickness of 30 nm were prepared using spin coating technique. For swelling experiments, films were coated on SiO_2/Si wafer whereas for conductivity measurements films were also coated on SiO_2 wafer but with interdigitated array (IDA) of gold electrodes. The procedure to fabricate IDA electrodes is described in detail elsewhere [53], [56], [68], [69]. The spin-coated samples were kept in vacuum oven (22 mm of Hg) for 20 hours to dry out at 40 °C or to anneal at 160 °C. To prepare the Co exchanged thin films, the dried or annealed samples were

soaked in excess amount of 0.1 M cobalt sulfate solution at room temperature (~ 23 °C) for 48 hours to make sure that the thin ionomer films were fully exchanged. Next, Co-exchanged thin films were rinsed using DI water several times to assure that there is no extra Co solution on the surface of the film. Subsequently, the Co exchanged samples were placed in the vacuum oven at 40 °C for 20 hours to make them ready for next steps.

5.2.3. Quantification of Co^{2+} exchange

To establish that Co exchange had occurred in the ionomer thin films and determined the Co exchange level, we applied inductively coupled plasma triple quadrupole mass spectrometer (ICPQQQMS-8900). The prepared Co exchanged thin film needed to be dissolved so, Dimethylformamide (DMF) solution (Sigma Aldrich) was used for dissolution of the ionomer thin film. After this step the dissolved sample were sonicated for 10-20 minutes followed by Co and S element content measurement via ICP-MS technique. For each ionomer, solution from two independent samples was prepared and triplicate ICP-MS measurements were performed for each solution. The reported variability from multiple experiments for each ionomer is presented in Table 1. One Co^{2+} cation would replace $2H^+$ ion. Accordingly, it was determined that 95% H^+ in PFSA ionomers and 96% H^+ in PFIA ionomer was replaced by Co^{2+} (Table 5.1). The difference in Co/S molar ratio for PFSA and PFIA raised from the different structure of their respective side chain. PFIA has three sulfur and two protogenic group whereas PFSA ionomers have one sulfur and one protogenic group in their side chain.

Table 5.1. The results obtained using ICP-MS technique for ionomers' Co2+ exchange quantification.

Ionomer	S (mg/Lit)	Co (mg/Lit)	Co/S Molar ratio	Co exchange rate (%)
Nafion	10.6 ± 0.04	9.4 ± 0.03	0.48	96
3M	87.7 ± 0.33	78.9 ± 0.35	0.49	98
Aquivion	12.5 ± 0.2	10.5 ± 0.1	0.46	92
PFIA	72.5 ± 0.8	42.7 ± 0.51	0.32	96

5.2.4. Conductivity measurement

Conductivity measurements were carried out on ionomer films on IDA electrodes by following the approach described in earlier papers from our group [53], [56], [68]. Briefly, impedance is measured on the films on IDA using a two – microprobe connected to a SP - 200 potentiostat (Bio - Logic Science Instrument, France) which was controlled by EC – Lab software that used for impedance measurement and electrochemical impedance spectroscopy (EIS) data modeling (analysis tool such as Z Fit). An environmental chamber (model MCBHS – 1.2-.33-.33-H/AC, MicroClimate compact chamber from CSZ products LLC., USA) is used to control relative humidity (RH) and temperature. Temperature was maintained at 80^{o}C. The repeatability experiments for ionic conductivity for selected samples (Nafion 100 EW, 3M 725 EW, Aquivion 830 EW and PFIA 620 EW) at high RH (RH > 70% RH) yielded a variation of less than 5% for all samples except Aquivion (830 EW) which had variation as high at 7.3%. A combined humidity and temperature sensor (CMOSENS Tec., Switzerland) was utilized to monitor the local temperature and RH by placing the sensor near the sample.

5.2.5. Water uptake measurement

The water uptake of thin films at each humidity was determined by measuring the change in the film thickness at given RH compared to its thickness at zero humidity (i.e. dry film). A custom-built environmental chamber, capable of controlling temperature and humidity combined with M 2000 Ellipsometer (J. A. Woollam Inc., USA) were employed to measure the thickness of thin film of various RHs. The details of the setup are provided elsewhere [69], [117].

For thickness measurements, a sample was first kept at dry conditions of 0% RH at 80ºC in the environmental chamber for more than 2 hours and the dry thickness (h_o) of the ionomer thin film was used for determination of water content. Next, the RH of the system was increased in the increments of 20 up to 80% and finally to 90% RH. The sample was maintained at each RH for approximately half an hour to make sure that the system is equilibrated completely (until ellipsometer response become steady). At the end, RH of the system were got back to the 0% RH to let it dry. The water content, λ, i.e. the number of the water molecules per protogenic group, of the ionomer is calculated [69], [81] according to the following equation:

$$\lambda = \frac{mol\ (H_2O)}{mol\ (SO_3)} = \frac{(h_{RH} - h_0)}{h_0}\left(\frac{EW}{M_{H_2O}}\right)\left(\frac{\rho_{H_2O}}{\rho_{ionomer}}\right) \quad (5.1)$$

where, EW is the equivalent weight of the ionomers in g/mol, M_{H2O} is the molecular weight of water which is 18.01 g/mol, h_0 is the thickness of the ionomer thin film at dry condition, h_{RH} is the thickness at specific RH in each step, ρ_{H2O} is the density of water (g/cm^3) and $\rho_{ionomer}$ is the density of ionomer (g/cm^3). In all calculations, it is assumed that the density and thickness of thin film are uniform all over the sample surface. It must be noted that λ is set to be 0 for dry films, as assumed by many groups, although it has also been argued that even in dry state one hydronium ion may be associated with a sulfonic group. The repeatability of water uptake measurement for selected

ionomers (Nafion 1100 EW, 3M 825 EW, Aquivion 830 EW and PFIA 620 EW) yielded a variation between 7.5% to 12.6 %.

5. 3. Results and Discussion

5.3.1. Surface morphology of the films before and after Co^{2+} exchange

The dried, spin-coated films were characterized for film thickness and surface morphology by ellipsometer and atomic force microscopy (AFM) (Figure 5.3), respectively. It was confirmed that the thickness and the surface morphology of the samples did not change after Co exchange and no precipitation occurred on the surface of the samples.

a) Before Co exchange

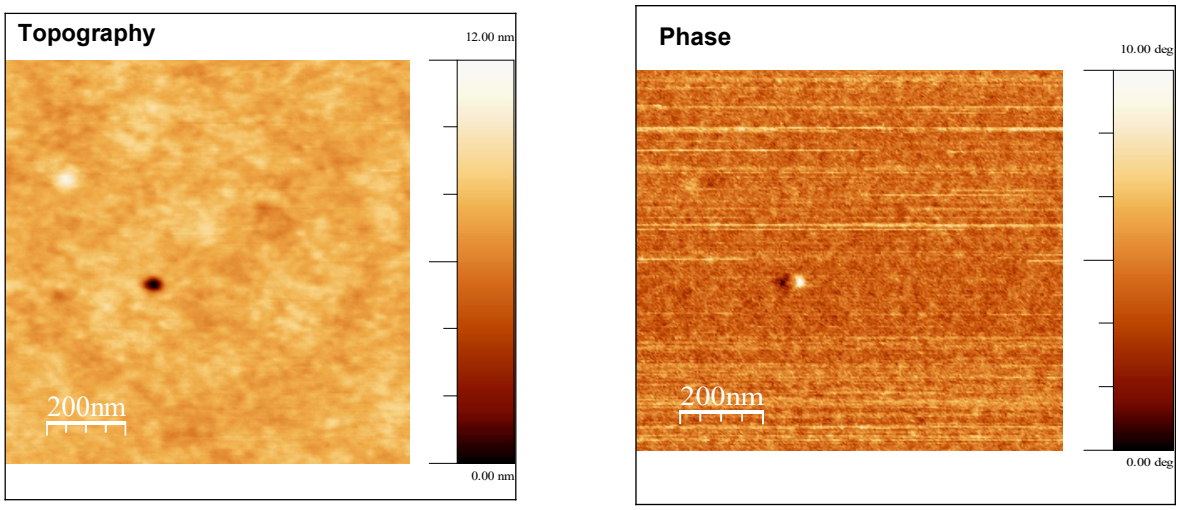

b) After Co exchange

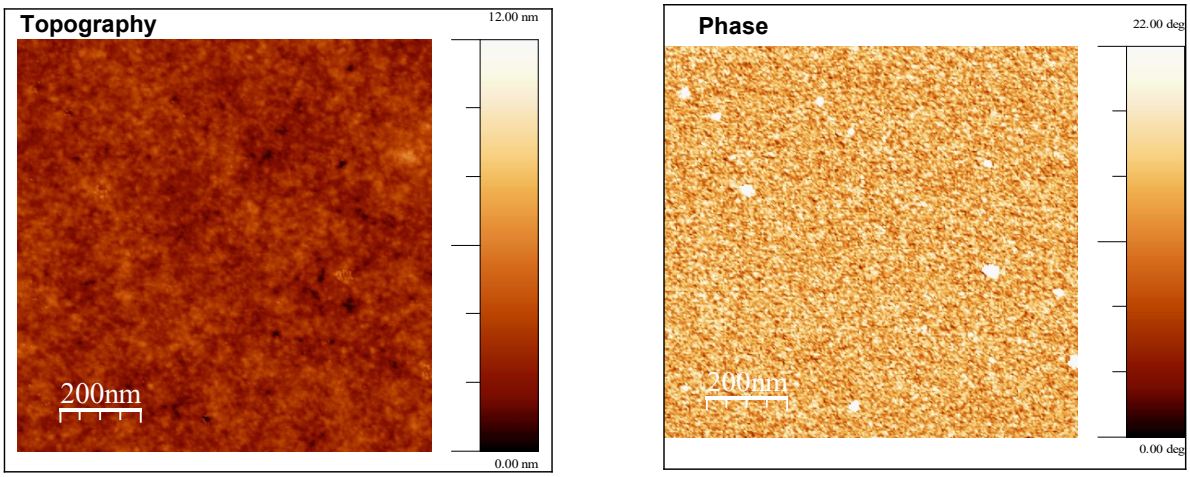

Figure 5.3. AFM topography and corresponding phase image of ~30 nm Nafion sample a) before and b) after Co exchange.

5.3.2. Effect of thermal annealing and liquid water exposure

In a set of early experiments, to achieve the Co exchange, when the Nafion films (dried at 40 °C in vacuum oven) were exposed to Cobalt sulfate solution, often they floated away. We discovered that if the films were annealed at high temperatures and then exposed to Cobalt solution for ion exchange, they remained adherent to the substrate.

Surprisingly, the conductivity measurement revealed that at higher relative humidity (RH), the Co-exchanged (Co^{2+} form) samples exhibited higher conductivity than annealed H^{+} form (or pre-exchanged) samples. We hypothesized that the seemingly counter-intuitive behaviour of Co^{2+} exchanged ionomer films exhibiting higher conductivity occurred due to differences in the pre-treatment of the two samples. The ionomer film samples during Co^{2+} exchange process are exposed to aqueous solution which can relax the structure and plasticize the ionomer. On the other hand, H-form samples were not exposed to liquid water. In a previous study from our group, it was observed that the water uptake and ionic conductivity of annealed ionomer thin films dropped

significantly upon thermal annealing at 160ºC [51-52]. However, when the same annealed sample was exposed to liquid water overnight, the conductivity could be nearly recovered to the pre-annealed conductivity level [53], [68]. Whereas our protocol in the previous studies [53] was to dry film at 40 °C, we carried out a systematic study to examine the impact of thermally treating the films on their conductivity at 30°C over a wide range of relative humidity. The set of experiments carried out in developing the protocol for ensuring similitude of hygrothermal history of samples is depicted in Figure 5.4a.

To decouple the effect of Co exchange on the conductivity of the ionomer films from that of the liquid exposure of annealed films, a set of experiments were carried wherein the H^+ form of films, annealed at 160ºC, were exposed to liquid water for the same period of time as that for exposure in cobalt solution. This comparison is presented in Figure 5.4b. It can be noted that the ionic conductivity of Co-form of Nafion is lower than the Ionic conductivity of water exposed but higher than annealed H- form of Nafion. For all films, it was observed that upon liquid water exposure, the 160ºC annealed film almost recovered the conductivity equivalent to that of unannealed ones. Thus, exposure of annealed Nafion films to cobalt solution has two opposing effects. The liquid water relaxes and plasticizes the polymer allowing higher water uptake (compared to annealed films) in subsequently dried films whereas the Co exchange results in lower ionic conductivity compared to un-exchanged or proton-form of films.

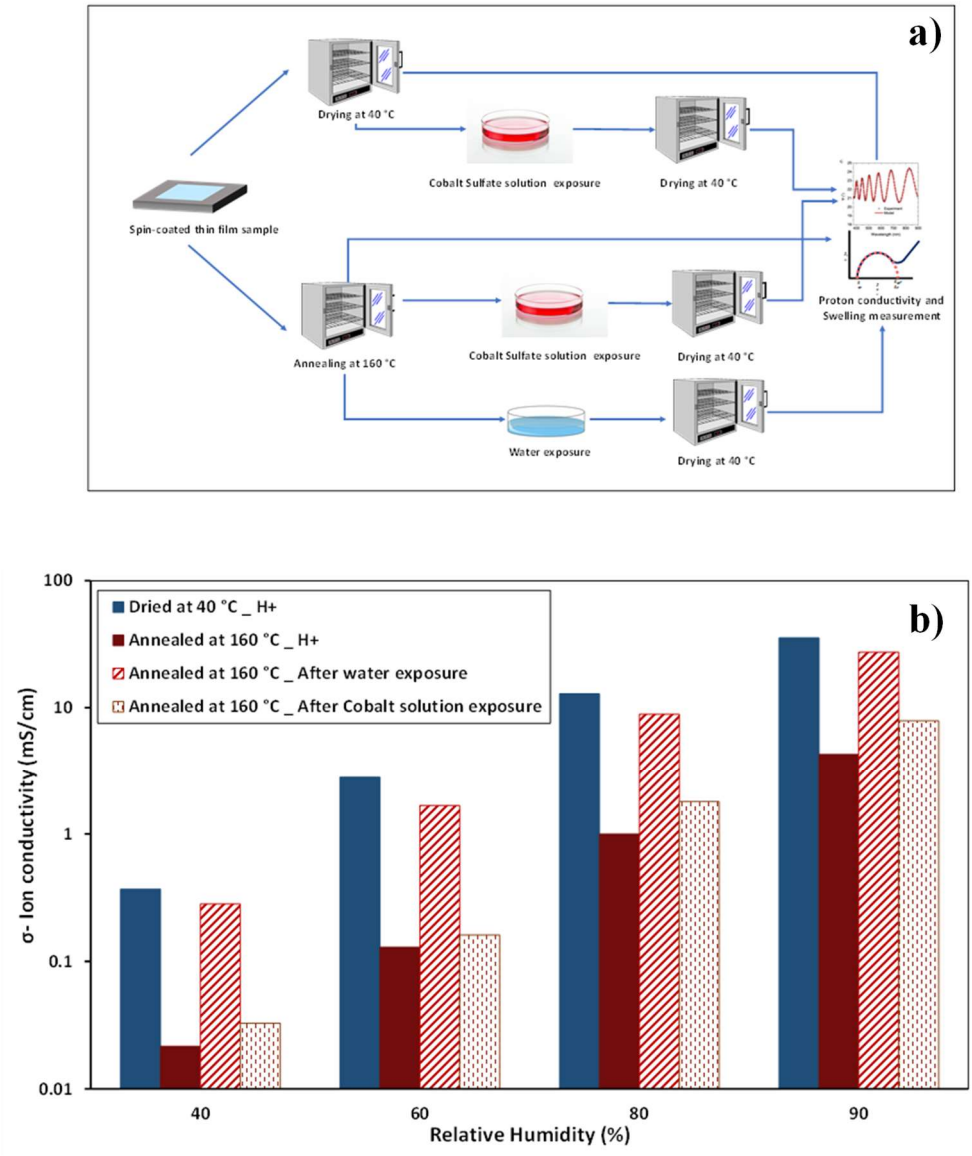

Figure 5.4. a) Schematic depiction of different film treatment conditions and film characterization applied. b) Ionic conductivity of 30 nm Nafion film measured at 80 °C at various relative humidity (RH) and thermal treatment for H^+ form and Co^{2+} form sample.

These results affirm that it is essential to compare the Co-form of ionomers with water exposed H-form of ionomers. For the rest of the paper, all comparison between H-form and Co-

exchanged films are made between liquid water exposed and Cobalt solution exposed samples, respectively.

5.3.3. Ionic conductivity of H^+ form and Co-exchanged Nafion thin film

The ionic conductivities of H^+ form and Co-exchanged thin films of Nafion as a function of relative humidity at 80 °C were measured. As expected, irrespective of the cation type, the ionic conductivity of Nafion increased by increasing the relative humidity. It can be noted that Co – exchange expectedly results in a systematic reduction of ionomer's conductivity at all RH values (Fig 5.4b). As can be seen, the percentage decrease in ionic conductivity ranges ~40% at high RH (90% RH) to nearly 99% at 40%RH.

5.3.4. Water uptake of H^+ form and Co-exchanged Nafion thin film

It is well-known that water content of ionomers affects its ionic conduction strongly and in several different ways. It affects the dissociation of sulfonic acid and thereby the 'effective' concentration of mobile ions. The intrinsic mobility of the ions is also a function of water content. Further, the shape/size and connectivity of the ionic domains/channels water affects the long-range ion transport. These factors will also affect the ionic transport of cation-exchanged ionomers. Thus, quantification of water content of the ionomer is important to get insight into whether the hydration level difference is the dominant factor for differences in the observed conductivity. In this work, the water content of the film has been determined from the RH-dependent swelling data measured by ellipsometry. Assuming that the polymer matrix density is constant, the thickness change due to water sorption can be used to determine the mass change, which can be then used to compute the number of water molecules per protogenic group (i.e., SO_3^- for PFSA ionomer; and SO_3^- and NH – SO for PFIA ionomer) or the water content parameter (λ).

Figure 5.5a shows the water content (λ) of Nafion film measured at 30 °C as a function of RH. Two sets of measurements are reported. One set corresponds to the water content for annealed film subjected to water exposure (H^+ form) and the second set refers to film subjected to Co exchange (Co^{2+} form). Both films were vacuum dried at 40°C after water/solution exposure. As can be seen in Figure 5.5a, the water content of Nafion films is generally higher in H^+ form samples than in Co^{2+} form, but these differences widen as RH increases. The presentation of complete set of data makes it difficult to discern the impact of equivalent weight and ionomer structure (side chain structure). Accordingly, results at a single RH examining the effect of EW and H^+ or Co^{2+} is discussed later. A number of theoretical ideas have been put forth regarding the hydration behaviour of PFSA ionomers as summarized in recent review by Kusoglu and Weber [31]. ^1H NMR investigations have revealed that three different regimes dependent on "state" of water exists [166]. This has also observed to be true for Nafion thin films as discussed by Karan [30] who reanalyzed the only reported NMR measurement on Nafion thin films [141] but considered the more recent water content data. Bound water is expected to be present at $\lambda < 2$, exchanged water up to λ of 4-6, and free water at λ above 7. If ionic cluster model is considered wherein clusters of SO_3^-/ H^+ ion-pairs exist in the clusters or domains, then it is thought that the initial water uptake is driven by tendency to form hydration shell around the H^+. Thus, water uptake under such conditions is driven by enthalpy of hydration of the ions. At higher RH, after the primary hydration shell is formed, the water uptake is driven by entropic effects. In an early but seemingly obscure work, Dolar et al [167] had analyzed the RH-λ data to extract the free energy of hydration of ionic clusters. Here, a distinction must be drawn between the energy of hydration of ions, which is the energy of gaseous ions dissolved in excess water (infinite dilution), and the energy of hydration of ionic clusters. In the former, the reference energy is that of free ion (without any counter ion) and

liquid water. In the latter, the reference energy is that of ionic cluster comprising the anion (SO_3^-) and the counterion or cation (H^+ or CO^{2+}), wherein the electrostatic interaction between the anion and cation exists in the dry state and is disrupted by the addition of water, considered to be in a condensed state.

We have employed a similar approach as that of Dolar et al [167] to determine the free energy of hydration of ionic cluster calculated at different RH for H^+ - and Co^{2+} - form of ionomers:

$$\Delta\bar{G}_{SW} = -RT \int_{a_{H_2O}\to 0}^{a_{H_2O}} \lambda_{H_2O} \cdot d \ln a_{H_2O} + RT\, \lambda_{H_2O} \ln a_{H_2O} \quad (5.2)$$

where, $\Delta\bar{G}_{SW}$ is the Gibbs free energy of swelling of the water (kJ/mol), R is the universal gas constant, T is the temperature and $a_{H_2O}$is the water activity.

$\Delta\bar{G}_{SW}$ of Nafion was plotted against λ_{H_2O} (Figure 5.5b). As can be seen, the Gibbs free energy change of water absorption is negative. $\Delta\bar{G}_{SW}$ decreases by increasing λ, and it increases after Co exchange which is similar with other reports [57], [58], [168] and comparison of hydration Gibbs free energy change for different form of ionomers (i.e. proton form and Co form of ionomers like Nafion) shed light on the interaction of water with ionic moiety Co^{2+}/H^+ or ionic cluster of $SO^-_3H^+/(SO_3)_2^-Co^{2+}$. Above 60 % RH, for both H-form (λ ≈ 7) and Co-form (λ≈ 4-5) of ionomers, the water uptake increases rapidly and the ionomer thin film swelling increase with increasing RH is high. Correspondingly, the free energy change of water sorption increased only slightly which is consistent with the completion of hydration of ion-pairs and transition to free water state for the added water[140], [168]. At a given λ, the Gibbs free energy change for hydration is higher for H^+ form of ionomer compared to Co^{2+} exchanged form, indicating stronger affinity of water to H^+ than to Co^{2+} in Nafion (Figure 5.5b).

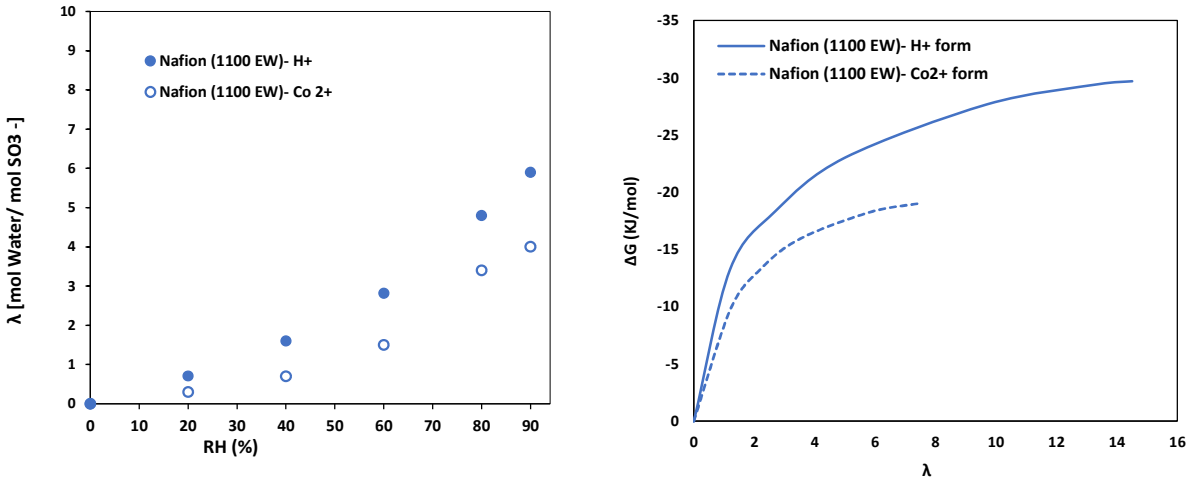

(a) (b)

Figure 5.5. a) Water uptake (λ) of 30 nm Nafion thin film at 80 °C as a function of relative humidity. b) Free energy of swelling ($\Delta\bar{G}_{SW}$) as a function of λ for 30 nm Nafion thin film.

It must be noted that the hydration enthalpy of cations play an important role for ionomer's water uptake, especially for monovalent cations. Cations with higher hydration enthalpy are less hydrophilic, which implies that they form weaker bonds with water molecules resulting in lower water uptake of ionomer films[169]–[172]. For ionomers exchanged with divalent cation (Co^{2+}) the charge density (z/r_c) of cations plays an important role in water uptake and other dependent properties. At low RH, the "bound water" exists and its mobility is restricted and as such the difference between proton form and Co^{2+} form of the ionomer is small and it indicates that the initial water uptake is less effected by Co^{2+} cation size which agrees well with the results reported in Shi et al's work [81]. On the other hand, at high RH water content increases and the system enters the "free water" regime wherein ions (like protons) can transport freely through the water channels. Larger cation (Co) form stronger pairs with sulfonate groups. Thus, there is a competition between the sulfonate group and water to interact with Co^{2+}. Hence, the result would be stronger electrostatic interaction which would lower the cation's mobility [173]–[175]. The

smaller water content results in smaller cationic mobility too. These two factors cause a reduction in ion conductivity in ionomers after Co exchange [46], [58].

5.3.5. Effect of ionomer equivalent weight and structure

The ionic conductivity of PSFA and PFIA ionomers before and after Co exchange are compared in Figure 5.6a. Irrespective of ionomer type and ionic moiety (PFSA vs PFIA), as expected, ionic conductivity increases with an increase in relative humidity. Consistent with prior membrane studies [36], [37], [58], [81], [152], [159] and the recent ionomer thin film study [165] comparing ionic conductivity of H^+ and Co^{2+} forms of PFSA, we also observed significant reduction in conductivity of Co^{2+} form compared to H^+ form at all RH. PFIA has the highest conductivity among all tested ionomers in both proton and Co form. On the other hand, Nafion has the lowest conductivity in both form of ionomers. To investigate the effect of EW of ionomers on ionic conductivity, ionic conductivity of ionomers in proton and Co form are compared in Figure 5.6b. As expected, ionomers with lower EW have higher conductivity in proton and Co form. at low RH (Figure 5.6b), we observed conductivity differences between proton and Co form of ionomer is higher (two order of magnitude higher in proton form) at low RH and these differences is smaller at high RH (two to three times higher in proton form) (Figure 5.6b). It is known that ionic conductivity is dependent on water content.

The ionic conductivity of ionomers increases with a decrease in the EW, i.e. an increase in the sulphonic group content. PFIA (620 EW) ionomer exhibits the highest conductivity. For the ionomers with similar EWs, e.g. ~830EW (3M EW 825 and Aquivion 830) and ~1000 EW (3M 980 and Acquivion 1000), 3M ionic conductivity is slightly higher than Aquivion conductivity. Nafion and 3M ionomers have similar EW but at the same RH, 3M ionomer has a better performance, and it comes from its different side chain structure (Aquivion has the shortest side

chain (SSC)length and Nafion hast the longest side chain (LSC) and 3M known as the medium side chain (MSC) length ionomer). After Co exchange, the conductivity of all ionomers is reduced. However, PFIA exhibits the least suppression in conductivity after Co^{2+} exchange. The conductivity suppression at 90%RH at 30C for PFIA is lowest at ~40% and highest for Nafion at ~85%. For ionomers with EW lower than 800, PFIA shows better performance compared to the 3M. For ionomers with EW higher than 800, 3M and Aquivion exhibit similar performance, and they are better than Nafion. All these behaviours are because of their differences in sidechain structure.

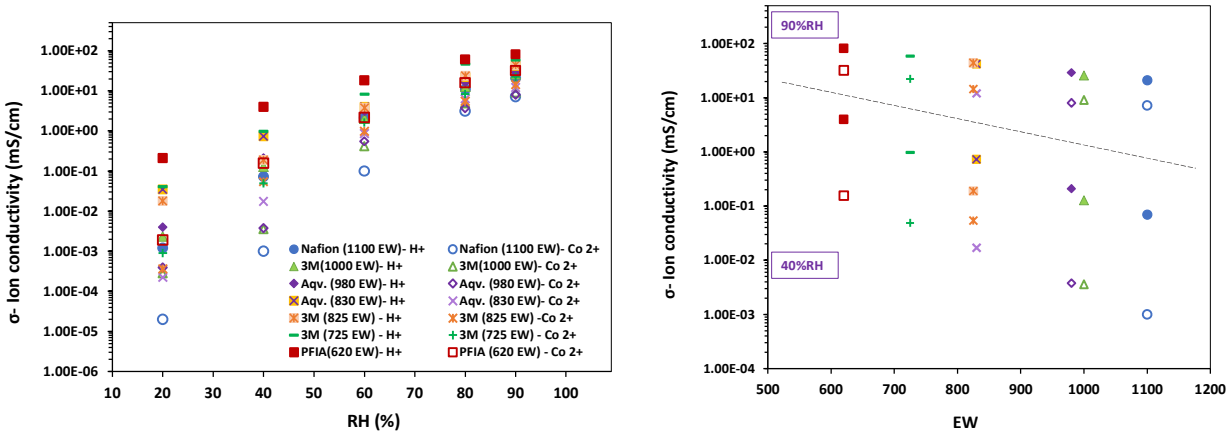

(a) (b)

Figure 5.6. Figure 5.6. Ionic Conductivity at 80 °C of ~30 nm ionomer thin films before and after Co exchange as a (a) function of relative humidity (RH), (b) function of equivalent weight (EW) at low RH (40% RH) and high RH (90% RH).

The differences in conductivity at a given RH for ionomer with different EW can arise from the differences in water content, λ. Accordingly, we determined λ of all ionomers over a range of RH in Figure 5.7. As expected, the water content of the ionomers increases with an increase in the RH. PFIA has higher water content than the other ionomers in both proton and Co

forms of the ionomers (Figure 5.7a). It is interesting to note that at low RH, the differences between water content of the ionomers are very small (negligible) (Figure 5.7b) while the differences in conductivity at similar low RH was high (Figure 5.6b). On the other hand, at high RH the differences in λ is larger compared in contrast to the conductivity, which were close to each other at high RH.

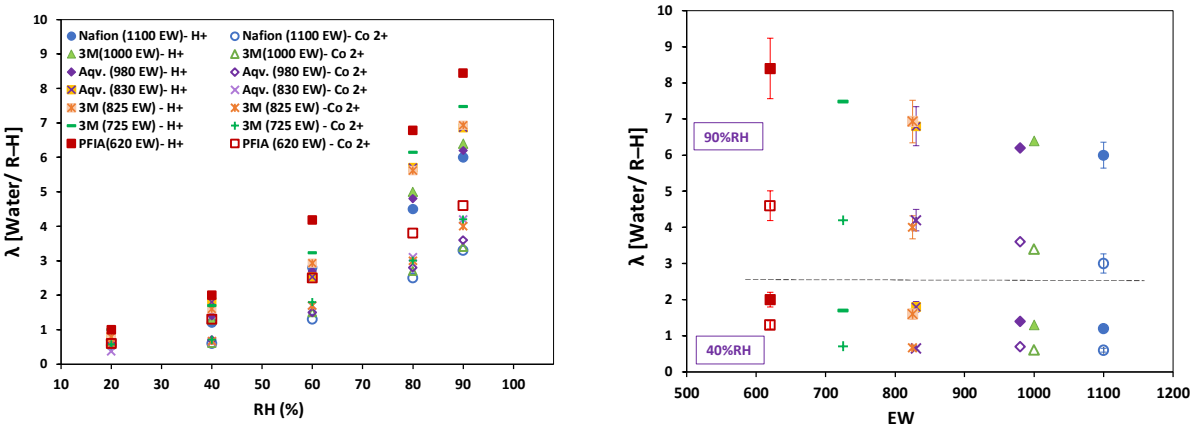

(a) (b)

Figure 5.7. Water uptake at 80 °C of ~30 nm ionomer thin films before and after Co exchange as a (a) function of relative humidity (RH), (b) function of equivalent weight (EW) at low RH (40% RH) and high RH (90% RH)

5.3.6. Discussion

Consistent with prior membrane studies and, also, with the recent ionomer thin film studies, significant differences between the H^+ and Co^{2+} forms of PFSA was observed with a significant reduction in conductivity of Co^{2+} form compared to H^+ form at all RH. The complementary measurements of ionomer swelling revealed lower water uptake for Co^{2+} form compared to H^+ form. Thus, qualitatively one can deduce that lower ionic conductivity is due to lower water uptake of the ionomer films. The question then arises is whether the two different forms have similar

conductivity at comparable water content. If so, the water content could be deemed to be the main determinant of the ionic conductivity of these systems. Accordingly, we have plotted the conductivity of H^+ form and CO^{2+} form of ionomer thin films as a function of the corresponding water content (λ) (Figure 5.8). Two interesting observations can be made from the data. First, the large differences in ionic conductivity for unexchanged ionomers (H^+ form) at any specific RH as noted in Figure 5.6a appear to be less so when plotted as a function of water content. Second, although significant decrease in conductivity of PFIA ionomer thin film was noticed after Co exchange, this difference also appears to be less prominent when expressed as a function of water content.

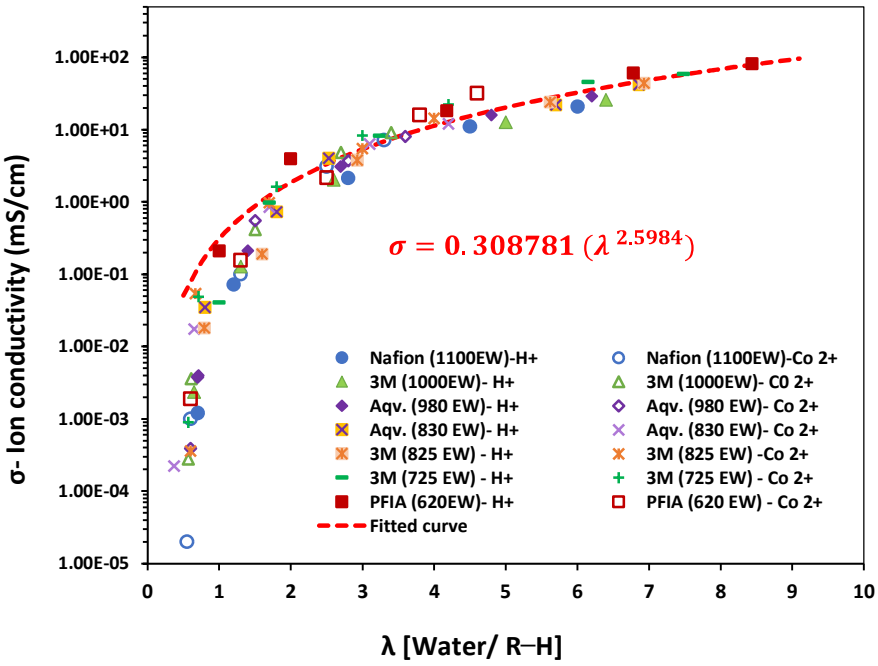

Figure 5.8.Ionic Conductivity at 80 °C of ionomer films, before and after Co exchange as a function of water content (λ).

The ionic conductivity-water content relationship reveals that lower conductivity of Co^{2+} exchanged ionomer is lower than H^+ form ionomer films due partially to lower water content of Co-exchanged ionomer. However, at lower RH significant differences in conductivity is noted at similar water content, indicating the influence of other parameters which may arise from differences in ionomer makeup. It has been shown [31] that domain-spacing of ionomers are also affected by the ionomer molecular structure. The differences in domain spacing may influence geometric factors such as tortuosity of the hydrophilic domains. The effective ionic conductivity can be expressed as a product of three factors: mobile species concentration, mobility of the ionic species, and a morphological factor accounting for the volume fraction (ε) and tortuosity (τ) of the conducting phase. Of these three factors, two of them – mobility and ε/τ – depend on the water content. The mobility is expected to have a complex relationship with water content. At lower water content, the cation/anion pair would be strongly attracted to each other and lower the effective concentration of mobile cation. At higher water content, the ions would be dissociated but also have increased size due to hydration shell. The ε/τ would increase since the water volume fraction would increase and with an increase the connectivity would improve resulting in decrease in tortuosity. If for simplicity's sake, we consider that the network of hydrated channels for both H^+ and Co^{2+} are similar, then at a given water content (water content per SO_3^-), the differences in conductivity could be attributed to the product of mobility and effective concentration of mobile ions. The data of Figure 5.8 is plotted for selected ionomers to examine this hypothesis. Since, experimentally, the controllable variable is RH and not λ, we plot the conductivity for H^+ and Co^{2+} forms of the ionomer thin films at integer values of λ for ionomers (Nafion, 3M and Aquivion and PFIA). We note that the conductivity of H^+ is clearly more than three times that of Co^{2+} form. This implies that conductivity reduction is not merely due to decrease in concentration of mobile ions

but likely to the differences in the mobility of cations. At higher λ, it may be expected that the cations are dissociated from the counter-ion. However, the mobility at comparable λ would still be different since the complete hydration of cations and their mobility differ.

To investigate the ionic conductivity of Nafion thin film in proton form and Co form at different temperature, the ionic conductivity reported by Han et al at different temperature [165] and this work data were plotted in Figure 5.9. It was shown that our data and its trend is in a good agreement with Han et al data. Ionic conduction at different temperature and Co contamination level could use to have Arrhenius plot, for calculating the activation energy of proton conduction associated with the proton conduction mechanism (Slope of Arrhenius plot). The activation energy for 30 nm Nafion thin film in proton form at 90% RH was found to be 17.35 kJ/mol which is higher than the reported activation energy for Nafion membrane (9-15 kJ/mol) [31], [53], [65], [66] and may be attributed to the confinement effect in thin films that cause reduction in proton mobility [30], [31]. The activation energy of Co form of the Nafion was found to be 25.6 kJ/mol and is higher than the proton form because the Co ion is bound to sulfonic acid group more tightly and it cause an increase in activation energy and a change in ion transport mechanism in Co form. Han et al. reported the activation energy for 40 nm film at proton form and cobalt form to be 17 kJ/mol (in proton form), 20 kJ/mol (at 73% contaminated with Co) and 27 kJ/mol (at 86% contaminated with Co). Our results are in good agreement with their findings.

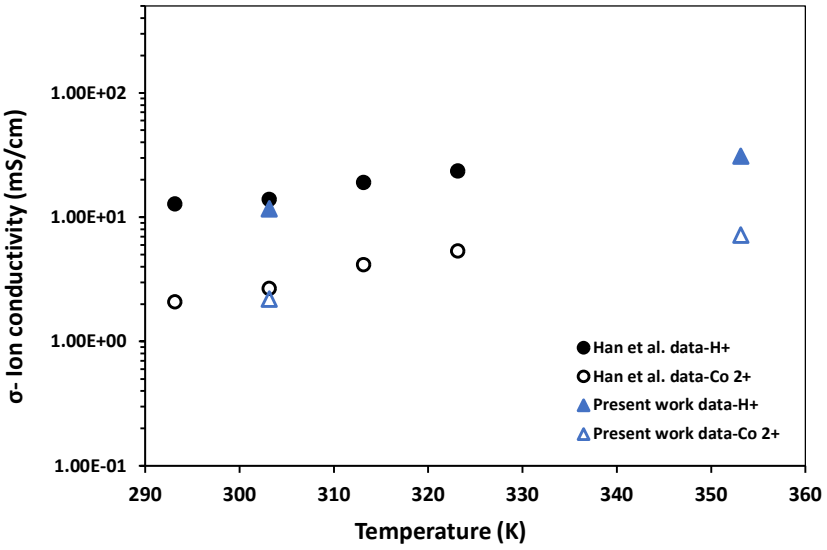

Figure 5.9. Comparison of ionic Conductivity of Nafion films in proton and Co from as a function of temperature, based on the reported values of 40 nm Nafion film at C(H+) in M= 0.28 from Han et al. [165] and 30 nm Nafion film this work.

We also compare the RH-dependency of catalyst layer ionic conductance and membrane conductance reported by Cai et al. [152] with RH-dependency of 30 nm Nafion thin film from the present work. It is noted that CL ionic conductivity cannot be easily defined [117] since the ionomer distribution is non-homogeneous through the CL including variation in the ionomer film thickness [160]. The thickness-dependency of water content and proton conductivity implies that an average thickness or property cannot be assigned. In contrast, the ionomer films in the present study are continuous and of well-defined thickness. Nonetheless, we thought it would be interesting to examine the differences and similarities in the CL ionic conductance (and membrane ionic conductance) and ionomer thin film conductivity. From Figure 5.10 below, we can note that the RH-dependency at lower RH for thin films (present study) is quite strong compared to that reported for CL ionic and membrane ionic conductance. At higher RH, the RH-dependency (slope

of the plots) are similar. The extent of suppression of conductance upon Co^{2+} exchange reported by Cai et al is much larger than that observed for thin films. Note that our results for suppression of ionic conductivity of thin films are very similar to that observed by Han et al (Figure 5.9). The origin of these differences can only be surmised at this point and may be due to the vastly difference microstructural characteristics, such as ionomer connectivity and discontinuous films in CL as well as nanoscopic structural differences induced by the substrate (Pt and C substrate in CL versus SiO_2 substrate used for thin film studies.

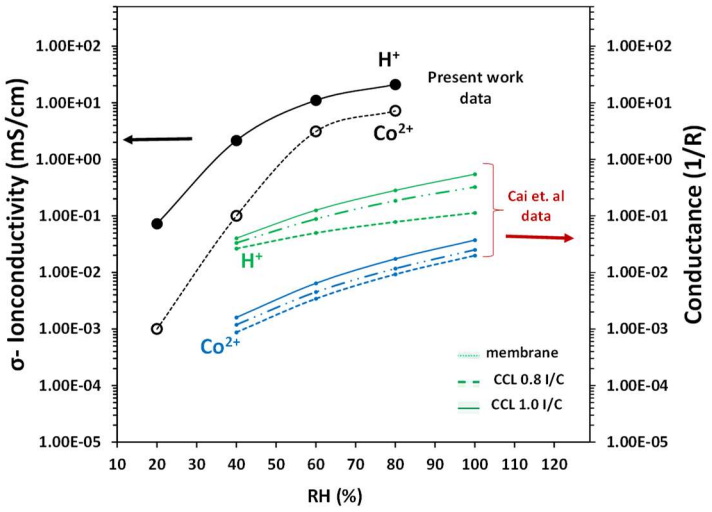

Figure 5.10. Ion conductivity of 30 nm Nafion thin films (this work) and ionic conductance (1/R) of catalyst layer and membrane reported by Cai et al. [152] as a function of RH .

5.4. Conclusions

This study provides interesting insights on the effect of Co contamination on hydration dependent properties (ion conductivity and water uptake) of PFSA and PFIA ionomer thin films (30 nm) with different equivalent weight (EW)(620 to 1100 g/mole of sulphonic acid) and side-chain length at 80 ˚C.

The ionic conductivity of ionomers thin films was measured using impedance spectroscopy. The changes in ionic conductivity in all ionomers showed similar behaviour. All ionomers exhibited suppression of ionic conductivity by Co contamination (a decrease of over two orders of magnitude at low RH), consistent with the earlier studies. The new insight provided from the present study is thar this suppression in conductivity arises from the suppression in water uptake of the ionomer films upon Co^{2+} exchange. RH dependent swelling measurement revealed lower swelling, i.e. lower water uptake, of ionomer films upon Co^{2+} exchange. Our study also highlighted that thermal annealing and liquid water exposure can dramatically impact the conductivity of the films. Thus, it is important when comparing conductivity and water uptake of H+ form of films with Co^{2+} form of ionomer films to subject the films to similar hygro-thermal pre-treatment. Co^{2+} has a larger impact on hydration dependent properties of ionomer thin films at lower RH. The impact was lower for PFIA ionomer than PFSA ionomer and is attributed to different side chain structure of PFIA ionomer, which has two acid sites on its side chain. In conductivity – water uptake relationship, the differences between H+ form and Co^{2+} form of ionomer films becomes less when the water content increases. Accordingly, a new universal relationship for ionic conductivity and water content of the ionomer films is introduced in this work.

Chapter Six: Water Sorption in Ionomer Thin Films: Investigation of Substrate and Hysteresis Effects

6.1. Introduction

Ionomer, carbon support and *Pt* catalyst are three main component of catalyst layers (CLs) in a fuel cell. Ionomer thin films play an important role of facilitating ion transport within the CL and between the membrane and the CL [22], [23], [68], [176]. Ion transport is strongly dependent on water content of the ionomer. Water is fed to the fuel cell system via humidified gases is also produced at the cathode via oxygen reduction reaction [177]. Water in the feed gases are transported through gas diffusion layer (GDL), catalyst layer (CL), ionomer and finally from electrode to the membrane where acts as a charge transport vehicle (Figure 6.1) [178]. The kinetics of water absorption/desorption in ionomers in fuel cell is of particular interest for fuel cell operations [115], [179]. Since the early work by Siroma and co-workers [66] reporting the decrease of proton conductivity with decreasing Nafion film thickness, studies on the relationship between interfacial structure of PFSA ionomers and proton transport properties have increased. It is now acknowledged that the ionomer thin film transport properties are influenced by the interaction between the ionomer and the substrate [56], [68], [70], [180]. Studies on ionomer films with thickness less than 100 nm on different substrates have been reported [30], [31], [187], [52], [68], [181]–[186]. Different techniques like Neutron Reflectometry [188]–[192], GISAXS [67], [68], [132], [183], FTIR [193], [194], Ellipsometry [68], [118], [183], [195]–[197] and QCM [54], [68], [182], [189], [195]–[197] and even coarse-grained molecular dynamics simulations [198] were used.

There are significant reports of the investigation of the properties of Nafion thin film (less than 100 nm) supported on Si and SiO_2 substrates [54], [66], [67], [69], [132], [199]. However, there have been questions about the relevance of these measurements to fuel cells where precious metal and carbon are used as catalyst part and ionomers are in contact with these catalytic substrates. It was observed that the morphology of ionomer depends on the substrate [68], [183], [190], [180]. Other studies investigated the effect of hydrophobicity of the substrate on water uptake and morphology of ionomer thin films [183], [195]. They found that the thin films on hydrophilic substrate absorb more water compared to the films on hydrophobic substrate [186], [187].

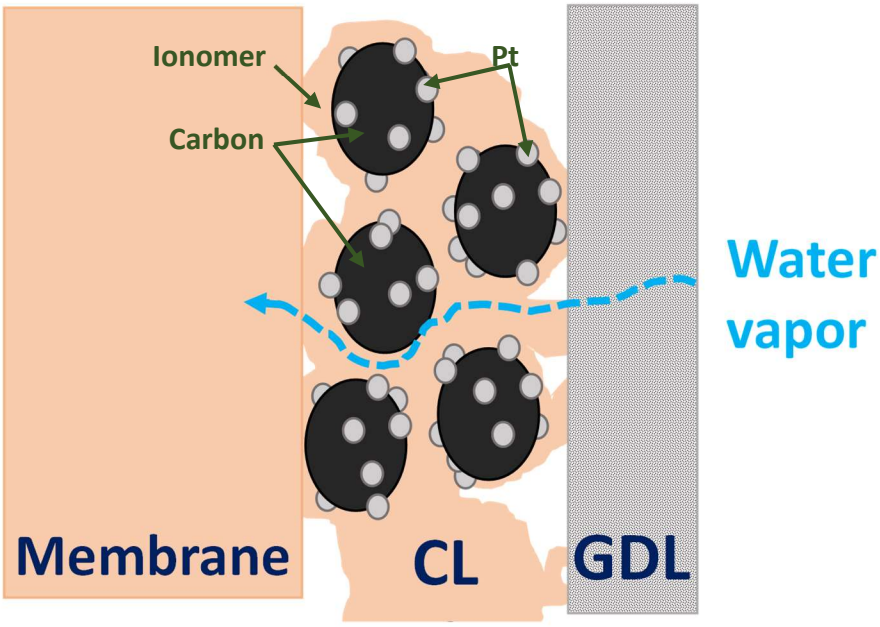

Figure 6.1. Schematic of the water vapor pathway.

Water transport through Nafion membrane has been investigated for decades by different methods [179], [200]–[202]. Reported diffusion coefficient using different methods varied by order of magnitude depend on the method of measurements like steady state permeation, NMR

diffusion or dynamic water uptake/loss. Majsztrik et al. provide an excellent summary of reported diffusion coefficient and trends for membrane [177]. Satterfield et al. discussed that effect of activity and phase of water on the permeation and sorption and indicated that the effective water permeability may be limited by interfacial mass transport, diffusion, or polymer swelling dynamics [203]. Majsztrik et al.[177], [204] found that the effective water diffusion coefficient decreased with decreasing water activity, causing diffusion to become rate limiting at low water activity. However, despite the number of studies were focused on Nafion membrane, there are limited number of studies on water diffusivity in Nafion thin film. Eastman et al. [132] studied Nafion thin films (20 - 222 nm), they found that the water sorption in thin films (< 60 nm) is thickness dependent and confinement effects are more dominant than interfacial effects [132]. Davis et al. [205] measured water sorption and diffusion in a Nafion thin film using in-situ polarization modulation infrared reflection absorption spectroscopy (PM-IRRAS), they found that the interfacial mass transport limitation is minimal and water diffusion coefficient in thin films was 4 – 5 order of magnitude lower than bulk membrane and was dependent on the initial hydration state of the Nafion [205]. This study was opposed to the other studies that find water transport as mainly governed by interfacial mass transport [132], [182].

Nevertheless, nearly all recent studies were restricted to one ionomer (Nafion) and to thickness of more than 20 nm (except one study on 4 nm self-assembled Nafion [68]). For better understanding of the relationship between ionomer properties and hydrophobicity of the substrate and ionomer /substrate interaction, we need to extend our study in length scale of 10 nm for different ionomers with different structure to provide us an insight into the effective factors on CL transport resistance. The main goal of this chapter is to investigate the substrate (SiO_2, Carbon and Pt) effect on morphology and properties of ionomer (Nafion, 3M, Aquivion) thin films (~10 nm).

More specifically, the effects of wetting property of the substrates (hydrophilicity/hydrophobicity), and operating condition (temperature and RH) are investigated in determining the morphology, wettability and water uptake of the ionomer thin films and at the end, the water diffusion coefficient in CCL thin films (10 nm films) was investigated to see what would control it and quantify the effect of water activity in ionomer on water diffusion[206] .

6.2. Experimental

6.2.1. Materials

In this work, three different ionomers, Nafion dispersion - EW1100 (Ion Power Inc. (USA)), the 3M PFSA-825 EW (3M Fuel cells Component Group, MN, USA) and Aquivion – 830 EW (Solvay Company (Italy)) were investigated. All ionomers were used to make diluted (0.2wt. %) solutions using isopropyl alcohol (IPA) (Sigma Aldrich) to have desired ionomer thin film thickness with spin coating method. The diluted dispersion was placed at room temperature for 24 hours for equilibrating and after that sonicated to make sure that the dispersion is homogenous and ready to use. Substrates including silicon with native SiO_2, C and Pt were used in this work. For C and Pt, a thin physical layer of the respective materials has been deposited on the silicon wafer. Pt substrate was obtained from NINT, Alberta and Carbon substrate was prepared, optimized, and characterized in house.

6.2.2. Substrate cleaning and Film preparation:

The SiO_2 and Pt substrates were soaked into acetone for 30 min, followed by 2 min sonication in each of the following solvents: IPA, acetone, and DI water. At the end, they were washed with IPA, acetone and Millipore water, then dried by N_2 blow for a few min and kept under UV light at O_3 atmosphere for 30 min and made them ready for ultrathin film preparation on them.

The substrate with carbon layer were gently washed by IPA and dried by N2 blow before UV light at O_3 atmosphere.

After cleaning the substrates, the ~10 nm thin films were prepared using spin coating. The diluted in IPA (0.2% wt) ionomer solutions were deposited on substrates using spin-coating (at 5000 rpm for 30 Sec). Then, Samples were dried at vacuum oven at 40 C for 24 hours. The water uptake and conductivity measurements were done immediately after samples were removed from vacuum oven to minimize the aging effects.

6.2.3. Film characterization

In this work, the surface morphology, roughness, and film thickness of the ionomer thin films were examined by AFM while wettability of the thin films were studied by water contact angle measurements. The proton conductivity of thin films on Carbon and Pt has not investigated due to the conductive nature of the substrate. However, the water uptake of the thin films was measured using Quartz Crystal Microbalance (QCM) and Ellipsometry techniques.

6.3. Result and discussion:

6.3.1. Surface wettability by water contact angle measurement:

For the surface wettability characterization, contact angle measurements (via Goniometer) with water were used. Water contact angle can be used to quantify the hydrophilicity (θ <90 degrees) and hydrophobicity (θ >90 degrees) of the surface. Based on the value of water contact angle, the ionomer thin films and substrates can be classified into three categories: a) hydrophilic b) hydrophobic, and c) intermediate. The water contact angle of the blank substrates and ~10 nm ionomer thin films on different substrate were measured and shown in Figure 6.2.

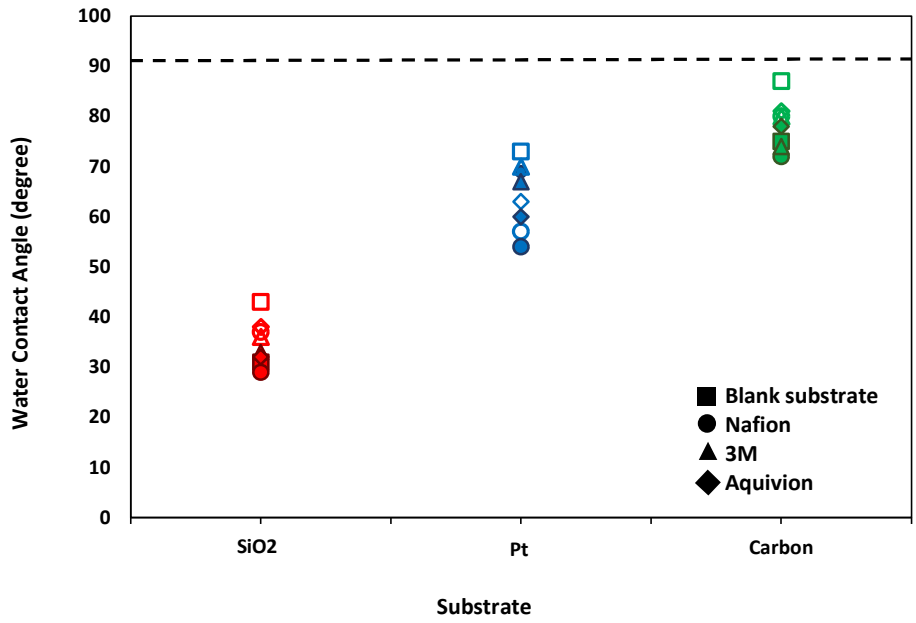

Figure 6.2. Water contact angle of ~10 nm ionomers (Nafion, 3M and Aquivion) thin films on SiO_2, Carbon and Pt substrate. squares, blank substrate; circles, Nafion thin film; triangles, 3M thin film; and diamonds, Aquivion thin films. Open symbols are as prepared samples (dried at 40 ^oC in vacuum oven); solid symbols are samples after experiencing high temperature (80 ^oC) and high humidity (90% RH).

As we expected, the substrate dependency of the water contact angle of ionomer thin films was observed as presented in Figure 6.2. Water contact angle of all ionomers on all substrate decreases after experiencing high humidity (90% RH) and high temperature (80˚ C) indicating organization of the ionomer including the free surface. The contact angle of ionomer thin films on SiO_2 is considerably lower than the films on Carbon and Pt. The water contact angle of SiO_2 substrate was measured to be as low as 31 degrees while that for carbon and Pt were found to be 75 and ~59 degrees, respectively. lower contact angle was expected for Pt as metals are known as super hydrophilic material. This could be the result of absorption of impurities from air on the surface of the Pt substrate during the experiments. The lower contact angle of ~10 nm ionomers

on SiO_2 show that the surface is highly hydrophilic, comparable to findings by Paul et al. who reported data for self-assembled Nafion thin films (4 and 10 nm) [98] while the contact angle of 70 and 80 degrees for ionomers on Carbon and Pt substrates indicate that the surfaces of these samples are more hydrophobic (less hydrophilic). SiO_2 substrate with hydrophilic surface generated hydrophilic film surface while Carbon and Pt with intermediate (less hydrophilic compared to the SiO_2 substrate) substrate surface generated less hydrophilic film surface. It shows that the hydrophilic substrate wetting interaction have a great influence on the molecular orientation of ionomer thin films but the nature of this interaction is not fully understood. The same behavior has been observed by Mohamed et al. [184] and Paul et al. [89] examined the wettability of spin coated and self- assembled Nafion thin films on different substate, respectively, using contact angle.

Among these three ionomers, Nafion is the more hydrophilic one on different substrate and Aquivion has the highest water contact angle (less hydrophilic) on all three substrates. The wettability changes can be induced due to changes in the roughness [30], [198], [207]. Hence, the surface roughness of the films and substrates was examined using AFM. The root mean square (RMS) roughness of the films on Carbon varied from 0.27 to 0.67 nm, whereas that on Pt varied from 0.32 to 0.58 nm. Based on the RMS roughness of all ionomer film surfaces and substrates, it could be concluded that the roughness of the films do not play any significant role in the observed wettability differences. On the other hand, due to the very low thickness of the films, confinement and interfacial interactions induced organization are expected to play a role in the surface wettability of ionomers tin films on different substrate [30]. In thin films, the ionomers aggregate oriented parallel to the surface therefore the surface of the substrate dictate the level of the hydrophobicity of the thin film surface [30], [208].

6.3.2. Film topology by AFM:

The film topology investigated by AFM is presented in the Figure 6.3 below. AFM images and surface roughness of blank substrates (SiO_2, Carbon and Pt) show that the surface was smooth with negligible roughness. After the film preparation, images of films surface on different substrates were presented. It was found that the film morphology depends on substrate surface energy which SiO_2 has higher surface energy compared to the Carbon and Pt (Carbon and Pt surface energy are close to each other). the aggregation pattern or the morphology of the films changed by changing the substrate [89]. For all three ionomers, it was observed that the ionomers on SiO_2 are less aggregated compared to the films on Carbon or Pt. and this is the comparable results that Paul et al [55], [89] reported for self-assembled Nafion thin film on different substrates.

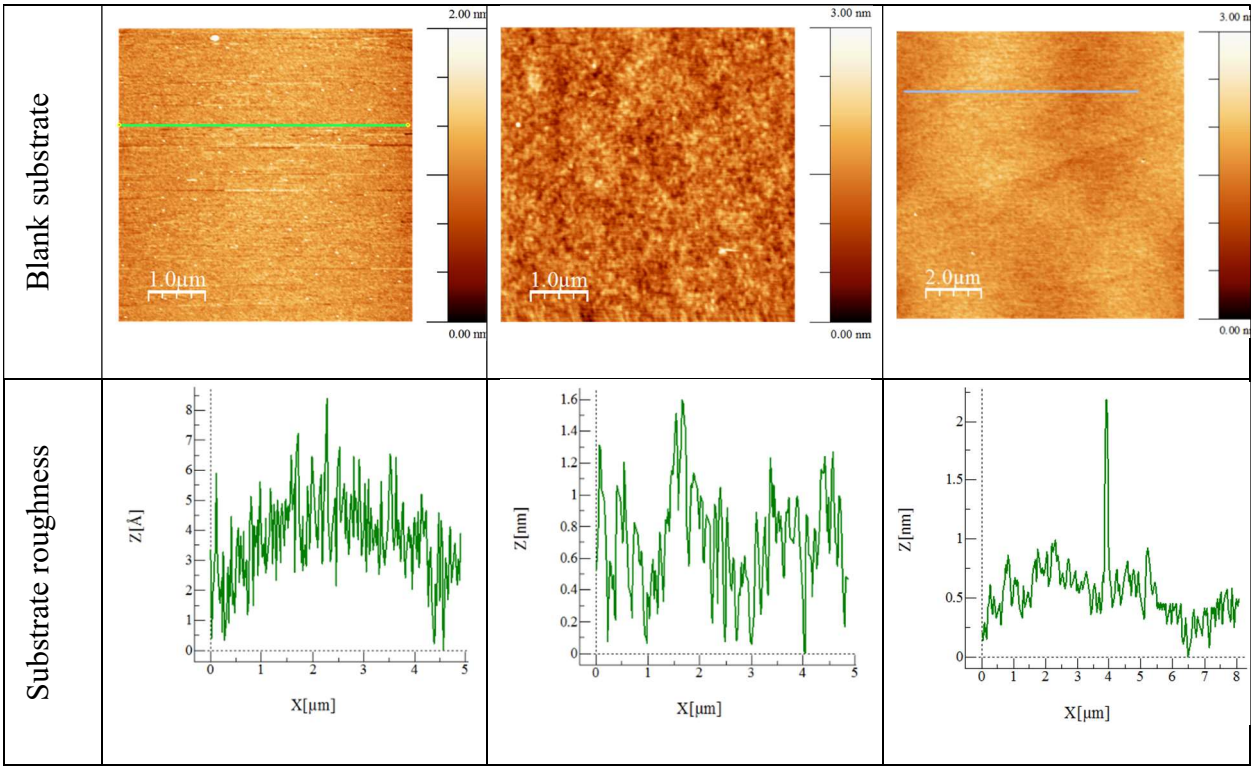

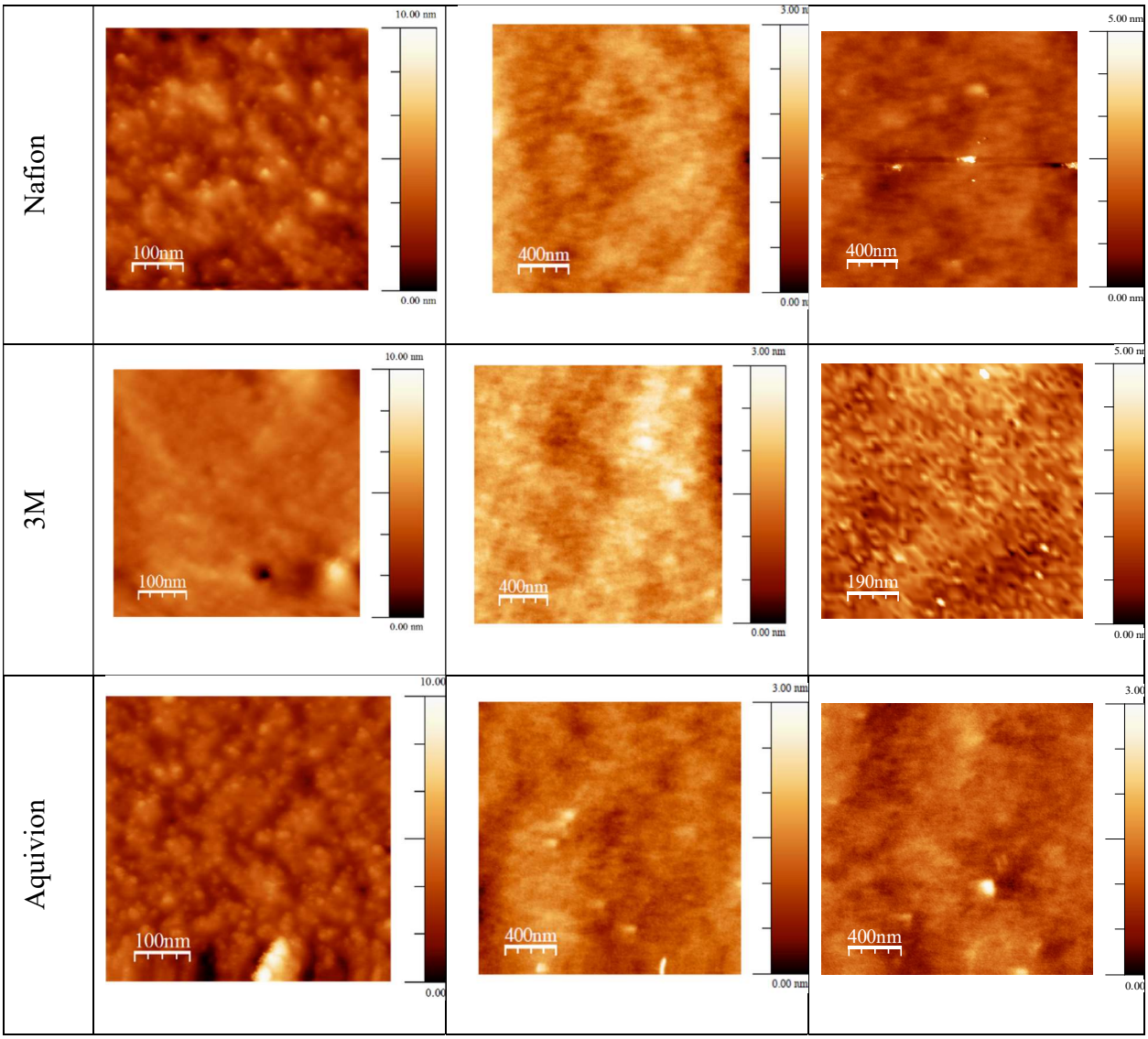

6.3.3. Substrate influence on water uptake of ionomer thin films

Swelling of all three ionomers thin film on SiO_2, Carbon and Pt were measured by Ellipsometry at 80 ˚C. The main goal of this work is to investigate whether the substrate and its hydrophilic nature could have any effect on the water uptake of ultrathin ionomer films. Figure 6.4

Figure 6.3. AFM images of (2 x 2 µm²) of blank substrate and 10 nm ionomer (Nafion, 3M ad Aquivion) thin films on SiO2, Carbon and Pt substrate.

shows the swelling of ionomer thin films on different substrate (SiO_2, Pt and Carbon) as a function of relative humidity.

It was observed that the changes in swelling of ionomers on Pt is the highest followed by films on SiO_2 and Carbon. The nominal thickness of all ionomers is 10 nm. Hence, the confinement effects would be similar for all substrates and the source of these differences comes from the interactions with the substrate and different structural organization of ionomers on substrates. Based on the proposed structural organization for Nafion thin film on SiO_2 substrate by Paul et al. [89], it is suggested that the 10 nm films of ionomers on SiO_2 substrates would be multi-lamellar films with water-rich inter-lamellar layer. The substrate wettability appears to control the film organization on substrate surface. The sulfonic groups are hydrophilic, and the Teflon backbone is hydrophobic. Hence, the backbones are expected to orient parallel to the surface. In this work, all three substrates are hydrophilic (they have different level of hydrophilicity) so, the orientation of ionomers on substrate may be similar. Therefore, the water rich inter layer will cause the differences between the water uptake of the ionomers on different substrate. Shrivastava et al [209] employed neutron reflectometry (NR) and quartz crystal microbalance (QCM) to quantify the interfacial and bulk water in ionomer thin films on Pt. Interfacial water layer for Nafion films on SiO_2 was observed by Dura et al. [190]. Hence, the differences between swelling rate of the ionomers on different substrate may partially arise from differences in interfacial water content for ionomer on different substrates. Additionally, the differences in ionomers structure and rearrangement, water network cluster size and their connectivity of ionomers on different substrate may be the cause of observed differences in the swelling rate.

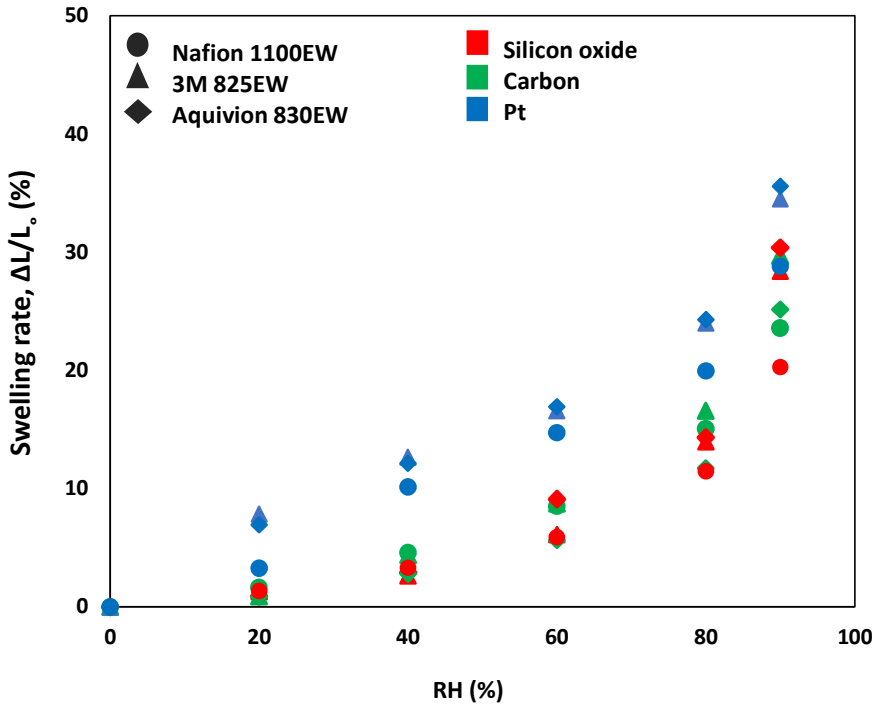

Figure 6.4. Water vapor sorption of ~10 nm ionomer thin films (Nafion, 3M and Aquivion) on different substrate (SiO_2, Carbon and Pt) as a function of relative humidity at 80 ˚C. circles, Nafion thin film; triangles, 3M thin film; and diamonds, Aquivion thin films. Red color, films on SiO_2 substrate; green color, films on carbon substrate and blue color, films on Pt substrate.

Previous studies suggested the presence of thin oxide layer on the SiO_2 and Pt surface under humidified condition [68], [210], [211]. Hence, electrostatic interactions between the hydronium ions and negatively charged oxygen atoms on the surface of substrate and sulfonic – acid moieties results in more stabled hydronium and sulfonic acid groups pair which result in more water uptake in ionomers on the surface of Pt and SiO_2 substrate [67], [68], [210], [212], [213].

By increasing the humidity, the difference in the water content for ionomers on different substrate decreased and water content of ionomers on Pt and SiO_2 substrate are found to be closer to each other at high RH (> 70% RH), specially for ionomers with low EW (i.e. Aquivion830 and 3M

825). Considering the low lambda (λ) values at low to mid RHs (up to 70% RH), the absorbed water can be considered to solvate the sulfonic group but remains as bound and exchanged water. This affects the swelling of hydrophilic domains to a small extent. 3M and Aquivion ionomers have similar swelling behavior due to the similarity of their EWs. At higher RH (more than 70% RH), swelling increases due to higher uptake of free water molecules specially for low EW ionomers because of their high sulfonic- group density.

Another interesting observation is the difference in swelling between ionomers for the same substrate. Among all ionomer thin films on substrates, Aquivion exhibits the highest change in thickness following 3M and Nafion. This is in agreement with the findings of Shrivastava et al. [209] and our previous studies about the effect of EW on ionomer thin films hydration properties. This trend was seen in all three substrates, and it shows that this correlation between ionomer structure (like side chain length) and water uptake of ionomer thin films exists in all three substrates.

6.3.4. Impact of humidity cycling on swelling of ionomer thin films

During fuel cell operations, ionomer in the catalyst layer is expected to experience different humidity during to shutdown, start-up, and variable current/load. The response of ionomer films to RH cycling with increasing and decreasing the RH several times was investigated by monitoring the film thickness during the cycles. First, a thin film under study was exposed to dry air to make sure there is no humidity in the film environment and thereby establish a baseline for dry film. Next, the humidity was increased up to 90% RH. This sequence was repeated two more times and at the end thin films were exposed to dry air for more than 12 hours (overnight) for final thickness measurement. The thickness of all ionomers thin films was measured at each step for water content calculation. Figure 6.5 shows the RH cycle protocol used for experiments and analysis.

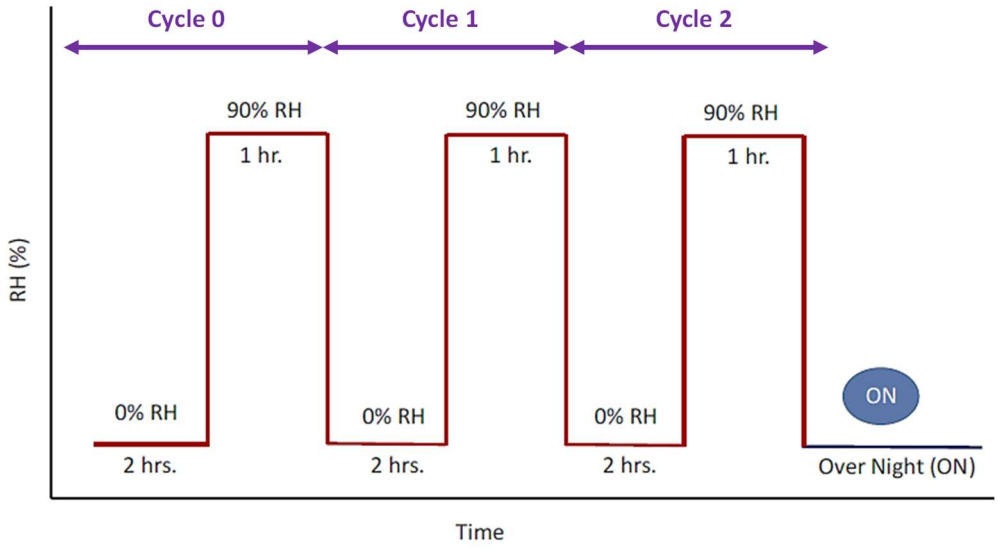

Figure 6.5. RH protocol used for humidity cycling investigation experiment.

For swelling rate and water content calculations, to quantify the differences of the ionomer's water content at each step compared to the as prepared ionomer thin film, the reference dry thickness (h_0) was set to the equilibrated dry thickness at ~0% RH in first cycle, and the saturated thickness at each cycle was set to the thickness of the film at 90% RH of each cycle.

Figure 6.6 shows the change in thickness of ionomers during RH cycling. At dry condition (0% RH). the swelling of ionomers increased after exposed to humid environment for the first time. Even after drying the ionomer overnight (more than 12 hours), there is still a sub-layer of water in the ionomer that is so difficult to be removed and it confirmed the formation of a water rich interface in ionomer thin films.

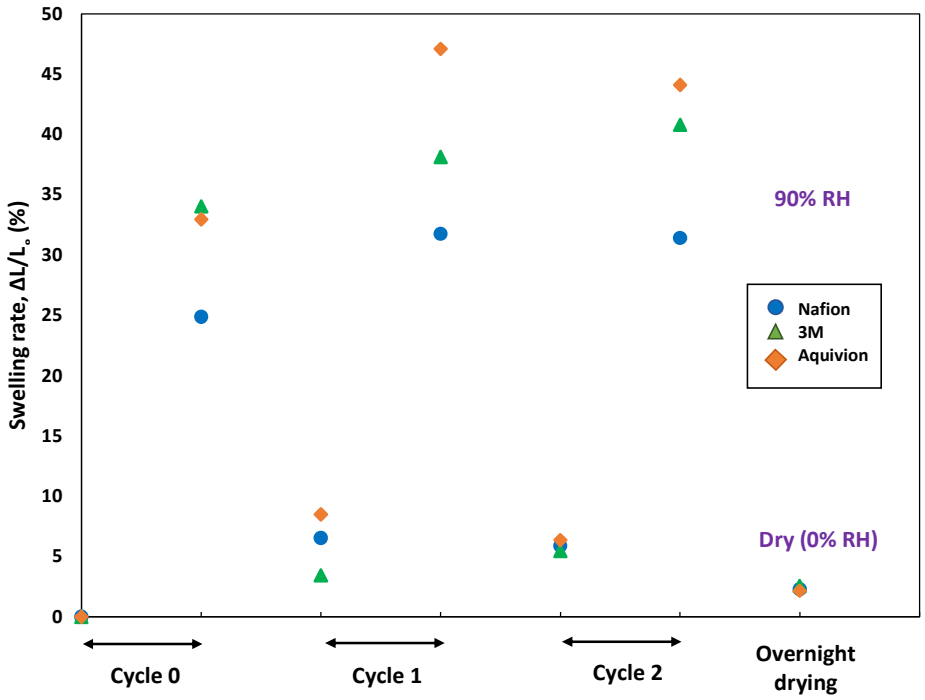

Figure 6.6. Swelling rate of ~10 nm ionomers (Nafion, 3M and Aquivion) on SiO2 substrate at 80 C as a function of relative humidity cycling.

At humid condition (90% RH) (Figure 6.6), the swelling of the ionomers increased after first cycle. The data in Figure 6.6 show that the swelling and de-swelling (relaxation) of the ionomers occurred by changing RH, increased the maximum swelling rate capacity. In Cycle 2, a slight reduction in the swelling rate was seen. However, it was observed that after several RH cycling, the swelling rate of ionomers merged to a stable value which is higher than that observed for the first round (cycle 0) of RH cycling. The humidity in the first round causes the structure relaxation and plasticization in ionomer and allowing higher swelling occurred in the next cycles. The results shows that this impact is long-lasting and the hydration properties (swelling rate of the ionomer/ water content) of the ionomer did not come back to the stage before humidity cycling

start (cycle 0). These results indicate that the humidity cycling has stronger effect on ionomer thickness swelling (water content) than ionomer structure. These trends were similar for all ionomers, and it shows that it is not dependent to the EW of ionomer or side chain length or structure.

6.3.5. Water vapor sorption in ionomers

To understand the water uptake kinetics of ionomer thin films (10 nm), Quartz Crystal Microbalance (QCM) (Inficon, East Syracuse, NY) was used and data analyzed assuming Sauerbrey equation holds. Ionomer thin films were deposited on gold QCM using spin coating the diluted in IPA (0.2% wt.) ionomer solutions were deposited on substrates using spin-coating (at 5000 rpm for 30 Sec). Then, Samples were dried at vacuum oven at 40 C for 24 hours. QCM crystal was sealed in its holder and place in a custom-made chamber for in-situ monitoring the relative humidity and temperature of the environment.

The experimental procedure for all the samples were similar. All measurements were performed at 30˚C due to the limitation of QCM crystal specification. Two different RH change protocols were used to investigate the absorption and desorption of water. In the first protocol, the sample was equilibrated at 30°C and 0% RH and the RH of the system was increased step by step up to 90% RH and then decreased step by step as shown in Figure 6.7a. At each RH, the measurement was carried until a quasi-equilibrium or steady state was reached. This was arbitrarily defined as frequency change of less than +/-1 Hz over 10 minutes period. Once this quasi-equilibrium state was achieved, the humidity was changed to the next value in the RH. The second protocol was similar to humidity cycling experiment described in section (6.3.4), the RH change rapidly between 0 and 90% RH (Figure 6.7b). The frequency of coated QCM crystal measured after equilibration at each RH and used for water uptake calculation.

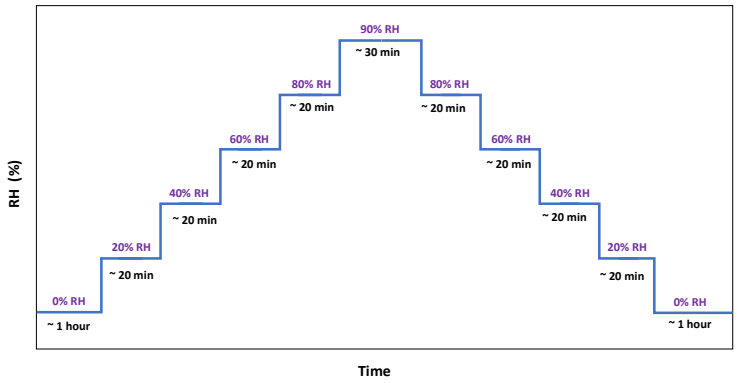

(a)

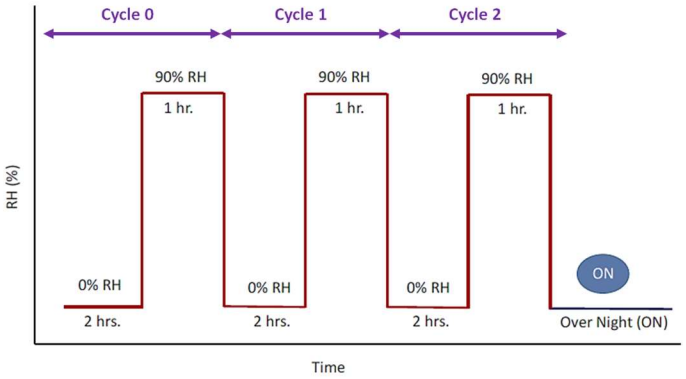

(b)

Figure 6.7. a), b) The humidity profile adopted for investigating the effect of RH at constant temperature (30 °C) on Ionomer thin film water content.

The water sorption and desorption were calculated using frequency change (Δf) measurement conducted by using QCM and Sauerbrey equation and founding the mass change based on the frequency change (Equation 6.1) (full QCM details can be found in section (3.1.3)).

$$Water\ (mass) uptake = \frac{m_{RH} - m_{dry}}{m_{dry}} = \frac{\Delta f_{RH} - \Delta f_{dry}}{\Delta f_{dry}} \qquad (6.1)$$

where, m_{RH} is the mass of the ionomer at specific RH that was measured, m_{dry} is the mass of the dry ionomer film that was measured at dry condition (0% RH), Δf_{RH} is the frequency change of

the ionomer at specific RH that was measured and Δf_{dry} is the frequency change of the dry ionomer film that was measured at dry condition (0% RH).

Figure 6.8 a, b shows a sample of frequency and mass change respectively in measuring water uptake in blank QCM gold crystal using QCM technique at 30˚ C.

a)

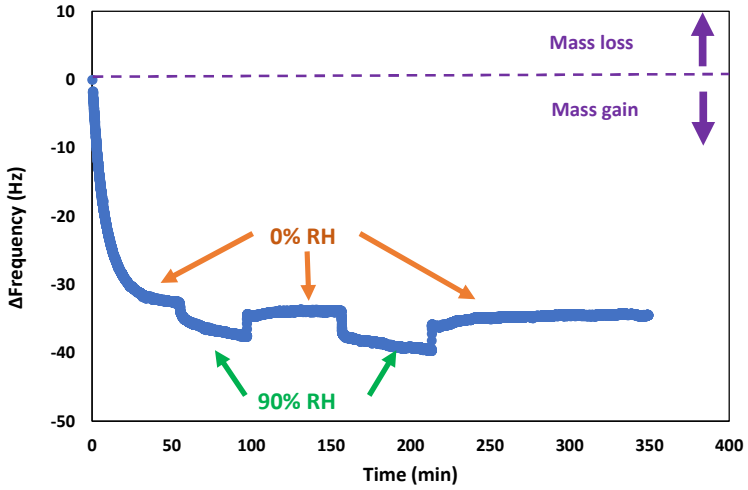

b)

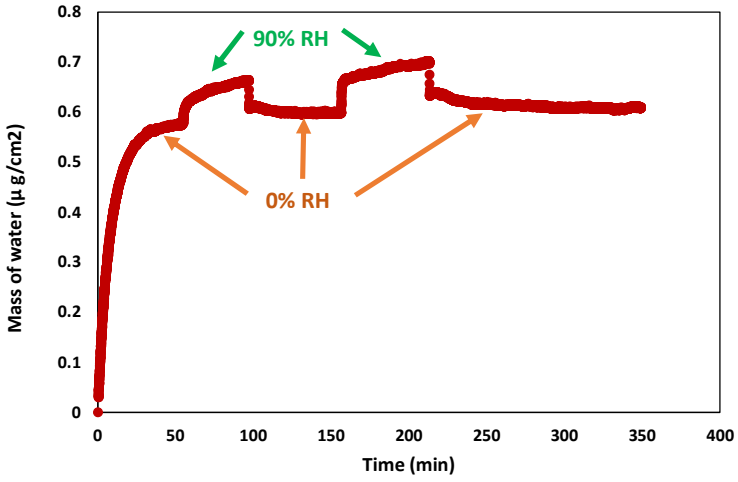

Figure 6.8. representation of a) frequency change and b) mass change of a bare gold QCM crystal under RH changes at 30˚ C.

6.3.5.1. Diffusion Coefficient of Water in Ionomer Thin Films

Fickian model is commonly used for diffusion coefficient evaluation [200], [201], [214]. However, it was noticed that some ionomers did not exhibit Fickian behavior [132], [178] like coefficient dependency on ionomer thickness [179], [204], [205], and concentration [179], [204], [215], [216] and the difference between adsorption and desorption diffusion coefficient [179], [215], [217], [218].

In this study, Fickian model was used to compute the diffusion coefficient of water ionomers at 30 C. It is known that the Fickian model may not adequately capture the water diffusion kinetics when there is high humidity differentials for a step-change, e.g., RH change from in one step from 0% and 90% RH. For protocol-1, the step change is around 20% so it could give us a good estimation for water absorption/desorption Diffusion Coefficient [132], [177], [219], [220].

For this purpose, at first, as shown in Figure 6.9, the water mass uptake is plotted vs. the square root of absorption/ desorption time. Assuming constant or average diffusivity over the absorption/desorption time, the mass uptake is predicted to follow the following relationship [220]:

$$\frac{\mathrm{M\ (t)}}{M_\infty} \approx \frac{2}{\sqrt{\pi}} \sqrt{\frac{D\ t}{l^2}} \qquad (1)$$

M_∞ is the mass at saturated condition (i.e. at infinite time), M(t) is the mass at time, t is the time (Sec.) and L is the film thickness. When mass loading plotted vs. $t^{1/2}$ this curve produces a straight line for the initial stage of absorption. The slope of the straight line is used for diffusivity calculation. The dashed line in Figure 6.9 is an example of what is mentioned above for calculating the slope in each stage.

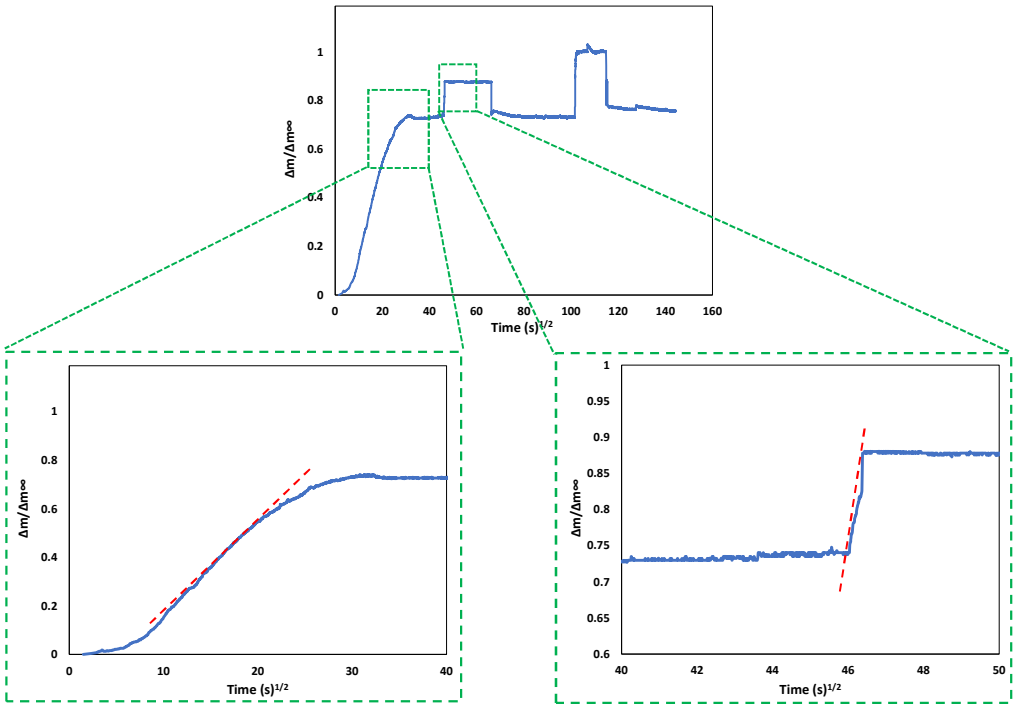

Figure 6.9. Mass loading of 10 nm Nafion measured at 30 C vs. square root of absorption time. The red dashed line is a fit to Fickian diffusion (eq. (1)).

The diffusion coefficient of ionomer thin films (~10 nm) for the two different RH step change protocols are reported in Table 6.1 and Table 6.2. The absorption diffusion coefficient column defined when RH changes from 0 to 90% and the desorption diffusion coefficient column defines when RH varied from 90 to 0 % RH. Table 6.1 shows water absorption and desorption diffusion coefficient of ionomer thin films as a function of for RH (RH changes gradually) at 30 ˚C. 3M and Aquivion ionomer showed similar behavior to the Nafion thin film.

The absorption and desorption kinetics of all ionomers increased by increasing the RH. Water desorption is seen to be (~ an order of magnitude) faster than water absorption in all RHs. Most of the research were focused on investigating the kinetics of water sorption in ionomer

membrane and there are few studies on diffusivity of water sorption in thin films for comparison. The water diffusion coefficient in Nafion thin films was reported ~2×10^{-13} cm^2/s for 20 nm Nafion using Polarization-Modulation Infrared Reflection−Absorption Spectroscopy (PM-IRRAS) method and ~ 2×10^{-12} cm^2/s for 50 nm Nafion using QCM method [132]. Krtil et al also reported ~4×10^{-14} cm^2/s for Nafion diffusion coefficient using QCM method [221]. These differences in diffusion coefficient may arise from different experimental measurement techniques, conditions, and history of samples.

Table 6.1. Diffusion Coefficient (cm2/s) of ionomers thin films at 30 °C when RH was changed in steps 0 to 20, 20 to 40, 40 to 60, 60 to 80, and 80 to 90.

Diffusion Coefficient (cm^2/s)						
	Nafion		**3M**		**Aquivion**	
RH (%)	**Absorption**	**Desorption**	**Absorption**	**Desorption**	**Absorption**	**Desorption**
20	0.4×10^{-18}	1.2×10^{-17}	0.2×10^{-16}	1.8×10^{-15}	0.5×10^{-16}	1.5×10^{-15}
40	1.5×10^{-18}	1.8×10^{-17}	1.2×10^{-15}	0.84×10^{-14}	1.1×10^{-15}	1.3×10^{-14}
60	1.8×10^{-17}	1.1×10^{-16}	1.5×10^{-14}	1.2×10^{-14}	1.7×10^{-14}	1.6×10^{-14}
80	3.3×10^{-17}	4.2×10^{-16}	4.3×10^{-14}	6.2×10^{-14}	4.7×10^{-14}	5.8×10^{-14}
90	4.8×10^{-17}	6.3×10^{-16}	5.9×10^{-14}	9.5×10^{-14}	5.5×10^{-14}	8.7×10^{-14}

Table 6.2. Diffusion Coefficient (cm^2/s) of ionomers thin films at 30 °C when RH step change from 0% to 90% RH and 90% to 0% is applied.

Diffusion Coefficient (cm^2/s)						
	Nafion		**3M**		**Aquivion**	
Cycle	**Absorption**	**Desorption**	**Absorption**	**Desorption**	**Absorption**	**Desorption**
0	4.3×10^{-18}	1.5×10^{-16}	1.2×10^{-16}	2×10^{-15}	0.4×10^{-16}	1.8×10^{-15}
1	0.4×10^{-16}	0.6×10^{-16}	0.9×10^{-15}	3.7×10^{-15}	1.2×10^{-15}	2.3×10^{-15}
2	1.6×10^{-16}	2.3×10^{-16}	2.3×10^{-15}	6.5×10^{-15}	2.7×10^{-15}	7.6×10^{-15}

Table 6.2 shows water absorption and desorption diffusion coefficient of ionomer thin films as a function of for RH (RH changes from 0 to 90% and vice versa instantly) at 30 ˚C. It is observed that the desorption diffusion coefficient is bigger than absorption diffusion coefficient for all ionomers which shows desorption happened faster than absorption for all ionomers. This behavior is in a good agreement with previous research reports[178], [200], [221]. The absorption coefficient of ionomers for the first cycle is smaller than the subsequent cycles. 3M and Aquivion ionomer showed similar behavior to the Nafion thin film.

The differences between kinetics of absorption and desorption of water in ionomers suggest complex interplay between diffusion mechanism and microstructure of the films. There are two processes involved in the sorption of water in ionomers film: a) interfacial mass transport from water vapor into the film, b) diffusion of water within the film through the hydrophilic domains [200]. The state of the ionomer, i.e. the connectivity of hydrophilic domains and the relaxation of polymer chains is certainly different at different water content. Thus, the differences in diffusivity

at low RH and high RH can be attributed, if not entirely, then significantly to the differences in the ionomer microstructure. It is noted that diffusion coefficient for desorption is larger than that for absorption. This difference can also be attributed partially to differences in relaxation state and hydrophilic domain connectivity. It is suggested that if the dry ionomer is exposed to water vapor for the first time, after initial water uptake, ionomer structure will rearrange and become more relaxed to accommodate the water into the hydrophilic domains of ionomers. On the other hand, during desorption, the polymer does not need to shrink before water leaves the ionomer. Thus, this difference in the polymer microstructure can also explain the differences in diffusivity for absorption and desorption processes.

6.4. Conclusion

To investigate the impact of substrate (Pt and carbon) on ionomer structure and properties, wettability of ionomer films and RH-dependent swelling rate were measured. The hysteresis of water sorption/desorption from ionomer was also investigated.

The wettability study of ionomers on Pt, carbon and SiO_2 substrate showed that the surface of ionomers on SiO_2 substrate are more hydrophilic than ionomers on Pt and carbon substrate. It shows that the tendency of forming SO_3H cluster groups on carbon and Pt substrate is not as strong as SiO_2 substrate. The swelling rate of 10 nm ionomer on Pt substrate were observed to be higher than those on carbon and SiO_2 substrates. These results indicate that the strong binding of ionomer on Pt does not adversely impact the water sorption. In fact, the opposite is true. The differences in wettability and swelling rate of ionomer film on carbon and platinum substrate indicate that the interactions between ionomers and substrate affects internal structure of ionomers as well as the film surface especially in ultra thin films (< 10 nm).

Moreover, water sorption studies on ionomer thin films shows that water absorption is slower than water desorption. It could indicate that the rate of water absorption controlled by the rate of interfacial transport and swelling while the desorption rate mainly controls by interfacial mass transport.

Chapter Seven: Conclusions and Recommendations for Future Work

7.1 Conclusions

In this thesis, new data for hydration-driven properties, pertinent to fuel cell catalysts layer, of ionomer thin films were generated. The work was undertaken to fill the gap in knowledge pertaining the quantitative information on the key functional properties - water sorption and proton conductivity - of new ionomers that have become available. Although the ionomers investigated in the present thesis all belong to the perfluorosulphonic acid (PFSA) class of polymer, the extent to which the molecular variation (side-chain length and inter side-chain distance) affect the water sorption and proton conductivity were not fully quantified. The these reports a comprehensive dataset comprising the aforementioned properties of thin films (<100 nm) of seven different ionomers over a wide range of relative humidity 0-90% and temperature (30, 60 and 80^{o}C). The new data generated for specific ionomers is expected to useful for scientists and engineers responsible for electrode fabrication and design. The comprehensive set of data also allowed investigation of a universal relationship or generalized behaviour of ionomer thin films. This thesis has made several contributions towards the advancement of the PEFC research field. These key findings are summarized below.

Effect of ionomer equivalent weight and side-chain characteristics: First contribution of this work is the generation of new data for water content and proton conductivity of seven PFSA ionomers (30 nm films for PFSA ionomers with different equivalent weight – from 620 to 1100 g/mole of sulphonic acid – and varying in side-chain length) as a function of relative humidity.

The collective analyses of the data revealed that the acid content of the ionomer, i.e., inverse of EW, was the strongest determinant of the water content and proton conductivity at any given relative humidity. Thus, water content and proton conductivity were found to decrease monotonically with increasing EW. All ionomer exhibited the expected exponential-type dependency of proton conductivity on water content. A single universal correlation for all ionomers could describe the trend but the influence of side-chain characteristics – length and interspacing – was significant at low water content ($\lambda<4$) . Proton conductivity data indicated that for all ionomer at higher water content there was a trend to reach an asymptotic value of ≈0.1 S/cm. The present study also showed why it is important to quantify the properties at fuel cell operating temperature (80°C) rather than commonly reported measurements at room temperatures (~30°C). At comparable relative humidity, the data in the thesis established that both water content and proton conductivity are significantly higher at fuel cell operating conditions (80°C) than at room temperature (30°C). The differences in proton conductivity arise from differences in water content. The important finding from the thesis is that the differences in proton conductivity at two temperatures diminish at comparable water content. The new data provides a more relevant source for use in fuel cell catalyst layer modeling. The availability of water content data also allowed correlation between literature reported oxygen transport resistance and ionomer water content.

Effect of cobalt exchange and thermal/aqueous treatment: An important contribution of this study has been the quantification of the extent of suppression of hydration properties when proton-form of ionomers are contaminated by Co^{2+} ion. All ionomers exhibited suppression of ionic conductivity by Co contamination (a decrease of over two orders of magnitude at low RH), consistent with the earlier studies. The new insight provided from the present study is that this suppression in conductivity arises from the suppression in water uptake of the ionomer films upon

Co^{2+} exchange. The RH dependent swelling measurement revealed lower swelling, i.e., lower water uptake, of ionomer films upon Co^{2+} exchange. The study also highlighted that thermal annealing and liquid water exposure can dramatically impact the conductivity of the films. Thus, it is important when comparing conductivity and water uptake of H^+ form of films with Co^{2+} form of ionomer films to subject the films to similar hygro-thermal pre-treatment. Co^{2+} has a larger impact on hydration-dependent properties of ionomer thin films at lower RH. The impact was lower for PFIA ionomer than PFSA ionomer and is attributed to different side chain structure of PFIA ionomer, which has two acid sites on its side chain. From conductivity – water uptake relationship, the differences between H^+ form and Co^{2+} form of ionomer films becomes less when the water content increases. Accordingly, a new universal relationship for ionic conductivity and water content of the ionomer films is introduced in this work.

Effect of substrate and hydration hysteresis: The swelling rate of 10 nm ionomer thin films on Pt, carbon and SiO_2 substrate revealed that films on Pt substrate have higher swelling rate than those on carbon and SiO_2 substrates. These results prove the evidence of better water network and higher proton conductivity in ionomers on Pt substrate. An important implication of the result is that it provides a counter argument for local oxygen transport resistance caused by densification of ionomer on Pt. The higher hydration level implies that oxygen transport through hydrophilic domain would be facile. The results also indicate that the interactions between ionomers and substrate affects internal structure of ionomers as well as the film surface especially in ultra thin films (< 10 nm). The combined results for hydration (swelling) and wettability study of ionomers on Pt, carbon and SiO_2 substrate reveals that both bulk and surface morphology of ionomer films are affected by the substrate.

Moreover, water sorption studies on ionomer thin films shows that water absorption is slower than water desorption. It could indicate that the rate of water absorption controlled by the rate of interfacial transport and swelling while the desorption rate mainly controls by interfacial mass transport.

7.2 Recommendations for Future Work

Although this thesis has contributed in several ways towards the quantification of the properties of thin films of ionomers with different structure (different side chain length and structure), yet some areas of the topic remained unexplored. Based on the key findings achieved throughout the thesis, following are the suggestions that must be considered to further advance the knowledge of ionomers in CL:

- Investigate the water uptake and proton conductivity of ionomers thin films (10 nm) on substrates with different hydrophobicity (hydrophilic Pt, hydrophobic and hydrophilic carbon substrate) at fuel cell operational temperature (~80^{o}C) to advance our knowledge about the effective parameters on controlling the proton transport in CL.
- Quantify the water uptake of catalyst layer at fuel cell operational temperature (~80^{o}C) and correlate with thin film water uptake as well with proton conductivity in catalyst layer.
- Investigate thermal expansion of different ionomer thin films (10 nm) on different substrate (Pt and carbon) using heated cell ellipsometry to gather more data about the effect of ionomers and substrate and their interaction and its effect on ionomer properties.
- Investigate the substrate-dependent properties of cobalt exchanged ionomer thin films. Hydration and thermal expansion properties of contaminated ionomers could be examined on different substrate (Pt and carbon) using ellipsometry to gather more data about the effect of substrate on the effect of contamination on ionomers properties.

References

[1] H. Ritchie, M. Roser, and P. Rosado, "Energy," *Our World Data*, 2020.

[2] IEA, "Material efficiency in clean energy transitions," Paris, 2019.

[3] I. Staffell *et al.*, "The role of hydrogen and fuel cells in the global energy system," *Energy Environ. Sci.*, vol. 12, no. 2, pp. 463–491, 2019.

[4] N. McCarthy, "Air Pollution Contributed To More Than 6 Million Deaths In 2016 [Infographic]," *Forbes*, 2018.

[5] WHO, "Air pollution and health." [Online]. Available: https://www.who.int/airpollution/en/.

[6] J. Tollefson, "Fuel oF the Future ? " T," *Nature*, vol. 464, no. April, pp. 1262–1264, 2010.

[7] US Energy Department, "International Energy Outlook 2018," 2018.

[8] C. A. Horowitz, "Paris Agreement," *Int. Leg. Mater.*, vol. 55, no. 4, pp. 740–755, 2016.

[9] O. M. Babatunde, J. L. Munda, and Y. Hamam, "Power system flexibility: A review," *Energy Reports*, vol. 6, pp. 101–106, 2020.

[10] IEA (2020), "IEA (2020), Energy Technology Perspectives," 2020.

[11] J. Schmidt *et al.*, "A new perspective on global renewable energy systems: why trade in energy carriers matters," *Energy Environ. Sci.*, vol. 12, no. 7, pp. 2022–2029, 2019.

[12] T. S. Uyar and D. Beşikci, "Integration of hydrogen energy systems into renewable energy systems for better design of 100% renewable energy communities," *Int. J. Hydrogen Energy*, vol. 42, no. 4, pp. 2453–2456, 2017.

[13] X. Liu, G. Liu, J. Xue, X. Wang, and Q. Li, "Hydrogen as a carrier of renewable energies toward carbon neutrality: State-of-the-art and challenging issues," *Int. J. Miner. Metall. Mater.*, vol. 29, no. 5, pp. 1073–1089, 2022.

[14] M. Winter and R. J. Brodd, "What Are Batteries, Fuel Cells, and Supercapacitors?," *Chem. Rev.*, vol. 104, no. 10, pp. 4245–4270, Oct. 2004.

[15] S. Curry-Nkansah, Maria and Driscoll, Daniel and Farmer, Richard and Garland, Roxanne and Gruber, Jill and Gupta, Nikunj and Hershkowitz, Frank and Holladay, Jamelyn and Nguyen, Kevin and Schlasner, "Hydrogen Production Roadmap. Technology Pathways to the Future, January 2009," 2009.

[16] P. Bruce, Sam and Temminghoff, Max and Hayward, Jenny and Schmidt, E and Munnings, Christopher and Palfreyman, Doug and Hartley, "National hydrogen roadmap, Pathways to an economically sustainable hydrogen industry in Australia," *Aust. CSIRO*, 2018.

[17] F. C. and H. J. U. (FCHJU), "Hydrogen Roadmap Europe," *Fuel Cells Hydrog. Jt. Undert. Bietlot, Belgium*, 2019.

[18] Y. Li and F. Taghizadeh-Hesary, "The economic feasibility of green hydrogen and fuel cell

electric vehicles for road transport in China," *Energy Policy*, vol. 160, p. 112703, 2022.

[19] T. Yoshida and K. Kojima, "Toyota MIRAI Fuel Cell Vehicle and Progress Toward a Future Hydrogen Society," *Electrochem. Soc. Interface*, vol. 24, no. 2, pp. 45–49, 2015.

[20] Y. Sando, "Research and Development of Fuel Cell Vehicles at Honda," 2009.

[21] S. H. Kim *et al.*, "Development of Hyundai's Tucson FCEV," in *SAE 2005 World Congress & Exhibition*, 2005.

[22] A. Kongkanand and M. F. Mathias, "The Priority and Challenge of High-Power Performance of Low-Platinum Proton-Exchange Membrane Fuel Cells," *J. Phys. Chem. Lett.*, vol. 7, no. 7, pp. 1127–1137, 2016.

[23] A. Z. Weber and A. Kusoglu, "Unexplained transport resistances for low-loaded fuel-cell catalyst layers," *J. Mater. Chem. A*, vol. 2, no. 41, pp. 17207–17211, 2014.

[24] K. A. Page and B. W. Rowe, "An overview of polymer electrolyte membranes for fuel cell applications," *ACS Symp. Ser.*, vol. 1096, pp. 147–164, 2012.

[25] S. J. Peighambardoust, S. Rowshanzamir, and M. Amjadi, "Review of the proton exchange membranes for fuel cell applications," *Int. J. Hydrogen Energy*, vol. 35, no. 17, pp. 9349–9384, Sep. 2010.

[26] US Office of energy efficiency & renewable energy, "3.4 Fuel Cells," *Fuel Cell Technol. Off. Multi-Year Res. Dev. Demonstr. Plan*, vol. 2015, pp. 3.4.1-3.4.58, 2017.

[27] J. Weber, A. Z.; Newman, "Transport in Polymer-Electrolyte Membranes," *J. Electrochem. Soc.*, vol. 150, no. 7, pp. A1008–A1015, 2003.

[28] M. N. Stamenkovic VR, Strmcnik D, Lopes PP, "Energy and Fuels from Electrochemical Interfaces," *Nat. Mater*, vol. 16, no. 1, pp. 57–69, 2016.

[29] K. Karan, "PEFC catalyst layer: Recent advances in materials, microstructural characterization, and modeling," *Curr. Opin. Electrochem.*, vol. 5, no. 1, pp. 27–35, 2017.

[30] K. Karan, "Interesting Facets of Surface, Interfacial, and Bulk Characteristics of Perfluorinated Ionomer Films," *Langmuir*, vol. 35, no. 42, pp. 13489–13520, 2019.

[31] A. Kusoglu and A. Z. Weber, "New Insights into Perfluorinated Sulfonic-Acid Ionomers," *Chem. Rev.*, vol. 117, no. 3, pp. 987–1104, 2017.

[32] A. Kongkanand, W. Gu, and M. F. Mathias, "Proton-Exchange Membrane Fuel Cells with Low-Pt Content," in *Encyclopedia of Sustainability Science and Technology*, R. A. Meyers, Ed. New York, NY: Springer New York, 2017, pp. 1–20.

[33] RuiyuJiang *et al.*, "A review of core-shell nanostructured electrocatalysts for oxygen reduction reaction," *Energy Storage Mater.*, vol. 12, pp. 260–276, 2018.

[34] L. Wang *et al.*, "Core–Shell Nanostructured Cobalt–Platinum Electrocatalysts with Enhanced Durability," *ACS Catal.*, vol. 8, no. 1, pp. 35–42, 2018.

[35] Y. Cai *et al.*, "Electrode Edge Cobalt Cation Migration in an Operating Fuel Cell: An In Situ Micro-X-ray Fluorescence Study," *J. Electrochem. Soc.*, vol. 165, no. 6, pp. F3132–

F3138, 2018.

[36] H. Li *et al.*, “Effect of Co2+ on oxygen reduction reaction catalyzed by Pt catalyst, and its implications for fuel cell contamination,” *Electrochim. Acta*, vol. 55, no. 8, pp. 2622–2628, 2010.

[37] H. Li *et al.*, “PEM fuel cell cathode contamination in the presence of cobalt ion (Co 2+),” *Electrochim. Acta*, vol. 55, no. 20, pp. 5823–5830, 2010.

[38] F. Maillard, L. Dubau, J. Durst, M. Chatenet, J. André, and E. Rossinot, “Durability of Pt3Co/C nanoparticles in a proton-exchange membrane fuel cell: Direct evidence of bulk Co segregation to the surface,” *Electrochem. commun.*, vol. 12, no. 9, pp. 1161–1164, 2010.

[39] J. Braaten, A. Kongkanand, and S. Litster, “Oxygen Transport Effects of Cobalt Cation Contamination of Ionomer Thin Films in Proton Exchange Membrane Fuel Cells,” *ECS Trans.*, vol. 80, no. 8, pp. 283–290, 2017.

[40] H. Eskandari, V. Ozhukil Kollath, and K. Karan, “Effect of Cobalt Ion Exchange and Thermal Pretreatment of Ionomer Thin Films on Conductivity, Water Uptake and Swelling,” *Meet. Abstr.* , vol. MA2018-02, no. 43, p. 1452, Jul. 2018.

[41] S. Authayanun, K. Im-orb, and A. Arpornwichanop, “A review of the development of high temperature proton exchange membrane fuel cells,” *Chinese J. Catal.*, vol. 36, no. 4, pp. 473–483, 2015.

[42] S. Ott *et al.*, “Ionomer distribution control in porous carbon-supported catalyst layers for high-power and low Pt-loaded proton exchange membrane fuel cells,” *Nat. Mater.*, 2019.

[43] A. Orfanidi, P. Madkikar, H. A. El-Sayed, G. S. Harzer, T. Kratky, and H. A. Gasteiger, “The key to high performance low pt loaded electrodes,” *J. Electrochem. Soc.*, vol. 164, no. 4, pp. F418–F426, 2017.

[44] K. Y. and K. S. Kazuyuki Sato, Atsushi Ohma, “Analysis of Water Transport in Catalyst Layers: The Effect of Carbon Supports,” *ECS Trans.*, vol. 25, no. 1, pp. 273–283, 2009.

[45] G. Gebel and R. B. Moore, “Small-Angle Scattering Study of Short Pendant Chain Perfuorosulfonated Ionomer Membranes,” *Macromolecules*, vol. 33, no. 13, pp. 4850–4855, 2000.

[46] T. Okada, H. Satou, M. Okuno, and M. Yuasa, “Ion and water transport characteristics of perfluorosulfonated ionomer membranes with H+ and alkali metal cations,” *J. Phys. Chem. B*, vol. 106, no. 6, pp. 1267–1273, 2002.

[47] W. Y. Hsu and T. D. Gierke, “Ion transport and clustering in nafion perfluorinated membranes,” *J. Memb. Sci.*, vol. 13, no. 3, pp. 307–326, Feb. 1983.

[48] T. D. Gierke, G. E. Munn, and F. C. Wilson, “The morphology in nafion perfluorinated membrane products, as determined by wide- and small-angle x-ray studies,” *J. Polym. Sci. Polym. Phys. Ed.*, vol. 19, no. 11, pp. 1687–1704, Nov. 1981.

[49] J. Peron *et al.*, “Fuel cell catalyst layers containing short-side-chain perfluorosulfonic acid ionomers,” *J. Power Sources*, vol. 196, no. 1, pp. 179–181, Jan. 2011.

[50] K. D. Kreuer *et al.*, "Short-side-chain proton conducting perfluorosulfonic acid ionomers: Why they perform better in PEM fuel cells," *J. Power Sources*, vol. 178, no. 2, pp. 499–509, Apr. 2008.

[51] D. Wu, S. J. Paddison, and J. A. Elliott, "Effect of Molecular Weight on Hydrated Morphologies of the Short-Side-Chain Perfluorosulfonic Acid Membrane," *Macromolecules*, vol. 42, no. 9, pp. 3358–3367, 2009.

[52] R. Hiesgen, T. Morawietz, M. Handl, C. Oldani, K. Karan, and K. A. Friedrich, "Structure, Properties, and Degradation of Ultrathin Ionomer Films in Fuel Cell Catalytic Layers," *Meet. Abstr.* , vol. MA2018-01, no. 30, p. 1769, Apr. 2018.

[53] D. K. Paul and K. Karan, "Conductivity and wettability changes of ultrathin nafion films subjected to thermal annealing and liquid water exposure," *J. Phys. Chem. C*, vol. 118, no. 4, pp. 1828–1835, 2014.

[54] M. A. Modestino *et al.*, "Self-Assembly and Transport Limitations in Confined Nafion Films," *Macromolecules*, vol. 46, no. 3, pp. 867–873, Feb. 2013.

[55] M. Handl, T. Morawietz, D. K. Paul, K. A. Friedrich, K. Karan, and R. Hiesgen, "Structure, Properties, and Degradation of Nanothin Ionomer Films in Fuel Cell Catalytic Layers," *ECS Trans.* , vol. 85, no. 13, pp. 889–903, Jun. 2018.

[56] D. K. Paul, A. Fraser, and K. Karan, "Towards the understanding of proton conduction mechanism in PEMFC catalyst layer : Conductivity of adsorbed Na fi on fi lms," *Electrochem. commun.*, vol. 13, no. 8, pp. 774–777, 2011.

[57] J. Peng, M. Tian, N. M. Cantillo, and T. Zawodzinski, "The ion and water transport properties of K+ and Na+ form perfluorosulfonic acid polymer," *Electrochim. Acta*, vol. 282, pp. 544–554, 2018.

[58] J. Peng, K. Lou, G. Goenaga, and T. Zawodzinski, "Transport Properties of Perfluorosulfonate Membranes Ion Exchanged with Cations," *ACS Appl. Mater. Interfaces*, vol. 10, p. 38418−38430, 2018.

[59] and F. H. G. Brian Kienitza,, Bryan Pivovarb, Tom Zawodzinskic, "Cationic Contamination Effects on Polymer Electrolyte Membrane Fuel Cell Performance," *J. Electrochem. Soc.*, vol. 158, no. 9, p. B1175_B1183, 2011.

[60] F. CW *et al.*, "Structure in Thin and Ultrathin Spin-Cast Polymer Films," *Science (80-.).*, vol. 273, pp. 912–917, 1996.

[61] M. Alcoutlabi and G. B. McKenna, "Effects of confinement on material behaviour at the nanometre size scale," *J. Phys. Condens. Matter*, vol. 17, no. 15, pp. R461–R524, Apr. 2005.

[62] B. D. Vogt, "Mechanical and viscoelastic properties of confined amorphous polymers," *J. Polym. Sci. Part B Polym. Phys.*, vol. 56, no. 1, pp. 9–30, Jan. 2018.

[63] D. Chen, A. Kongkanand, and J. Jorne, "Proton Conduction and Oxygen Diffusion in Ultra-Thin Nafion Films in PEM Fuel Cell: How Thin?," *J. Electrochem. Soc.* , vol. 166, no. 2, pp. F24–F33, Jan. 2019.

[64] Y. Ono and Y. Nagao, “Interfacial Structure and Proton Conductivity of Nafion at the Pt-Deposited Surface,” *Langmuir*, vol. 32, no. 1, pp. 352–358, Jan. 2016.

[65] D. K. Paul, R. McCreery, and K. Karan, “Proton Transport Property in Supported Nafion Nanothin Films by Electrochemical Impedance Spectroscopy,” *J. Electrochem. Soc.*, vol. 161, no. 14, pp. F1395–F1402, Oct. 2014.

[66] Z. Siroma, R. Kakitsubo, N. Fujiwara, T. Ioroi, S. Yamazaki, and K. Yasuda, “Depression of proton conductivity in recast Nafion® film measured on flat substrate,” *J. Power Sources*, vol. 189, no. 2, pp. 994–998, Apr. 2009.

[67] A. Kusoglu, T. J. Dursch, and A. Z. Weber, “Nanostructure / Swelling Relationships of Bulk and Thin-Film PFSA Ionomers,” *Adv. Funct. Mater.*, vol. 26, no. 27, pp. 4961–4975, 2016.

[68] A. Kusoglu, D. Kushner, D. K. Paul, K. Karan, M. A. Hickner, and A. Z. Weber, “Impact of Substrate and Processing on Confinement of Nafion Thin Films,” *Adv. Funct. Mater.*, vol. 24, no. 30, pp. 4763–4774, Aug. 2014.

[69] D. K. Paul, H. K. K. Shim, J. B. Giorgi, and K. Karan, “Thickness dependence of thermally induced changes in surface and bulk properties of Nafion ® nanofilms,” *J. Polym. Sci. Part B Polym. Phys.*, vol. 54, no. 13, pp. 1267–1277, Jul. 2016.

[70] Y. Nagao, “Proton-Conductivity Enhancement in Polymer Thin Films,” *Langmuir*, vol. 33, no. 44, pp. 12547–12558, Nov. 2017.

[71] H. A. Gasteiger, S. S. Kocha, B. Sompalli, and F. T. Wagner, “Activity benchmarks and requirements for Pt, Pt-alloy, and non-Pt oxygen reduction catalysts for PEMFCs,” *Appl. Catal. B Environ.*, vol. 56, no. 1-2 SPEC. ISS., pp. 9–35, 2005.

[72] M. P. Ralph, T. R.; Hogarth, “Catalysis for Low Temperature Fuel Cells PART I: THE CATHODE CHALLENGES,” *Platin. Met. Rev.*, vol. 46, no. 1, pp. 3–14, 2002.

[73] M. Mathias *et al.*, “Two Fuel Cell Cars In Every Garage?,” *Interfaces (Providence).*, vol. 14, Sep. 2005.

[74] L. Dubau *et al.*, “Further insights into the durability of Pt 3 Co / C electrocatalysts : Formation of ‘ hollow ’ Pt nanoparticles induced by the Kirkendall effect,” *Electrochim. Acta*, vol. 56, no. 28, pp. 10658–10667, 2011.

[75] M. J. Kelly, G. Fafilek, J. O. Besenhard, H. Kronberger, and G. E. Nauer, “Contaminant absorption and conductivity in polymer electrolyte membranes,” *J. Power Sources*, vol. 145, no. 2, pp. 249–252, Aug. 2005.

[76] H. Li *et al.*, “Durability of PEM fuel cell cathode in the presence of Fe3+and Al3+,” *J. Power Sources*, vol. 195, no. 24, pp. 8089–8093, 2010.

[77] M. Sulek, J. Adams, S. Kaberline, M. Ricketts, and J. R. Waldecker, “In situ metal ion contamination and the effects on proton exchange membrane fuel cell performance,” *J. Power Sources*, vol. 196, no. 21, pp. 8967–8972, 2011.

[78] L. B. and T. M. Jing Qi, Xiaofeng Wang, Ugur Pasaogullaria, “Effect of Al3+ Contaminant

on Polymer Electrolyte Fuel Cell Performance," *J. Electrochem. Soc.*, vol. 160, no. 9, p. F916_F922, 2013.

[79] J. Qi *et al.*, "Effect of cationic contaminants on polymer electrolyte fuel cell performance," *J. Power Sources*, vol. 286, pp. 18–24, 2015.

[80] J. G. Goodwin, K. Hongsirikarn, S. Greenway, and S. Creager, "Effect of cations (Na+, Ca2+, Fe3+) on the conductivity of a Nafion membrane," *J. Power Sources*, vol. 195, no. 21, pp. 7213–7220, 2010.

[81] S. Shi, A. Z. Weber, and A. Kusoglu, "Structure-Transport Relationship of Perfluorosulfonic-Acid Membranes in Different Cationic Forms," *Electrochim. Acta*, vol. 220, pp. 517–528, 2016.

[82] J. Dumont *et al.*, "Effect of Cerium, Cobalt and Nickel Contaminants on the Oxygen Reduction Reaction at Platinum Electrodes," *ECS Trans.*, vol. 80, pp. 861–867, Aug. 2017.

[83] T. Okada, Y. Ayato, M. Yuasa, and I. Sekine, "The Effect of Impurity Cations on the Transport Characteristics of Perfluorosulfonated Ionomer Membranes," *J. Phys. Chem. B*, vol. 103, no. 17, pp. 3315–3322, Apr. 1999.

[84] J. Curtin, S.; Gangi, "State of the States: Fuel Cells in America 2016," *U.S. Dep. Energy, Energy Effic. &Renewable Energy*, pp. 1–46, 2016.

[85] L. Albe, N. D.; Bas, C.; Reymond, L.; Dane, A.; Rossinot, E.; Flandin, "Key Counter Ion Parameters Governing Polluted Nafion Membrane Properties.," *J. Polym. Sci. Part B Polym. Phys.*, vol. 47, no. 14, pp. 1381–1392, 2009.

[86] J. Li and S. Nemat-Nasser, "Micromechanical analysis of ionic clustering in Nafion perfluorinated membrane," *Mech. Mater.*, vol. 32, pp. 303–314, May 2000.

[87] T. Okada, Y. Ayato, M. Yuasa, and I. Sekine, "The Effect of Impurity Cations on the Transport Characteristics of Perfluorosulfonated Ionomer Membranes," pp. 3315–3322, 1999.

[88] M. Y. and I. S. Tatsuhiro Okada, Norito Nakamura, "Ion and Water Transport Characteristics in Membranes for Polymer Electrolyte Fuel Cells Containing H + and Ca2 + Cations," *J. Electrochem. Soc.*, vol. 144, no. 8, p. 2744_2750, 1997.

[89] P. Devproshad K, "Structure and Properties of Self-Assembled Sub-Micron Thin Nafion Films," Queen's University, 2013.

[90] J. W. E. Co., "Ellipsometry Tutorial: Light and Materials." [Online]. Available: http://www.jawoollam.com/tutorial_4.html.

[91] D. P. Subedi, "Contact Angle Measurement for The Surface Characterization of Solids," *Himal. Phys.*, vol. 2, no. 1, pp. 1–4, 2011.

[92] B. E. RANJITH RANGANATHAN, "SURFACE ACTIVITY AND EFFECTS AS MEASURED BY CONTACT ANGLE," Texas Tech University, 2003.

[93] A. F. Stalder, T. Melchior, M. Müller, D. Sage, T. Blu, and M. Unser, "Low-bond axisymmetric drop shape analysis for surface tension and contact angle measurements of

sessile drops," *Colloids Surfaces A Physicochem. Eng. Asp.*, vol. 364, no. 1–3, pp. 72–81, 2010.

[94] D. Wu, C. Peng, C. Yin, and H. Tang, "Review of System Integration and Control of Proton Exchange Membrane Fuel Cells," *Electrochem. Energy Rev.*, vol. 3, no. 3, pp. 466–505, 2020.

[95] Y. Wang, K. S. Chen, J. Mishler, S. C. Cho, and X. C. Adroher, "A review of polymer electrolyte membrane fuel cells: Technology, applications, and needs on fundamental research," *Appl. Energy*, vol. 88, no. 4, pp. 981–1007, 2011.

[96] K. Kodama, T. Nagai, A. Kuwaki, R. Jinnouchi, and Y. Morimoto, "Challenges in applying highly active Pt-based nanostructured catalysts for oxygen reduction reactions to fuel cell vehicles," *Nat. Nanotechnol.*, vol. 16, no. 2, pp. 140–147, 2021.

[97] T. Van Cleve *et al.*, "Dictating Pt-Based Electrocatalyst Performance in Polymer Electrolyte Fuel Cells, from Formulation to Application," *ACS Appl. Mater. Interfaces*, vol. 11, no. 50, pp. 46953–46964, Dec. 2019.

[98] K. Jiao *et al.*, "Designing the Next generation of proton-exchange membrane fuel cells," *Nature*, vol. 595, no. 7867, pp. 361–369, 2021.

[99] S. Farzin, A. Sarella, M. A. Yandrasits, and S. K. Dishari, "Fluorocarbon-Based Ionomers with Single Acid and Multiacid Side Chains at Nanothin Interfaces," *J. Phys. Chem. C*, vol. 123, no. 51, pp. 30871–30884, Dec. 2019.

[100] K. Kodama *et al.*, "Effect of the Side-Chain Structure of Perfluoro-Sulfonic Acid Ionomers on the Oxygen Reduction Reaction on the Surface of Pt," *ACS Catal.*, vol. 8, no. 1, pp. 694–700, Jan. 2018.

[101] X. Luo, S. Holdcroft, A. Mani, Y. Zhang, and Z. Shi, "Water, proton, and oxygen transport in high IEC, short side chain PFSA ionomer membranes: consequences of a frustrated network," *Phys. Chem. Chem. Phys.*, vol. 13, no. 40, pp. 18055–18062, 2011.

[102] J. Peron *et al.*, "Fuel cell catalyst layers containing short-side-chain perfluorosulfonic acid ionomers," *J. Power Sources*, vol. 196, no. 1, pp. 179–181, 2011.

[103] S. Shahgaldi, I. Alaefour, and X. Li, "The impact of short side chain ionomer on polymer electrolyte membrane fuel cell performance and durability," *Appl. Energy*, vol. 217, pp. 295–302, 2018.

[104] Y. Garsany, R. W. Atkinson, M. B. Sassin, R. M. E. Hjelm, B. D. Gould, and K. E. Swider-Lyons, "Improving PEMFC Performance Using Short-Side-Chain Low-Equivalent-Weight PFSA Ionomer in the Cathode Catalyst Layer," *J. Electrochem. Soc.*, vol. 165, no. 5, pp. F381–F391, 2018.

[105] F. N. Büchi, M. Wakizoe, and S. Srinivasan, "Microelectrode Investigation of Oxygen Permeation in Perfluorinated Proton Exchange Membranes with Different Equivalent Weights," *J. Electrochem. Soc.*, vol. 143, no. 3, pp. 927–932, 1996.

[106] C. Lei, D. Bessarabov, S. Ye, Z. Xie, S. Holdcroft, and T. Navessin, "Low equivalent weight short-side-chain perfluorosulfonic acid ionomers in fuel cell cathode catalyst layers," *J.*

Power Sources, vol. 196, no. 15, pp. 6168–6176, 2011.

[107] H. Xu, H. R. Kunz, L. J. Bonville, and J. M. Fenton, "Improving PEMFC Performance Using Low Equivalent Weight PFSA Ionomers and Pt-Co/C Catalyst in the Cathode," *J. Electrochem. Soc.*, vol. 154, no. 2, pp. B271–B271, 2007.

[108] A. Stassi *et al.*, "Performance comparison of long and short-side chain perfluorosulfonic membranes for high temperature polymer electrolyte membrane fuel cell operation," *J. Power Sources*, vol. 196, no. 21, pp. 8925–8930, 2011.

[109] Y.-C. Park, K. Kakinuma, H. Uchida, M. Watanabe, and M. Uchida, "Effects of short-side-chain perfluorosulfonic acid ionomers as binders on the performance of low Pt loading fuel cell cathodes," *J. Power Sources*, vol. 275, pp. 384–391, 2015.

[110] M. Yandrasits, M. Lindell, M. Schaberg, and M. Kurkowski, "Increasing fuel cell efficiency by using ultra-low equivalent weight ionomers," *Electrochem. Soc. Interface*, vol. 26, no. 1, pp. 49–53, 2017.

[111] N. J. Economou, J. R. O'Dea, T. B. McConnaughy, and S. K. Buratto, "Morphological differences in short side chain and long side chain perfluorosulfonic acid proton exchange membranes at low and high water contents," *RSC Adv.*, vol. 3, no. 42, pp. 19525–19532, 2013.

[112] N. Ramaswamy *et al.*, "Editors' Choice—Ionomer Side Chain Length and Equivalent Weight Impact on High Current Density Transport Resistances in PEMFC Cathodes," *J. Electrochem. Soc.*, vol. 168, no. 2, p. 24518, 2021.

[113] S. J. Hamrock and M. A. Yandrasits, "Proton exchange membranes for fuel cell applications," *J. Macromol. Sci. Part C Polym. Rev.*, vol. 46, no. 3, pp. 219–244, 2006.

[114] Y. Liu *et al.*, "A small-angle X-ray scattering study of the development of morphology in films formed from the 3M perfluorinated sulfonic acid ionomer," *Macromolecules*, vol. 45, no. 18, pp. 7495–7503, 2012.

[115] T. A. Zawodzinski *et al.*, "A Comparative Study of Water Uptake By and Transport Through Ionomeric Fuel Cell Membranes," *J. Electrochem. Soc.*, vol. 140, no. 7, pp. 1981–1985, 1993.

[116] D. Wu, S. J. Paddison, and J. A. Elliott, "A comparative study of the hydrated morphologies of perfluorosulfonic acid fuel cell membranes with mesoscopic simulations," *Energy Environ. Sci.*, vol. 1, no. 2, pp. 284–293, 2008.

[117] D. K. Paul and K. Karan, "Effect of Thermal Treatment on the Properties of Ultra-Thin Nafion Film," *ECS Trans.*, vol. 50, no. 2, pp. 951–959, 2012.

[118] U. N. Shrivastava, K. Suetsugu, S. Nagano, H. Fritzsche, Y. Nagao, and K. Karan, "Cross-correlated humidity-dependent structural evolution of Nafion thin films confined on a platinum substrate," *Soft Matter*, vol. 16, no. 5, pp. 1190–1200, 2020.

[119] R. Borup and A. Weber, "FC135 : FC-PAD : Fuel Cell Performance and Durability Consortium Presenter : Rod Borup," *2019 DOE Fuel Cell Technol. Off. Annu. Merit Rev.*, no. May, pp. 1–42, 2020.

[120] C. Zhang, M. Davies, and K. Karan, "Probing interfacial interactions of nafion ionomer: Thermal expansion of nafion thin films on substrates of different hydrophilicity/hydrophobicity," *J. Polym. Sci. Part B Polym. Phys.*, vol. 57, no. 6, pp. 343–352, Mar. 2019.

[121] H. K. (Key) Shim, D. K. Paul, and K. Karan, "Resolving the Contradiction between Anomalously High Water Uptake and Low Conductivity of Nanothin Nafion films on SiO2 Substrate," *Macromolecules*, vol. 48, no. 22, pp. 8394–8397, Nov. 2015.

[122] T. E. Springer, T. A. Zawodzinski, and S. Gottesfeld, "Polymer Electrolyte Fuel Cell Model," *J. Electrochem. Soc.*, vol. 138, no. 8, pp. 2334–2342, 1991.

[123] T. A. Zawodzinski, T. E. Springer, F. Uribe, and S. Gottesfeld, "Characterization of polymer electrolytes for fuel cell applications," *Solid State Ionics*, vol. 60, no. 1, pp. 199–211, 1993.

[124] D. Wu, S. J. Paddison, J. A. Elliott, and S. J. Hamrock, "Mesoscale Modeling of Hydrated Morphologies of 3M Perfluorosulfonic Acid-Based Fuel Cell Electrolytes," *Langmuir*, vol. 26, no. 17, pp. 14308–14315, Sep. 2010.

[125] J. T. Gostick and A. Z. Weber, "Resistor-Network Modeling of Ionic Conduction in Polymer Electrolytes," *Electrochim. Acta*, vol. 179, pp. 137–145, 2015.

[126] A. Eisenberg, "Clustering of Ions in Organic Polymers. A Theoretical Approach," *Macromolecules*, vol. 3, pp. 147–154, 1970.

[127] P. Choi, N. H. Jalani, and R. Datta, "Thermodynamics and Proton Transport in Nafion," *J. Electrochem. Soc.*, vol. 152, no. 3, p. E123, 2005.

[128] P. Choi, N. H. Jalani, T. M. Thampan, and R. Datta, "Consideration of thermodynamic, transport, and mechanical properties in the design of polymer electrolyte membranes for higher temperature fuel cell operation," *J. Polym. Sci. Part B Polym. Phys.*, vol. 44, no. 16, pp. 2183–2200, Aug. 2006.

[129] A. Kusoglu, M. H. Santare, A. M. Karlsson, A. Kusoglu, M. H. Sa, and A. M. Ka, "Mechanics-Based Model for Non-Affine Swelling in Perfluorosulfonic Acid (PFSA) Membranes Publisher ' s Statement Mechanics-based model for non-affine swelling in perfluorosulfonic acid (PFSA) membranes," vol. 50, no. 11, pp. 2481–2491, 2009.

[130] A. Kusoglu and A. Z. Weber, "Electrochemical/Mechanical Coupling in Ion-Conducting Soft Matter," *J. Phys. Chem. Lett.*, vol. 6, no. 22, pp. 4547–4552, Nov. 2015.

[131] A. Kusoglu, S. Savagatrup, K. T. Clark, and A. Z. Weber, "Role of Mechanical Factors in Controlling the Structure–Function Relationship of PFSA Ionomers," *Macromolecules*, vol. 45, no. 18, pp. 7467–7476, Sep. 2012.

[132] S. A. Eastman *et al.*, "Effect of Confinement on Structure, Water Solubility, and Water Transport in Nafion Thin Films," *Macromolecules*, vol. 45, no. 19, pp. 7920–7930, Oct. 2012.

[133] K. A. Page, A. Kusoglu, C. M. Stafford, S. Kim, R. J. Kline, and A. Z. Weber, "Confinement-Driven Increase in Ionomer Thin-Film Modulus," *Nano Lett.*, vol. 14, no. 5, pp. 2299–2304, May 2014.

[134] B. R. Frieberg *et al.*, "Mechanical Response of Thermally Annealed Nafion Thin Films," *ACS Appl. Mater. Interfaces*, vol. 8, no. 48, pp. 33240–33249, Dec. 2016.

[135] A. A. Voityuk and S. F. Vyboishchikov, "Fast and accurate calculation of hydration energies of molecules and ions," *Phys. Chem. Chem. Phys.*, vol. 22, no. 26, pp. 14591–14598, 2020.

[136] A. Malek, E. Sadeghi, J. Jankovic, M. Eikerling, and K. Malek, "Aquivion Ionomer in Mixed Alcohol–Water Solution: Insights from Multiscale Molecular Modeling," *J. Phys. Chem. C*, vol. 124, no. 6, pp. 3429–3438, 2020.

[137] C. Wang and S. J. Paddison, "Hydration and proton transfer in highly sulfonated poly(phenylene sulfone) ionomers: an ab initio study.," *J. Phys. Chem. A*, vol. 117, no. 3, pp. 650–660, Jan. 2013.

[138] S. Cui, J. Liu, M. E. Selvan, S. J. Paddison, D. J. Keffer, and B. J. Edwards, "Comparison of the hydration and diffusion of protons in perfluorosulfonic acid membranes with molecular dynamics simulations," *J. Phys. Chem. B*, vol. 112, no. 42, pp. 13273–13284, 2008.

[139] Y. Marcus and G. Hefter, "Ion pairing," *Chem. Rev.*, vol. 106, no. 11, pp. 4585–4621, 2006.

[140] U. N. Shrivastava *et al.*, "Water content and ionic conductivity of thin films of different anionic forms of anion conducting ionomers," *J. Phys. Chem. C*, vol. 124, no. 43, pp. 23469–23478, 2020.

[141] N. E. De Almeida, D. K. Paul, K. Karan, and G. R. Goward, "1H Solid-State NMR Study of Nanothin Nafion Films," *J. Phys. Chem. C*, vol. 119, no. 3, pp. 1280–1285, Jan. 2015.

[142] G. M. Su *et al.*, "Chemical and Morphological Origins of Improved Ion Conductivity in Perfluoro Ionene Chain Extended Ionomers," *J. Am. Chem. Soc.*, vol. 141, no. 34, pp. 13547–13561, 2019.

[143] T. Mabuchi and T. Tokumasu, "Effects of water nanochannel diameter on proton transport in proton-exchange membranes," *J. Polym. Sci. Part B Polym. Phys.*, vol. 57, no. 13, pp. 867–878, Jul. 2019.

[144] S. Shen, A. Han, X. Yan, J. Chen, X. Cheng, and J. Zhang, "Influence of Equivalent Weight of Ionomer on Proton Conduction Behavior in Fuel Cell Catalyst Layers," *J. Electrochem. Soc.*, vol. 166, no. 12, pp. F724–F728, 2019.

[145] D. Malevich *et al.*, "Effect of Microporous Layer on Impedance Response of PEM Fuel Cell Fed with H_2 and N_2," *ECS Meet. Abstr.*, vol. MA2009-02, no. 10, p. 977, 2009.

[146] A. Alaswad *et al.*, "Technical and Commercial Challenges of Proton-Exchange Membrane (PEM) Fuel Cells," *Energies* , vol. 14, no. 1. 2021.

[147] L. Du, V. Prabhakaran, X. Xie, S. Park, Y. Wang, and Y. Shao, "Low-PGM and PGM-Free Catalysts for Proton Exchange Membrane Fuel Cells: Stability Challenges and Material Solutions," *Adv. Mater.*, vol. 33, no. 6, p. 1908232, Feb. 2021.

[148] P. S. T.A. Greszler, D. Caulk, "The Impact of Platinum Loading on Oxygen Transport

Resistance," *J. Electrochem. Soc.*, vol. 159, pp. 831–840, 2012.

[149] T. Yoshitake *et al.*, "Preparation of fine platinum catalyst supported on single-wall carbon nanohorns for fuel cell application," *Phys. B Condens. Matter*, vol. 323, no. 1–4, pp. 124–126, Oct. 2002.

[150] A. A. Franco *et al.*, "PtxCoy Catalysts Degradation in PEFC Environments: Mechanistic Insights," *J. Electrochem. Soc.*, vol. 156, no. 3, p. B410, 2009.

[151] E. Antolini, J. R. C. Salgado, and E. R. Gonzalez, "The stability of Pt–M (M=first row transition metal) alloy catalysts and its effect on the activity in low temperature fuel cells: A literature review and tests on a Pt–Co catalyst," *J. Power Sources*, vol. 160, no. 2, pp. 957–968, 2006.

[152] Y. Cai, A. Kongkanand, W. Gu, and T. E. Moylan, "Effects of Cobalt Cation on Low Pt-loaded PEM Fuel Cell Performance," *ECS Trans.*, vol. 69, no. 17, pp. 1047–1061, 2015.

[153] S. Chen, H. A. Gasteiger, K. Hayakawa, T. Tada, and Y. Shao-Horn, "Platinum-Alloy Cathode Catalyst Degradation in Proton Exchange Membrane Fuel Cells: Nanometer-Scale Compositional and Morphological Changes," *J. Electrochem. Soc.*, vol. 157, no. 1, p. A82, 2010.

[154] N. Ramaswamy *et al.*, "High-Current Density Durability of Pt/C and PtCo/C Catalysts at Similar Particle Sizes in PEMFCs," *J. Electrochem. Soc.*, vol. 168, no. 2, p. 024519, 2021.

[155] S. Satyapal, "Hydrogen & Fuel Cells Program Overview," *U.S. Department of Energy Hydrogen and Fuel Cell Technologies Office Overview*, pp. 1–45, 2021.

[156] T. Okada, S. Møller-holst, O. Gorseth, and S. Kjelstrup, "Transport and equilibrium properties of Nafion® membranes with H+ and Na+ ions," *J. Electroanal. Chem.*, vol. 442, no. 1–2, pp. 137–145, 1998.

[157] T. Rockward, I. Urdampilleta, F. Uribe, E. L. Brosha, B. Pivovar, and F. H. Garzon, "The Effects of Multiple Contaminants on Polymer Electrolyte Fuel Cells," *ECS Trans.*, vol. 11, no. 1, pp. 821–829, 2019.

[158] J. Durst, M. Chatenet, and F. ric Maillard, "Impact of metal cations on the electrocatalytic properties of Pt / C nanoparticles at multiple phase interfaces w," *Phys. Chem. Chem. Phys.*, vol. 14, pp. 13000–13009, 2012.

[159] J. P. Braaten, X. Xu, Y. Cai, A. Kongkanand, and S. Litster, "Contaminant Cation Effect on Oxygen Transport through the Ionomers of Polymer Electrolyte Membrane Fuel Cells," *J. Electrochem. Soc.*, vol. 166, no. 16, pp. F1337–F1343, 2019.

[160] M. Lopez-Haro *et al.*, "Three-dimensional analysis of Nafion layers in fuel cell electrodes," *Nat. Commun.*, vol. 5, pp. 1–6, 2014.

[161] C. Bas, N. D. Albérola, and L. Flandin, "Effects of contaminant on thermal properties in perfluorinated sulfonic acid membranes," *J. Memb. Sci.*, vol. 363, no. 1–2, pp. 67–71, 2010.

[162] S. A. Eastman *et al.*, "E ff ect of Con fi nement on Structure, Water Solubility, and Water Transport in Na fi on Thin Films," *Macromolecules*, 2012.

[163] G. Gebel and O. Diat, “Neutron and X-ray Scattering : Suitable Tools for Studying Ionomer Membranes ,” no. 2, pp. 261–276, 2005.

[164] M. A. Hickner and B. S. Pivovar, “The Chemical and Structural Nature of Proton Exchange Membrane Fuel Cell Properties ,” no. 2, pp. 213–229, 2005.

[165] A. Han *et al.*, “Effect of cobalt ion contamination on proton conduction of ultrathin Nafion film,” *Int. J. Hydrogen Energy*, vol. 45, no. 46, pp. 25276–25285, 2020.

[166] C. Wakai, T. Shimoaka, and T. Hasegawa, “(1)H NMR Analysis of Water Freezing in Nanospace Involved in a Nafion Membrane.,” *J. Phys. Chem. B*, vol. 119, no. 25, pp. 8048–8053, Jun. 2015.

[167] D. Dolar, S. Lapanje, and L. Čelik, “Thermodynamics of water sorption by polymethylstyrenesulphonic acid and its sodium salt,” *Die Makromol. Chemie*, vol. 41, no. 1, pp. 77–85, 1960.

[168] K. K. Pushpa, D. Nandan, and R. M. Iyer, “Thermodynamics of Water Sorption by Perfluorosulphonate (Dowex 50W) Ion-exchange Resins at 298 _ + 1 K,” vol. 84, no. 6, pp. 2047–2056, 1988.

[169] J. E. R. Nightingale, “PHENOMENOLOGICAL THEORY OF ION SOLVATION. EFFECTIVE RADII OF HYDRATED IONS,” *J. Phys. Chem.*, vol. 63, no. 9, pp. 1381–1387, 1959.

[170] B. G. Pollet, I. Staffell, and J. L. Shang, “Current status of hybrid, battery and fuel cell electric vehicles: From electrochemistry to market prospects,” *Electrochim. Acta*, vol. 84, pp. 235–249, Dec. 2012.

[171] Y. Marcus, “Effect of Ions on the Structure of Water: Structure Making and Breaking,” *Chem. Rev.*, vol. 109, no. 3, pp. 1346–1370, 2009.

[172] M. Della Monica and L. Senatore, “Solvated radius of ions in nonaqueous solvents,” *J. Phys. Chem.*, vol. 74, no. 1, pp. 205–207, Jan. 1970.

[173] R. Tandon and P. N. Pintauro, “Divalent/monovalent cation uptake selectivity in a Nafion cation-exchange membrane: Experimental and modeling studies,” *J. Memb. Sci.*, vol. 136, no. 1–2, pp. 207–219, 1997.

[174] P. N. Pintauro and N. Orleans, “Water orientation and ion solvation effects during multicomponent salt partitioning in a Nafion cation exchange membrane,” *Chem. Eng. Sci.*, vol. 49, no. 23, pp. 3835–3851, 1994.

[175] S. H. Lee, S. S. Park, S. Parambadath, and C.-S. Ha, “Sulphonic acid functionalized periodic mesoporous organosilica with the bridged bissilylated urea groups for high selective adsorption of cobalt ion from artificial seawater,” *Microporous Mesoporous Mater.*, vol. 226, pp. 179–190, May 2016.

[176] S. Holdcroft, “Fuel Cell Catalyst Layers: A Polymer Science Perspective,” *Chem. Mater.*, vol. 26, no. 1, pp. 381–393, Jan. 2014.

[177] P. W. Majsztrik, M. B. Satterfield, A. B. Bocarsly, and J. B. Benziger, “Water sorption,

desorption and transport in Nafion membranes," *J. Memb. Sci.*, vol. 301, no. 1, pp. 93–106, 2007.

[178] A. L. Rangel-Cárdenas, S. J. Picken, and G. J. M. Koper, "Anomalous water sorption kinetics in supported Nafion thin-films as membrane-electrode assemblies," *J. Memb. Sci.*, vol. 650, no. February, p. 120368, 2022.

[179] T. A. Zawodzinski, M. Neeman, L. O. Sillerud, and S. Gottesfeld, "Determination of water diffusion coefficients in perfluorosulfonate ionomeric membranes," *J. Phys. Chem.*, vol. 95, no. 15, pp. 6040–6044, Jul. 1991.

[180] D. I. Kushner, A. Kusoglu, N. J. Podraza, and M. A. Hickner, "Substrate-Dependent Molecular and Nanostructural Orientation of Nafion Thin Films," *Adv. Funct. Mater.*, vol. 29, no. 37, p. 1902699, Sep. 2019.

[181] R. L. Wood, D. L., III; Chlistunoff, J.; Majewski, J.; Borup, "Nafion Structural Phenomena at Platinum and Carbon Interfaces," *J. Am. Chem. Soc.*, vol. 131, pp. 18096–18104, 2009.

[182] A. Kongkanand, "Interfacial Water Transport Measurements in Nafion Thin Films Using a Quartz-Crystal Microbalance," *J. Phys. Chem. C*, vol. 115, no. 22, pp. 11318–11325, Jun. 2011.

[183] M. A. Modestino, A. Kusoglu, A. Hexemer, A. Z. Weber, and R. A. Segalman, "Controlling Nafion Structure and Properties via Wetting Interactions," *Macromolecules*, vol. 45, no. 11, pp. 4681–4688, Jun. 2012.

[184] A. Ohira, S. Kuroda, H. F. M. Mohamed, and B. Tavernier, "Effect of interface on surface morphology and proton conduction of polymer electrolyte thin films," *Phys. Chem. Chem. Phys.*, vol. 15, no. 27, pp. 11494–11500, 2013.

[185] N. C. Buggy *et al.*, "Designing Anion-Exchange Ionomers with Oriented Nanoscale Phase Separation at a Silver Interface," *J. Phys. Chem. C*, vol. 125, no. 37, pp. 20592–20605, Sep. 2021.

[186] K. Alofari, E. Me´dici, K. Tajiri, and J. Allen, "Ionomer Films Impact on The Structure, Flow Regime, and The Wettability of The Catalyst Layer of PEMFC," *E3S Web Conf.*, vol. 334, p. 04019, 2022.

[187] T. A. M. Suter *et al.*, "Engineering Catalyst Layers for Next-Generation Polymer Electrolyte Fuel Cells: A Review of Design, Materials, and Methods," *Adv. Energy Mater.*, vol. 11, no. 37, p. 2101025, Oct. 2021.

[188] Y. Ogata, D. Kawaguchi, N. L. Yamada, and K. Tanaka, "Multistep Thickening of Nafion Thin Films in Water," *ACS Macro Lett.*, vol. 2, no. 10, pp. 856–859, Oct. 2013.

[189] S. Kim *et al.*, "Surface-Induced Nanostructure and Water Transport of Thin Proton-Conducting Polymer Films," *Macromolecules*, vol. 46, no. 14, pp. 5630–5637, Jul. 2013.

[190] J. A. Dura, V. S. Murthi, M. Hartman, S. K. Satija, and C. F. Majkrzak, "Multilamellar Interface Structures in Nafion," *Macromolecules*, vol. 42, no. 13, pp. 4769–4774, Jul. 2009.

[191] D. L. Wood, J. Chlistunoff, J. Majewski, and R. L. Borup, "Nafion Structural Phenomena

at Platinum and Carbon Interfaces," *J. Am. Chem. Soc.*, vol. 131, no. 50, pp. 18096–18104, Dec. 2009.

[192] S. C. DeCaluwe, A. M. Baker, P. Bhargava, J. E. Fischer, and J. A. Dura, "Structure-property relationships at Nafion thin-film interfaces: Thickness effects on hydration and anisotropic ion transport," *Nano Energy*, vol. 46, pp. 91–100, 2018.

[193] T. J. Zimudzi and M. A. Hickner, "Signal Enhanced FTIR Analysis of Alignment in NAFION Thin Films at SiO2 and Au Interfaces," *ACS Macro Lett.*, vol. 5, no. 1, pp. 83–87, Jan. 2016.

[194] R. M. Blanchard and R. G. Nuzzo, "An infrared study of the effects of hydration on cation-loaded nafion thin films," *J. Polym. Sci. Part B Polym. Phys.*, vol. 38, no. 11, pp. 1512–1520, Jun. 2000.

[195] G. C. Abuin, M. Cecilia Fuertes, and H. R. Corti, "Substrate effect on the swelling and water sorption of Nafion nanomembranes," *J. Memb. Sci.*, vol. 428, no. Complete, pp. 507–515, 2013.

[196] S. K. Dishari and M. A. Hickner, "Antiplasticization and Water Uptake of Nafion Thin Films," *ACS Macro Lett.*, vol. 1, no. 2, pp. 291–295, Feb. 2012.

[197] S. K. Dishari and M. A. Hickner, "Confinement and Proton Transfer in NAFION Thin Films," *Macromolecules*, vol. 46, no. 2, pp. 413–421, Jan. 2013.

[198] T. Mabuchi, S.-F. Huang, and T. Tokumasu, "Influence of Ionomer Loading and Substrate Wettability on the Morphology of Ionomer Thin Films Using Coarse-Grained Solvent Evaporation Simulations," *Macromolecules*, vol. 54, no. 1, pp. 115–125, Jan. 2021.

[199] T. A. Hill, D. L. Carroll, R. Czerw, C. W. Martin, and D. Perahia, "Atomic force microscopy studies on the dewetting of perfluorinated ionomer thin films," *J. Polym. Sci. Part B Polym. Phys.*, vol. 41, no. 2, pp. 149–158, Jan. 2003.

[200] M. B. Satterfield and J. B. Benziger, "Non-Fickian Water Vapor Sorption Dynamics by Nafion Membranes," *J. Phys. Chem. B*, vol. 112, no. 12, pp. 3693–3704, 2008.

[201] D. J. Burnett, A. R. Garcia, and F. Thielmann, "Measuring moisture sorption and diffusion kinetics on proton exchange membranes using a gravimetric vapor sorption apparatus," *J. Power Sources*, vol. 160, no. 1, pp. 426–430, 2006.

[202] S. Ge, X. Li, B. Yi, and I.-M. Hsing, "Absorption, Desorption, and Transport of Water in Polymer Electrolyte Membranes for Fuel Cells," *J. Electrochem. Soc.*, vol. 152, no. 6, p. A1149, 2005.

[203] M. B. Satterfield, *Mechanical and water sorption properties of Nafion and composite Nafion/titanium dioxide membranes for polymer electrolyte membrane fuel cells*. Princeton University, 2007.

[204] Q. Zhao, P. Majsztrik, and J. Benziger, "Diffusion and Interfacial Transport of Water in Nafion," *J. Phys. Chem. B*, vol. 115, no. 12, pp. 2717–2727, Mar. 2011.

[205] E. M. Davis, C. M. Stafford, and K. A. Page, "Elucidating Water Transport Mechanisms in

Nafion Thin Films," *ACS Macro Lett.*, vol. 3, no. 10, pp. 1029–1035, Oct. 2014.

[206] P. W. Majsztrik, "MECHANICAL AND TRANSPORT PROPERTIES OF NAFION{\textregistered} FOR PEM FUEL CELLS; TEMPERATURE AND HYDRATION EFFECTS," PRINCETON UNIVERSITY, 2008.

[207] T. ~A. Hill, C. ~W. Martin, and D. Perahia, "Wetting of Ionomers at Interfaces," in *APS March Meeting Abstracts*, 1998, p. M13.15.

[208] M. A. Modestino *et al.*, "Self-Assembly and Transport Limitations in Confined Nafion Films," *Macromolecules*, vol. 46, no. 3, pp. 867–873, Feb. 2013.

[209] K. Shrivastava, U. N.; Fritzsche, H.; Karan, "Interfacial and Bulk Water in Ultra-thin Films of Nafion, 3M PFSA and 3M PFIA Ionomers on Polycrystalline Platinum Surface," *Macromolecules*, vol. 51, no. 23, pp. 9839–9849, 2018.

[210] H. Luo, S. Park, H. Y. H. Chan, and M. J. Weaver, "Surface Oxidation of Platinum-Group Transition Metals in Ambient Gaseous Environments: Role of Electrochemical versus Chemical Pathways," *J. Phys. Chem. B*, vol. 104, no. 34, pp. 8250–8258, Aug. 2000.

[211] H. F. M. Mohamed, S. Kuroda, Y. Kobayashi, N. Oshima, R. Suzuki, and A. Ohira, "Possible presence of hydrophilic SO3H nanoclusters on the surface of dry ultrathin Nafion® films: a positron annihilation study," *Phys. Chem. Chem. Phys.*, vol. 15, no. 5, pp. 1518–1525, 2013.

[212] Z. Li, P. Beck, D. A. A. Ohlberg, D. R. Stewart, and R. S. Williams, "Surface properties of platinum thin films as a function of plasma treatment conditions," *Surf. Sci.*, vol. 529, no. 3, pp. 410–418, 2003.

[213] Q. He, N. S. Suraweera, D. C. Joy, and D. J. Keffer, "Structure of the Ionomer Film in Catalyst Layers of Proton Exchange Membrane Fuel Cells," *J. Phys. Chem. C*, vol. 117, no. 48, pp. 25305–25316, Dec. 2013.

[214] D. Rivin, C. E. Kendrick, P. W. Gibson, and N. S. Schneider, "Solubility and transport behavior of water and alcohols in Nafion^{TM}," *Polymer (Guildf).*, vol. 42, no. 2, pp. 623–635, 2001.

[215] C. H. Lee, H. B. Park, Y. M. Lee, and R. D. Lee, "Importance of Proton Conductivity Measurement in Polymer Electrolyte Membrane for Fuel Cell Application," *Ind. Eng. Chem. Res.*, vol. 44, no. 20, pp. 7617–7626, Sep. 2005.

[216] S. Didierjean *et al.*, "Theoretical evidence of the difference in kinetics of water sorption and desorption in Nafion® membrane and experimental validation," *J. Power Sources*, vol. 300, pp. 50–56, 2015.

[217] A. L. Rangel-Cárdenas and G. J. M. Koper, "Transport in Proton Exchange Membranes for Fuel Cell Applications—A Systematic Non-Equilibrium Approach," *Materials* , vol. 10, no. 6. 2017.

[218] V. S. Murthi, J. Dura, S. Satija, and C. Majkrzak, "Water Uptake and Interfacial Structural Changes of Thin Film Nafion® Membranes Measured by Neutron Reflectivity for PEM Fuel Cells," *ECS Trans.*, vol. 16, no. 2, pp. 1471–1485, 2008.

[219] D. T. Hallinan, M. G. De Angelis, M. Giacinti Baschetti, G. C. Sarti, and Y. A. Elabd, "Non-Fickian Diffusion of Water in Nafion," *Macromolecules*, vol. 43, no. 10, pp. 4667–4678, May 2010.

[220] O. Zybaylo *et al.*, "A novel method to measure diffusion coefficients in porous metal–organic frameworks," *Phys. Chem. Chem. Phys.*, vol. 12, no. 28, pp. 8093–8098, 2010.

[221] P. Krtil, A. Trojánek, and Z. Samec, "Kinetics of Water Sorption in NafionThin Films − Quartz Crystal Microbalance Study," *J. Phys. Chem. B*, vol. 105, no. 33, pp. 7979–7983, Aug. 2001.

Copyright Information

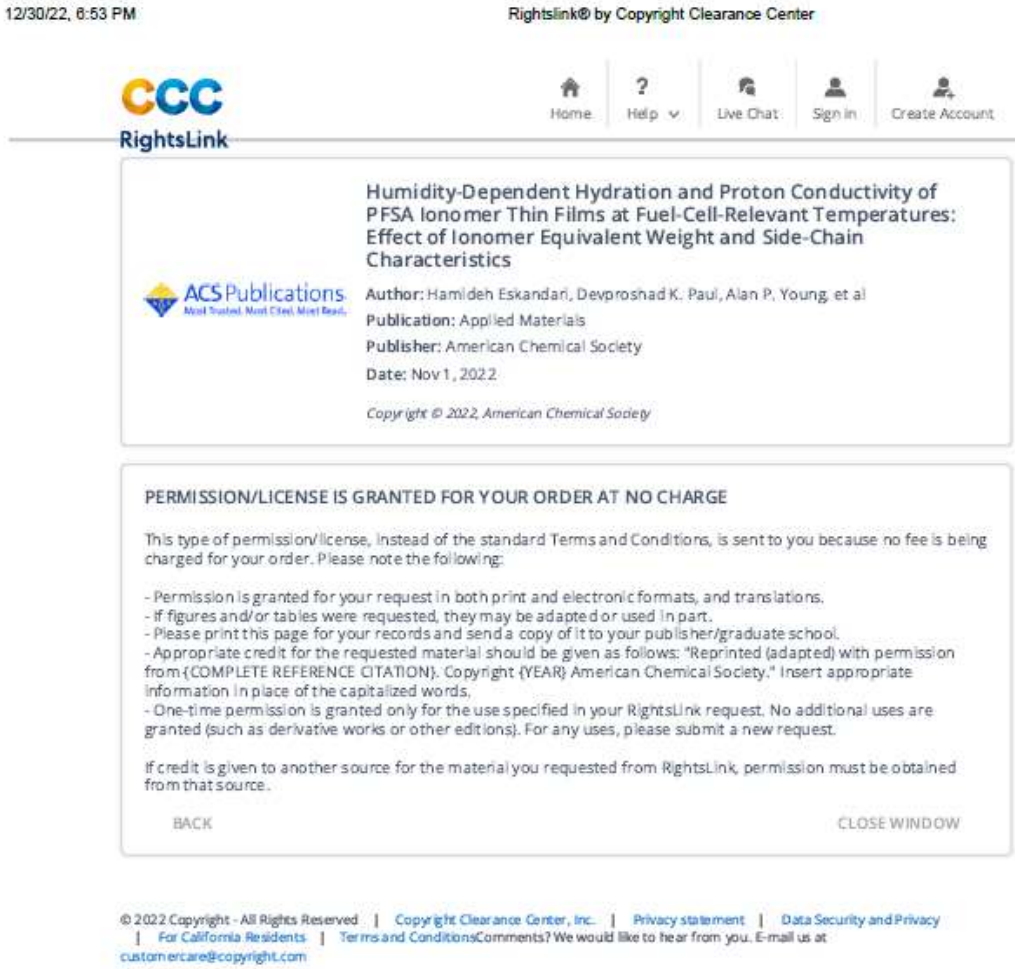

Copyright permission letters from the co-authors pertinent to this paper are provided below.

Subject: Permission to access manuscript

To
The University of Calgary Copyright Office

Dear Madam/Sir,

I, **Alan Young**, hereby grant permission to **Hamideh Eskandari** to include the following manuscript in her PhD dissertation:

"Humidity-Dependent Hydration and Proton Conductivity of PFSA Ionomer Thin Films at Fuel-Cell-Relevant Temperatures: Effect of Ionomer Equivalent Weight and Side Chain Characteristics"

Sincerely,

Alan Young
Electrodes Research Manager
Ballard Power Systems

Subject: Permission to access manuscript

To
The University of Calgary Copyright Office

Dear Madam/Sir,

I, **Devproshad Paul**, hereby grant permission to **Hamideh Eskandari** to include the following manuscript in his PhD dissertation:

"Humidity-Dependent Hydration and Proton Conductivity of PFSA Ionomer Thin Films at Fuel-Cell-Relevant Temperatures: Effect of Ionomer Equivalent Weight and Side Chain Characteristics"

Sincerely,

Devproshad paul. 03-01-2023

Devproshad Paul, Ph.D.
Senior Research Scientist – R&D
Ballard Power Systems

Chapter 5 of this thesis has been published in Journal of Physical Chemistry C, and it was reproduced with permission. According to the copyright policies of American Chemical Society, the authors retain the right to reproduce the article in whole or in part in a thesis or dissertation written by the authors provided acknowledgement is given to the original source of publication. An acknowledgement to the original published article has been prominently provided at the beginning of Chapter 5. Detailed information on the copyright policy of the ACS can be found at: https://pubs.acs.org/pb-assets/acspubs/Migrated/dissertation-1546558023843.pdf

The published article is available as *"Conductivity and Hygroscopic Expansion of Ionomer Thin Films: Effect of Cobalt Exchange and Thermal/Aqueous Treatment", J. Phys. Chem. C 2022, 126, 42, 17862–17874.* *https://doi.org/10.1021/acs.jpcc.2c05629*

Copyright permission letters from the co-author pertinent to this chapter and from the journals of the references used are provided below.

Subject: Permission to access manuscript

To
The University of Calgary Copyright Office

Dear Madam/Sir,

I, **Vinayaraj Ozhukil Kollath**, hereby grant permission to **Hamideh Eskandari** to include the following manuscript in her PhD dissertation:

"*Conductivity and Hygroscopic Expansion of Ionomer Thin films: Effect of Cobalt Exchange and Thermal/Aqueous Treatment*"

Sincerely,

Vinayaraj Ozhukil Kollath, Ph.D.

OPEN ACCESS

Proton Transport Property in Supported Nafion Nanothin Films by Electrochemical Impedance Spectroscopy

Devproshad K. Paul[1,2], Richard McCreery[4,3] and Kunal Karan[5,6,2]

Published 8 October 2014 • © The Author(s) 2014. Published by ECS.

Journal of The Electrochemical Society, Volume 161, Number 14

Citation Devproshad K. Paul *et al* 2014 *J. Electrochem. Soc.* **161** F1395

DOI 10.1149/2.0571414jes

1/3/23, 10:25 AM Proton Transport Property in Supported Nafion Nanothin Films by Electrochemical Impedance Spectroscopy - IOPscience

Interesting Facets of Surface, Interfacial, and Bulk Characteristics of Perfluorinated Ionomer Films

Kunal Karan*

Cite this: *Langmuir* 2019, 35, 42, 13489−13520
Publication Date: February 12, 2019
https://doi.org/10.1021/acs.langmuir.8b03721

New Insights into Perfluorinated Sulfonic-Acid Ionomers

Ahmet Kusoglu* and Adam Z. Weber

View Author Information

Cite this: *Chem. Rev.* 2017, 117, 3, 987−1104
Publication Date: January 23, 2017
https://doi.org/10.1021/acs.chemrev.6b00159

Case CSCSI0111548 solution proposed: PLEASE DO NOT REPLY

Comments:

01-03-2023 01:04:57 PM EST - Jawwad Saeed Additional comments

Dear Hamideh,

Your permission requested is granted and there is no fee for this reuse.

In your planned reuse, you must cite the ACS article as the source, add the direct link(s): <https://pubs.acs.org/doi/10.1021/acs.langmuir.8b03721>, and <https://pubs.acs.org/doi/10.1021/acs.chemrev.6b00159>, and include a notice to the readers that further permission related to the material excerpted should be directed to the ACS.

Please do not hesitate to contact me if you need any further assistance.

Regards,
Jawwad Saeed
ACS Customer Services & Information
https://help.acs.org